Aus dem

Institut für Kardiovaskuläre Physiologie und Pathophysiologie im Walter-Brendel-Zentrum für Experimentelle Medizin
Institut der Ludwig-Maximilians-Universität München



The Role of Dyrk3 in Centrosome Coherence during Cell Migration

Dissertation
zum Erwerb des Doctor of Philosophy (Ph.D.)
an der Medizinischen Fakultät
der Ludwig-Maximilians-Universität München

vorgelegt von Madeleine Tanja Schmitt

> aus Karlstadt

> > Jahr 2024

Mit Genehmigung der Medizinischen Fakultät der Ludwig-Maximilians-Universität München

Erstes Gutachten: Prof. Dr. Jörg Renkawitz

Zweites Gutachten: Dr. Ralph Böttcher

Drittes Gutachten: Prof. Dr. Annette Müller-Taubenberger

Viertes Gutachten: Priv. Doz. Dr. Franziska Hartig-Vielmuth

Dekan: Prof. Dr. med. Thomas Gudermann

Tag der mündlichen Prüfung: 30.09.2024

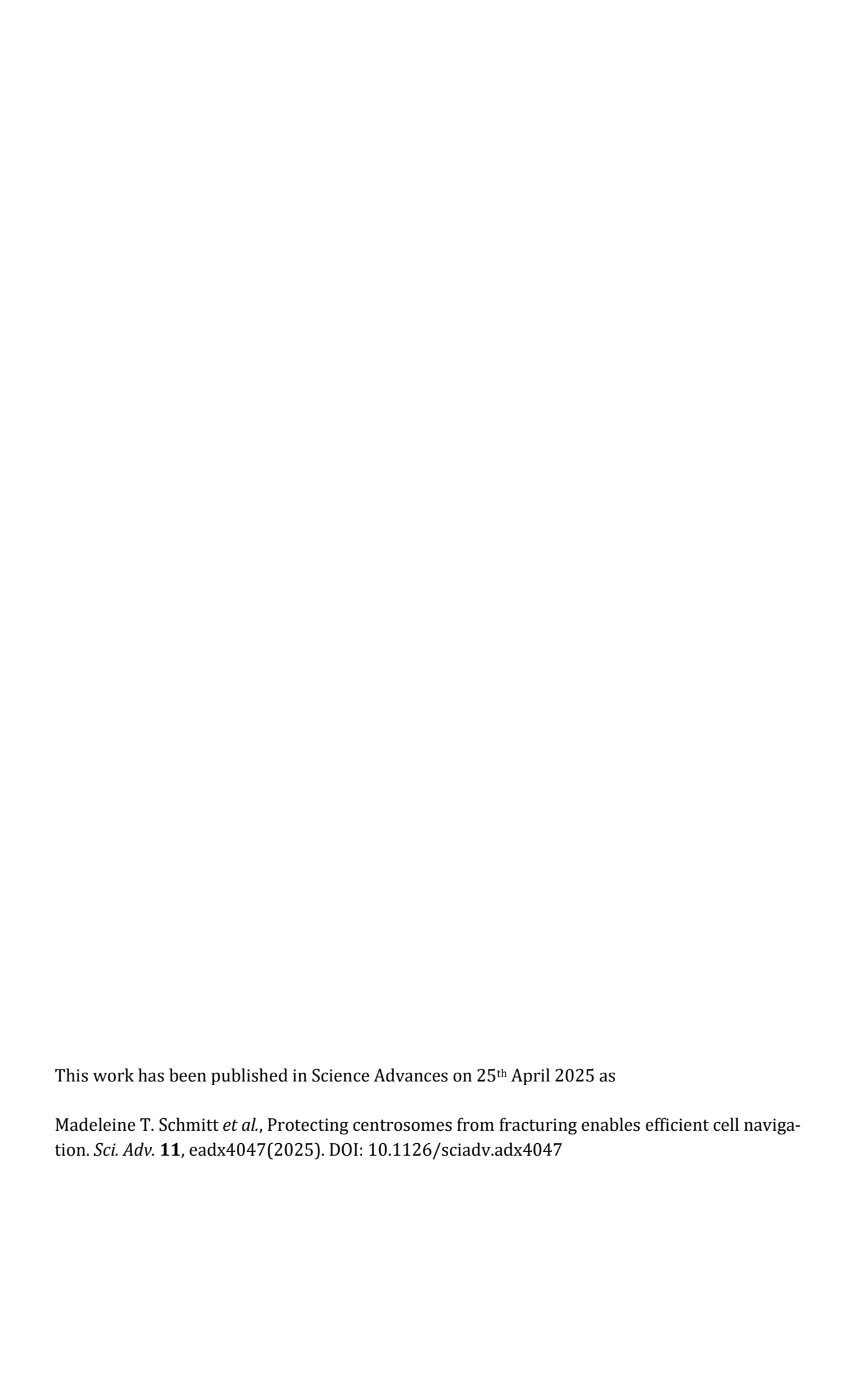


TABLE OF CONTENT

Tab	ole of conte	ent	7
Abs	stract		9
List	t of figures		11
	J		
LIST	t of tables.		12
List	t of abbrev	riations	13
1	Introd	uction	15
	1.1 Cell m	igration	15
	1.1.1	Cell migration modes	15
	1.1.2	Immune cell migration	17
	1.1.3	Cell shape coordination during migration	18
	1.2 The Ce	entrosome	19
	1.2.1	Architecture of the centrosome	19
	1.2.2	The centrosome cycle	21
	1.2.3	Centrosome function	
	1.3 The pr	rotein kinase Dyrk3	23
	1.3.1	DYRK kinases	
	1.3.2	Dyrk3 function	
	1.4 Aims o	of the thesis	
2	Materi	ial and Methods	27
		ial	
	2.1.1	Media, buffers, and reagents	
	2.1.2	Cell lines	
	2.1.3	Plasmids	
	2.1.4	Oligonucleotides	
	2.1.5	Antibodies and staining reagents	
	2.2 Metho	ods	
	2.2.1	Cell culture	
	2.2.2	Flow cytometry analysis	
	2.2.3	Mice	
	2.2.4	Generation of fluorescent reporter constructs	
	2.2.5	Transgene delivery	33
	2.2.6	Micro-fabricated devices	34
	2.2.7	Migration assays	35
	2.2.8	Immunofluorescence staining	36
	2.2.9	Imaging	
	2.2.10	Image analysis	38
	2.2.11	Statistical analysis	40

3	Result	ts	41
	3.1 Cell m	otility forces deform the centrosome	41
	3.2 Centro	osomes fracture in the absence of Dyrk3 activity	41
	3.2.1	Immune cell motility requires functional Dyrk3	41
	3.2.2	Dyrk3 kinase is active at the centrosome	46
	3.2.3	Dyrk3 impairment alters diffusion dynamics of centrosomal proteins	48
	3.2.4	The centrosome fractures during cellular pathfinding in the absence of activity	
	3.3 Mecha	anical centrosome fracturing	50
	3.3.1	The centrosomal linker protein C-Nap1 is required for centrosome cohe during cellular pathfinding	
	3.3.2	Actomyosin forces fracture the centrosome	53
	3.4 Centro	osome fracturing generates coexisting MTOCs	56
	3.5 Centro	osome fracturing impedes cellular navigation	59
	3.5.1	Mechanically unstable centrosomes impair cellular pathfinding	59
	3.5.2	Dendritic cells retain their polarity upon rendering Dyrk3 non-function	al66
	3.5.3	Emergence of two coexisting MTOCs causes cellular entanglement	68
4	Discus	ssion	71
	4.1 Evalua	ation of Dyrk3 function in vivo	71
	4.2 Forces	s acting on the centrosome resulting in fracturing	72
	4.3 How 6	exactly is Dyrk3 influencing centrosome cohesion?	75
	4.4 Funct	ional consequences of centrosome fracturing	77
Re	ferences		81
Со	ntribution	S	96
Ac	knowledge	ements	97
Af	fidavit		98
Со	nfirmation	of congruency between printed and electronic version of the doctoral th	esis 99
Lis	st of public	ations	100

ABSTRACT

Cell migration is a fundamental mechanism underlying numerous biological processes, such as development, immune responses, and wound healing, as well as cancer cell dissemination and metastasis formation (Te Boekhorst et al., 2016). Fast-migrating cells, such as immune cells, typically employ an amoeboid migration mode, characterized by frequent and highly dynamic shape changes and low adhesiveness to the substrate as they encounter complex microenvironments of heterogeneous composition while navigating through the body (Yamada & Sixt, 2019). To process diverse guidance cues and efficiently traverse these microenvironments, amoeboid migrating cells generate multiple exploratory protrusions simultaneously, which undergo continuous formation and retraction cycles (Leithner et al., 2016; Fritz-Laylin et al., 2017). The mechanical stress resulting from these dynamic cell shape changes and the surrounding environment affects the cell's interior and causes intracellular structures such as microtubules to become compressed and bent (Schaedel et al., 2015; Robison et al., 2016). In many cells, the centrosome functions as the primary microtubule-organizing center (MTOC), nucleating and anchoring microtubules, suggesting it can withstand such mechanical forces (Bettencourt-Dias & Glover, 2007). Given that the centrosome is a membraneless organelle consisting of two centrioles connected by a non-covalent linker and surrounded by a pericentriolar matrix, it raises the question of how cells maintain centrosome integrity while experiencing these mechanical forces.

This study reveals that the centrosome of migrating cells undergoes mechanical deformations during navigational pathfinding due to the formation of two simultaneous exploratory cell fronts. Importantly, these deformations are transient, indicating that cells have developed mechanisms to actively maintain centrosome integrity. Based on transcriptome analysis of migrating dendritic cells, I identified the dual-specificity tyrosine-regulated kinase 3 (Dyrk3) as crucial for immune cell motility. Dyrk3 localizes to the centrosome, and loss of Dyrk3 activity not only alters the phosphorylation status of multiple centrosome-associated proteins but also affects the diffusion dynamics of various pericentriolar matrix proteins, suggesting a direct role of Dyrk3 at the centrosome. In the absence of functional Dyrk3, centrosome cohesion is impaired, resulting in centrosome fracturing during cell migration in complex microenvironments. Similarly, genetic depletion of the centrosome linker protein C-Nap1 leads to mechanical centrosome fracturing during navigational pathfinding. Pharmacological inhibition experiments revealed that the fracturing force is exerted by the actomyosin cytoskeleton, as actin inhibition completely prevents Dyrk3-dependent centrosome fracturing. Furthermore, increased mechanical deformation of the surrounding pericentriolar material during cellular pathfinding is reduced when actin polymerization is inhibited. As a consequence of centrosome fracturing, two functional microtubule-organizing centers (MTOCs) form around the individual centrioles within a single cell, effectively anchoring and nucleating microtubules from two distinct locations. This emergence of two competing MTOCs impairs cell migration in complex microenvironments. While overall front-rear polarity remains unaffected in Dyrk3-deficient cells with intact centrioles, shape analysis of cells migrating within collagen networks shows an elongated cell shape, indicative of impaired cell shape coordination and cellular entanglement in Dyrk3-deficient cells. Consistently, cells with fractured centrosomes exhibit longer competing protrusions and take longer to make productive path decisions in complex microenvironments. Finally, pharmacological depletion of centrioles confirmed a direct link between the emergence of two MTOCs and cell entanglement, as centriole-depleted cells are not affected by Dyrk3 inhibition.

Altogether, this study demonstrates that cells actively maintain centrosome integrity to withstand mechanical forces during migration in complex microenvironments. Given that almost all cells in multicellular organisms experience mechanical forces, these results suggest that preserving centrosome stability is a fundamental mechanism.

LIST OF FIGURES

Figure	1: Mesenchymal and amoeboid migration modes	16
Figure	2: Centrosome structure	19
Figure	3: The centrosome duplication cycle	21
Figure	4: Mechanical centrosome deformations in motile cells	43
Figure	5: Transcriptome analysis of migrating dendritic cells	44
Figure	6: Pharmacological inhibition of Dyrk3 during dendritic cell migration	45
J	7: Pharmacological inhibition and expression of a kinase-dead point mutant of Dyrk3 during Jurkat T cell migration	46
_	8: Dyrk3 localization and phosphoproteome analysis of migrating dendritic cells upon Dyrk3 inhibition4	47
Figure	9: Fluorescence recovery after photobleaching (FRAP) of centrosomal proteins4	49
_	10: Centrosome deformation dynamics and fracturing frequency during dendritic cell migration upon Dyrk3 inhibition	52
_	11: Centrosome deformation dynamics and fracturing frequency during dendritic cell migration upon C-Nap1 deletion	53
Figure	12: Inhibition of actomyosin forces upon centrosome fracturing	54
Figure	13: Pericentriolar material shape deformations during dendritic cell migration	55
Figure	14: Characterization of intact centrosomes in dendritic cells	56
Figure	15: Microtubule nucleation in intact centrosomes	57
Figure	16: Characterization of individual centrioles upon centrosome fracturing	58
_	17: Dendritic cell migration in less complex environments in the presence of mechanically unstable centrosomes	61
	18: Dendritic cell migration in complex environments in the presence of mechanically unstable centrosomes	62
	19: Jurkat T cell migration in the presence of mechanically unstable centrosomes upon Dyrk3 inhibition	63
	20: Jurkat T cell migration in the presence of mechanically unstable centrosomes upon expression of dominant-negative Dyrk3 (K218M)	64
	21: Dendritic cell and Jurkat T cell shapes during migration in 3D collagen matrices upon rendering Dyrk3 non-functional	
	22: Dendritic cell polarity upon rendering Dyrk3 non-functional	
_	23: Dendritic cell nucleus-MTOC axis configuration upon rendering Dyrk3 non-functional	68
Figure	24: Consequences of centrosome fracturing on cellular navigation	70

LIST OF TABLES

27
28
28
28
28
29
29
30
30

LIST OF ABBREVIATIONS

2D Two-dimensional3D Three-dimensional

Arp2/3 Actin-related protein 2/3 BSA Bovine serum albumin

Ccdc88b Coiled-coil domain-containing protein 88B

CCL19 C-C motif chemokine ligand 19
CCL21 C-C motif chemokine ligand 21

Cdc42Cell division control protein 42 homologCdk5rap2CDK5 regulatory subunit-associated protein 2

CEP68 Centrosomal protein of 68 kDa
CEP152 Centrosomal protein of 152 kDa
CEP192 Centrosomal protein of 192 kDa

CETN2 Centrin-2

CLASP1 CLIP-associating protein 1
CLASP2 CLIP-associating protein 2

CP110 Centriolar coiled-coil protein of 110 kDa

DA Distal appendage

DAPI 4',6-diamidino-2-phenylindole

DC Dendritic cell

DOCK8 Dedicator of cytokinesis protein 8

DYRK 3 Dual-specificity tyrosine phosphorylation-regulated kinase 3

ECM Extracellular matrix
ER Endoplasmic reticulum

ERES ER exit site

ESCRT III Endosomal sorting complexes required for transport III

FACS Fluorescence-activated cell sorting
FBXW5 F-box/WD repeat-containing protein 5

FCS Fetal calf serum

Flt3l Fms-related tyrosine kinase 3 ligand

FRAP Fluorescence recovery after photobleaching

FRET Förster resonance energy transfer

GFP Green fluorescent protein

GM-CSF Granulocyte macrophage-colony stimulating factor

 γ TuRC γ -tubulin ring complex

HEPES 4-(2-Hydroxyethyl)-1-piperazineethanesulfonic acid

KO Knockout

Lfc Rho guanine nucleotide exchange factor 2

LLPS Liquid-liquid phase separation

LPS Lipopolysaccharide

LRRC45 Leucine-rich repeat-containing protein 45

MIP Microtubule inner protein
MAP Microtubule-associated protein
MEM Minimal essential medium

min Minutes

mRNA Messenger ribonucleic acid

MTOC Microtubule organizing center

mTORC1 Mechanistic target of rapamycin complex 1

Nek2
NPF
Nucleation-promoting factor
Odf2
ODT
Optical diffraction tomography
PBS
Phosphate-buffered saline
PCM
Pericentriolar material

PCM1 Pericentriolar material 1 protein

PCNT Pericentrin

PCR Polymerase chain reaction
PDMS Polydimethylsiloxane
PFA Paraformaldehyde

PMAP Plasma membrane-associated platform

PLK1 Polo-like kinase 1
PLK4 Polo-like kinase 4
RFP Red fluorescent protein
RPE1 Retinal epithelium cells

SAS4 Spindle assembly abnormal protein 4
SAS6 Spindle assembly abnormal protein 6
SCLT1 Sodium channel and clathrin linker 1

SDA Subdistal appendage

SRRM1 Serine/arginine repetitive matrix protein 1 **SRRM2** Serine/arginine repetitive matrix protein 2

STED Stimulated emission depletion WASH WASp and SCAR homolog

WASp Wiskott-Aldrich syndrome protein

WAVE WASp-family verprolin-homologous protein

WT Wildtype

1 Introduction

1.1 CELL MIGRATION

Cell migration is a fundamental mechanism underlying numerous biological processes, such as development, immune responses, wound healing, but also cancer cell dissemination and formation of metastasis (Te Boekhorst *et al.*, 2016). During migration in these multifaceted physiological contexts, cells encounter a variety of complex microenvironments, such as densely packed tissues, blood flow, or extracellular matrix in the interstitium, requiring the ability to adapt to these highly diverse surroundings. Cellular motility has been demonstrated to be affected by various environmental factors, including geometric features such as substrate topology spanning from one-dimensional fibrils to two-dimensional basement membranes and three-dimensional tissues, as well as pore sizes (Wolf *et al.*, 2009; Weigelin *et al.*, 2012; Doyle *et al.*, 2013). Likewise, mechanical properties such as the stiffness and deformability of collagen fibers or the elasticity of the extracellular matrix (ECM), which is also influenced by ECM composition, have been shown to influence migration (DuChez *et al.*, 2019). Gradients of, for instance, chemotactic signaling peptides can serve as navigational cues for cells within these complex environments (Yamada & Sixt, 2019).

1.1.1 CELL MIGRATION MODES

In response to these highly diverse and challenging microenvironments, cells developed a variety of different migratory modes, such as mesenchymal, amoeboid, or lobopodial migration (Yamada & Sixt, 2019).

Mesenchymal migration relies on the polymerization of actin filaments at the protruding cell front pushing the cell membrane outwards, and retrograde actin flow towards the cell rear with concomitant force coupling to extracellular substrates via e.g. focal adhesions (Caswell & Zech, 2018). Focal adhesions transmit actin-generated force in a 'molecular clutch' mechanism (Mitchison & Kirschner, 1988), as they are macromolecular protein assemblies comprising force-transducing proteins like vinculin or talin linking integrin transmembrane receptors, that strongly bind to ECM substrates in the extracellular environment, to the actin cytoskeleton (Doyle et al., 2022). Therefore, focal adhesions act as a pivotal site where tensile forces synchronize the actin cytoskeleton with neighboring matrix fibers, thereby enhancing the efficacy of force propagation and cellular motility (Doyle et al., 2022). As a consequence, mesenchymal cells are generally observed to be more elongated, as their internal actin arrangement frequently adjusts to the characteristics of their surrounding microenvironment (Yamada & Sixt, 2019). Since mesenchymal cells need to detach focal adhesions at the cell rear, this migration mode is rather slow ($\sim \mu m/h$) (Bear & Haugh, 2014). Of note, mesenchymal cells are able to extensively remodel the ECM by proteolytic digestion or pulling on ECM fibers in order to generate or widen pre-existing paths to facilitate their migration (Wolf et al., 2013). Therefore, mesenchymal migrating cells typically display a cell axis configuration, where the nucleus localizes to the cell rear and the centrosome as microtubule organizing center to the front (Fig. 1). This configuration supports vesicular transport towards the cell surface via microtubules originating from the centrosome and facilitates the secretion of proteases required for extracellular matrix degradation (Infante et al., 2018). For instance, this migratory strategy is utilized by neural crest, placodal, and neuronal cells during embryonic development, as these cells necessitate timely and organized migration to reach their specified destination, ensuring undisturbed developmental processes. Additionally, fibroblasts and certain cancer cells also employ this mode of migration (SenGupta *et al.*, 2021).

In contrast to mesenchymal migration, amoeboid migrating cells display a rounded cellular morphology, reduced adhesiveness, and frequent alterations in their cell shape driven by actin protrusions or membrane blebs, indicative of their heightened contractility (Lämmermann & Sixt, 2009). Unlike mesenchymal migrating cells, amoeboid migrating cells move independently of proteolytic degradation of the surrounding ECM (Wolf et al., 2003). Instead, amoeboid migration through narrow ECM pores involves the squeezing or mechanical enlargement of pores within their microenvironment (Gaertner et al., 2022). Therefore, amoeboid migrating cells rather fill existing gaps between ECM fibers with their protrusions (Fig. 1). Additionally, amoeboid migrating cells, such as dendritic cells or T cells, were shown to position their nucleus to the cell front (Renkawitz et al., 2019). Moreover, amoeboid migration is typically faster than mesenchymal migration (~ µm/min), as no remodeling of foal adhesion is required owing to low adhesive and traction forces (Yamada & Sixt, 2019). Forward locomotion is accomplished by exerting traction forces onto the substrate solely through the retrograde forces generated by actin polymerization (Renkawitz et al., 2009). Adhesion-independent force transmission to the substrate is therefore friction-mediated (Bergert et al., 2015). In vertebrates, the amoeboid migration mode is mainly represented by cells of the immune system and primordial germ cells (Yamada & Sixt, 2019).

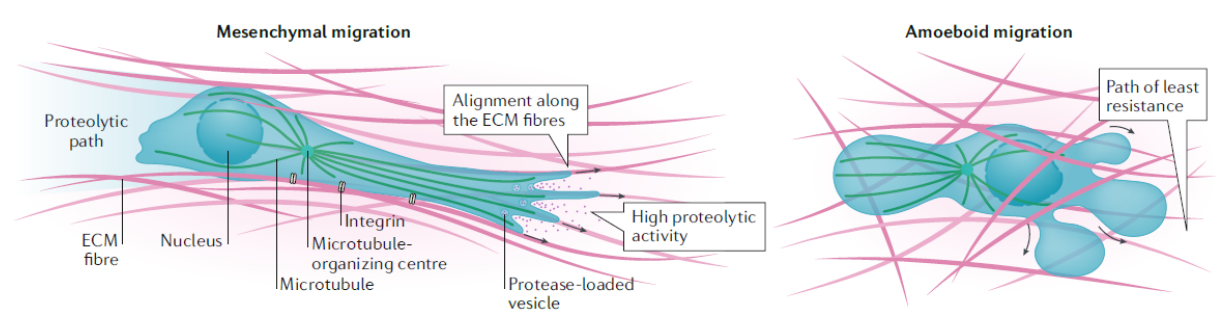


Figure 1: Mesenchymal and amoeboid migration modes. Mesenchymal migration is characterized by strong ECM adhesions and proteolytic ECM degradation. In this mode, the nucleus is located at the rear of the cell, while the centrosome is positioned to the front. In contrast, amoeboid migration is defined by its independence from adhesion and the lack of requirement of proteolytic activity, with the nucleus positioned at the front of the cell. (From Yamada & Sixt, 2019, reproduced with permission of Springer Nature)

More recently, besides mesenchymal and amoeboid migration, lobopodial migration has been identified as an additional migratory mode (Petrie *et al.*, 2014). Lobopodial migration relies on high myosin-II contractility to generate high intracellular hydrostatic pressure pushing the plasma membrane forward. By employing a nuclear piston mode, where the nucleus subdivides the cell in a front and rear compartment, intracellular pressure at the leading edge is increased resulting in the formation of a bleb-like lobopodial cell front (Petrie *et al.*, 2014). In order to facilitate lobopodial migration, a highly confining ECM is a key requirement for this migration mode (Petrie & Yamada, 2016).

Importantly, migrating cells are able to dynamically switch between different migration modes depending on their microenvironmental context. For instance, this migration plasticity can be observed in dendritic cells, where surface-bound CCL21 triggers integrin-mediated adhesive migration, whereas soluble CCL19 leads to non-adhesive migration (Schumann *et al.*, 2010). Of note, switching migration modes is also of relevance in disease context: cancer cells can similarly switch

between adhesive and non-adhesive migration modes, facilitating microenvironmental adaption and favoring the formation of metastasis (Petrie & Yamada, 2016; Te Boekhorst *et al.*, 2016).

1.1.2 IMMUNE CELL MIGRATION

In comparison to organismal development, rapidly moving leukocytes (white blood cells) during innate and adaptive immune responses often do not require precise migration accuracy owing to the significant numbers of cells engaged in the inflammatory response and the transient nature of this response (Yamada & Sixt, 2019). Yet, leukocytes evolved mechanisms to migrate efficiently, as this is essential for the induction, maintenance, and modulation of immune responses (Kameritsch & Renkawitz, 2020). Accordingly, impairment of leukocyte migration can lead to immunodeficiencies, autoimmunity, and inflammation (Badolato, 2013; Worbs *et al.*, 2017). On their way, leukocytes encounter diverse microenvironments of different composition resulting in various chemical and physical properties. For instance, leukocytes migrate from bone marrow into the blood circulation or lymph vessels, and transmigrate into tissues either to fulfill their function for tissue surveillance or upon inflammatory stimuli (Lämmermann & Germain, 2014; Weninger *et al.*, 2014). These challenging environments require adaptation to their microenvironments, as the cells face liquid flow within the vasculature systems of blood and lymph, squeeze through pores during transmigration and interstitial migration, and navigate in complex tissue microenvironments following different guidance cues (Kameritsch & Renkawitz, 2020).

Upon activation by pro-inflammatory stimuli, macrophages often employ a mesenchymal migration mode that is accompanied by proteolytic digestion of the surrounding ECM to facilitate tissue infiltration (van Goethem et al., 2010). Polymorphonuclear leukocytes (neutrophils) employ a crawling migration mode, closely resembling mesenchymal migration when encountering flow as it requires the establishment of focal adhesions to withstand shear forces (Lämmermann & Sixt, 2009). Similarly, a crawling mode can be observed for dendritic cells migrating in lymphatic capillaries, where they encounter slower flow velocities compared to those in the blood stream (Russo et al., 2016). Upon transmigration through the endothelial barrier, leukocytes undergo a switch in their migratory mode towards amoeboid migration through the interstitium. Here, immune cells encounter pores that are significantly smaller than their own diameter (Weigelin et al., 2012; Wolf et al., 2013). In order to facilitate migration through these microenvironmental barriers, leukocytes possess the ability to undergo extreme deformation of their cellular body. However, the nucleus, as the largest and stiffest organelle, represents a particular challenge during migration in complex 3D microenvironments. Extreme nuclear squeezing can lead to rupturing of the nuclear envelope resulting in chromatin leaking into the cytoplasm and eventually apoptosis (Denais et al., 2016; Irianto et al., 2017). To prevent this, the nuclear envelope is resealed by components of the repair machinery ESCRT III (Denais et al., 2016; Raab et al., 2016). Therefore, cells have developed different mechanisms to avoid nuclear damage. For instance, neutrophils reduce the nuclear stiffness by downregulation of A-type lamins, which constitute a major component of the nuclear lamina and confer mechanical stiffness (Friedl et al., 2011). Additionally, cells have evolved mechanisms to sense and avoid mechanical stress during migration. Cellular confinement below a certain threshold, determined by the nuclear envelope's stretch capacity, increases cell contractility through stretch-sensitive protein signaling, thereby causing a partial retraction out of the confining microenvironment (Lomakin et al., 2020; Venturini et al., 2020). When leukocytes migrate through complex environments, they typically explore multiple pores simultaneously at the same time by formation of multiple cellular and nuclear protrusions, resulting in highly dynamic and complex cell shapes (Kameritsch & Renkawitz, 2020). During this process, they use their nucleus as a mechanical gauge to probe for the pore (and path) of least resistance, which therefore also poses the lowest risk for nuclear envelope rupture (Renkawitz *et al.*, 2019). Recent findings indicate that amoeboid migrating cells, such as dendritic cells and T cells, are capable of integrating competing chemical chemokine and mechanical pore size cues to make efficient cellular pathfinding decisions, primarily through nuclear repositioning, a phenomenon also referred to as nucleokinesis (Kroll *et al.*, 2023). Such chemical guidance cues, like the chemotactic proteins CCL19 and CCL21 in the case of dendritic cells, or fMLP guiding neutrophils to inflammatory sites, are required to facilitate efficient migration through complex microenvironments, and are detected by multiple exploratory protrusions undergoing continuous cycles of formation and retraction (Worbs *et al.*, 2017; Lämmermann & Kastenmüller, 2019; Bodor *et al.*, 2020).

1.1.3 CELL SHAPE COORDINATION DURING MIGRATION

How do cells move and coordinate their cell body? Different cytoskeletal components are implicated in this complex process. The fundamental mechanism driving force generation involves actin polymerization at the leading edge of the cell and myosin-mediated contraction at the trailing edge, with extracellular substrate coupling primarily mediated by integrins or cadherins (Yamada & Sixt, 2019). Yet, actomyosin forces are essential not only for cellular forward locomotion but also for navigation through complex microenvironments and cell shape coordination. In neutrophils and immature dendritic cells, actomyosin forces are required for nuclear squeezing through perinuclear Arp2/3-driven actin polymerization, thus enabling nuclear deformation upon migration through complex microenvironments (Thiam et al., 2016). Mesenchymal cells coordinate distant cellular parts, therefore their shape, using actin stress fibers connecting focal adhesions in their protrusions (Cai & Sheetz, 2009). In contrast, amoeboid migrating neutrophils and dendritic cells employ thin veil-like structures that form rosettes at their protruding and are filled with branched F-actin. Impairment of branched F-actin nucleation by inhibition of the Arp2/3 complex or WAVE complex reduces these veil formations (Leithner et al., 2016; Fritz-Laylin et al., 2017). Although forward migration per se is not affected, cells without veils show reduced cellular turning and impaired chemokine sensing, further highlighting the importance of the actin cytoskeleton during shape coordination and navigation (Leithner et al., 2016; Fritz-Laylin et al., 2017). Furthermore, dendritic cells display cell shape alterations and migratory defects upon mutations of DOCK8, an upstream regulator of the small GTPase Cdc42 (Lämmermann et al., 2009; Harada et al., 2012). Similarly, deletion of the small GTPase Cdc42 in dendritic cells (DCs) leads to cellular entanglement in complex 3D microenvironments owing to the spatial and temporal dysregulation of protrusion dynamics resulting in impaired coordination of their leading edge (Lämmermann et al., 2009).

In addition, the microtubule cytoskeleton is often implicated in coordinative processes. For instance, in dendritic cells, microtubule depolymerization in losing protrusions leads to the local release of the RhoA exchange factor Lfc and therefore RhoA-controlled actomyosin contractility facilitating protrusion retraction. Loss of Lfc function results in cellular entanglement and cell fragmentation (Kopf *et al.*, 2020). Altogether, these discoveries indicate that the coordination of cell shape is an intricate process that involves the interaction of numerous signaling pathways and cytoskeletal components.

1.2 THE CENTROSOME

1.2.1 ARCHITECTURE OF THE CENTROSOME

Centrosomes are non-membrane bound organelles and consist of two interconnected centrioles and a surrounding protein matrix called pericentriolar material (PCM) (Fig. 2). Each individual centriole has an approximate length of 500 nm and a diameter of 200 nm and is composed of nine microtubule triplets (Fig. 2A). These microtubule triplets are arranged in a radial ninefold symmetry and display a proximal-distal polarity along their axis (Bornens, 2002; Li et al., 2012; Greenan et al., 2018). In each microtubule triplet, the innermost tubule is called A-tubule, followed by the so-called B-tubule and the outermost C-tubule. Towards the distal end, the centriole is composed of A-tubule/B-tubule doublets (Bettencourt-Dias & Glover, 2007). Consecutive microtubule triplets are interconnected via an A-C linker connecting the A-tubule of one triplet with the Ctubule of the adjacent microtubule blade (Fig. 2A) (Guichard et al., 2013; Li et al., 2019). A cartwheel ring with spokes located at the proximal centriole end serves as a centriole scaffold and is mainly composed of Spindle assembly abnormal protein 6 homolog (SAS6) as the major component (Nakazawa et al., 2007). Via pinhead structures, the microtubules are attached to the spokes of the cartwheel ring (Gönczy, 2012; Guichard et al., 2013; Nazarov et al., 2020). Centriolar microtubules are the target of several posttranslational modifications, such as polyglutamylation of tubulin (Janke et al., 2005; Gadadhar et al., 2017), and are presumably further stabilized by different microtubule inner proteins (MIPs) and microtubule-associated proteins (MAPs) (Li et al., 2012; Greenan et al., 2018), thereby promoting the required stability for conservative centriole formation (Kochanski & Borisy, 1990). Importantly, the two centrioles within one cell are not identical but are instead differentiated as mother and daughter centrioles, reflecting their formation during different cycles of cell division (Kuriyama & Borisy, 1981). The older mother centriole is decorated with appendages that are further classified into distal appendages (DAs) and subdistal appendages (SDAs) based on their localization (Fig. 2B). While DAs are crucial for ciliogenesis, SDAs are mainly implicated in microtubule anchoring during interphase (Delgehyr et al., 2005; Tanos et al., 2013). For instance, the microtubule anchoring protein Ninein is a SDA component interconnecting the centriole via its C-terminal domain and the γ -tubulin ring complex (γ TuRC) via its N-terminal domain (Delgehyr et al., 2005).

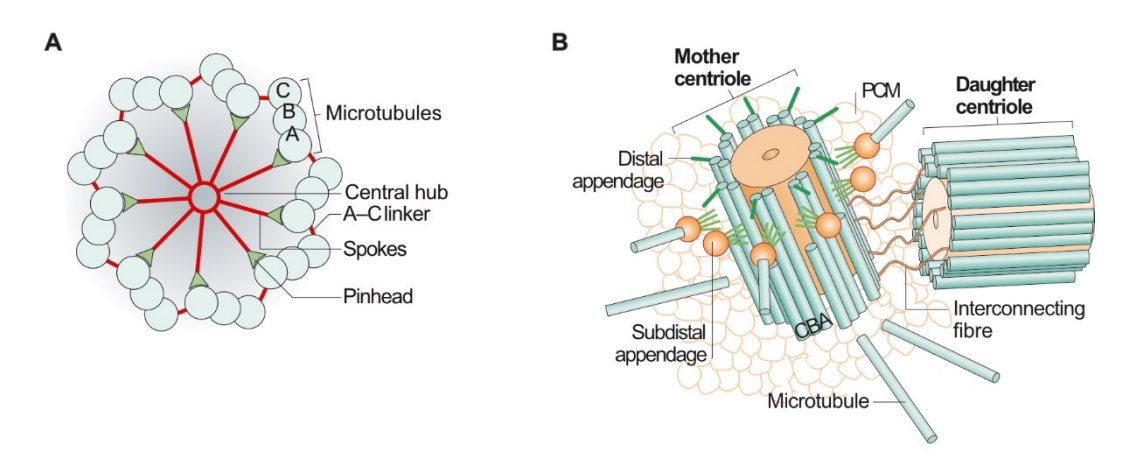


Figure 2: Centrosome structure. (A) Schematic view of the cross-section of the centriolar cartwheel structure. A-, B-, and C-microtubules are arranged in a radial ninefold symmetry. (From Gönczy, 2012, reproduced with permission from Springer Nature) **(B)** Schematic view of mother and daughter centrioles that are connected via protein fibers and surrounded by the proteinaceous pericentriolar material (PCM). The inner, middle, and outer microtubules of microtubule triplets are designated as A, B, and C. Note, that distal and subdistal appendages are only present at the mother centriole. (From Bettencourt-Dias & Glover, 2007, reproduced with permission from Springer Nature)

During interphase, the two centrioles are tightly connected via two simultaneous linker mechanisms. Most well-known is the non-covalent protein-based filamentous linker directly interconnecting the two centrioles. As revealed by STED super-resolution microscopy, the protein linker is an interwoven network of Rootletin and CEP68 forming filamentous structures that are attached to the proximal ends of centrioles via the adaptor protein C-Nap1 (Fry et al., 1998; Mayor et al., 2000; Bahe et al., 2005; Graser et al., 2007; Vlijm et al., 2018). More recently, other proteins such as LRRC45 or CEP215 (also known as Cdk5rap2) were described to be implicated in centriole connectivity (Graser et al., 2007; He et al., 2013). CEP215 was identified in a siRNA screen aiming at uncovering novel proteins implicated in centrosome cohesion (Graser et al., 2007). While being unaffected by depletion of the main linker components Rootletin, CEP68 or C-Nap1, the localization of CEP215 to the centrosome is strongly dependent on Pericentrin (Graser et al., 2007). LLRC45 was shown to locate between the two centrioles and form filamentous structures similar to Rootletin, where it also interacts with C-Nap1 and Rootletin. Upon phosphorylation by Nek2A during mitosis, LRRC45 dissociates from the centrosome. As depletion of LRRC45 results in premature centrosome splitting during G1 and G2 phases, LRRC45 is considered a critical component of the proteinaceous centrosome linker (He et al., 2013). How exactly this filament network provides centrosome cohesion remains elusive, although different models have been proposed, as eventually the weak multivalent interactions between the filamentous structures could be the basis of linker-based connectivity (Dang & Schiebel, 2022). Alternatively, liquid droplets of C-Nap1 arising via liquid-liquid phase separation at the proximal ends of the centrioles were suggested to connect the centrosomes (Mahen, 2022). However, the importance of different linker components contributing to centrosome connectivity seems to differ between different cell types (Theile et al., 2023). At the onset of mitosis, this linker is disassembled by Never in mitosis-related kinase 2 (Nek2) and Polo-like kinase 1 (PLK1) (Fry et al., 1998; Bahe et al., 2005).

In addition, a second centrosomal linker mechanism relies on microtubule-based connectivity. Based on the notion that C-Nap1 depleted RPE1 cells lacking a functional protein linker only show a modest increase in centriolar distance and no chromosome segregation defects, an additional microtubule-based linker was proposed (Panic et al., 2015). This was further supported by increased centriole separation upon alterations of microtubule dynamics by treatment with the microtubule depolymerizing agent nocodazole or the microtubule stabilizer taxol (Meraldi & Nigg, 2001). During mitosis, centrioles are separated by the tetrameric plus-end directed kinesin Eg5 generating an outward pushing force by crosslinking and sliding antiparallel microtubules apart (Kapitein et al., 2005). This outward pushing force is counteracted by the minus-end directed kinesin-14 KIF3C providing a cohesive force by pulling the centrosomes together (Hata et al., 2019). Therefore, knockdown or expression of mutated KIF3C without catalytic motor function further increases the cohesion defect of C-Nap1 depleted cells lacking a functional protein linker (Hata et al., 2019). For microtubule-based centrosome connectivity, KIF3C as a component of mother centriolar SDAs relies on the microtubule network emanating from the SDAs as well as the daughter centriolar PCM microtubule network for efficient microtubule crosslinking and antiparallel microtubule sliding (Hata et al., 2019). This microtubule-dependent mechanism becomes especially important during mitosis, when the Rootletin-based linker is disassembled via Nek2 and PLK1 (Fry et al., 1998; Bahe et al., 2005), and Eg5-driven outward pushing force needs to be counteracted to ensure precisely timed spindle body formation (Sawin et al., 1992; Blangy et al., 1995; Kapitein et al., 2005; Hata et al., 2019).

As mentioned, the two centrioles are surrounded by an electron-dense, proteinaceous matrix composed of hundreds of proteins called PCM, functioning as a key structure for the nucleation

and anchorage of microtubules (Fig. 2B). Due to its membraneless nature, the assembly and function of pericentriolar material depend on the localized concentration and organization of its components. These components are notably rich in disordered and coiled-coil domains, which increase their propensity for the self-interactions necessary for PCM scaffold assembly (Nido $et\ al.$, 2012). The inner PCM layer is composed of coiled-coil scaffolding proteins like CEP192, CEP152, and Pericentrin forming elongated fibrillar structures with their N-terminal ends that localize in the outer PCM layer, providing a scaffold for outer layer proteins. The outer PCM layer is composed of regulatory and microtubule nucleating proteins such as γ -tubulin and CEP215 (Lawo $et\ al.$, 2012; Mennella $et\ al.$, 2012; Sonnen $et\ al.$, 2012). As the cell prepares for mitosis, the PCM expands and increases its microtubule nucleating capacity, a process known as centrosome maturation (Cabral $et\ al.$, 2019).

1.2.2 THE CENTROSOME CYCLE

In cycling cells undergoing mitosis, centrosome duplication is a tightly controlled process, as each centriole has to duplicate exactly once per cell cycle and form a new daughter centriole that is attached to the already pre-existing one. In general, the centrosome duplication cycle can be described as four consecutive steps: I) daughter centriolar formation, which are also termed procentrioles before they acquire their full centriolar length, II) procentriole elongation, III) centrosome maturation and separation, and IV) centriole disengagement (Fig. 3) (Kuriyama & Borisy, 1981).

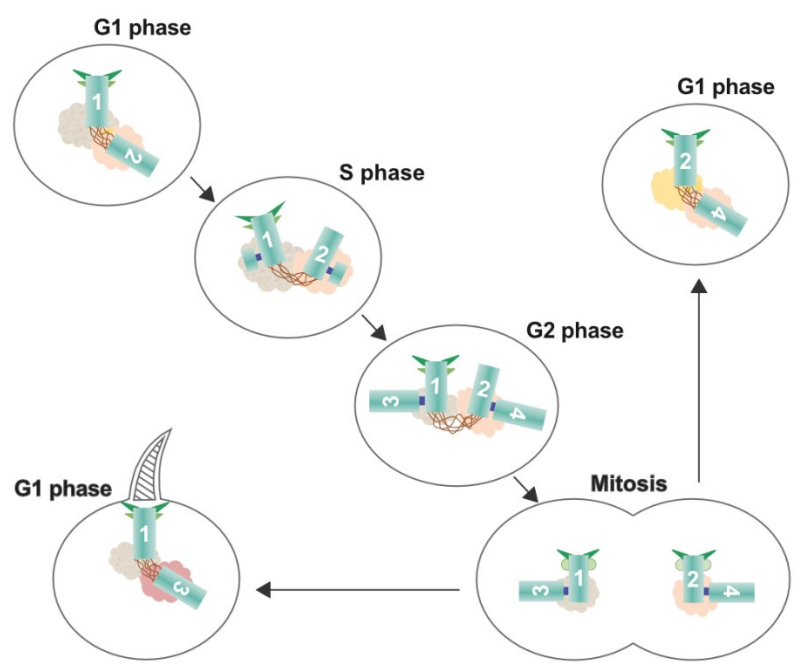


Figure 3: The centrosome duplication cycle. Schematic view of centrioles (cyan), distal and subdistal appendages (green), and surrounding PCM (grey, yellow, and pink). Note, that the proteinaceous linker (brown) is absent during mitosis, whereas the tether linking procentriole and parental centriole (dark blue) is disassembled upon re-entry into G1 phase. Numbers ranging from 1-4 indicate centriole origin for easier traceability. (From Nigg & Stearns, 2011, modified with permission from Springer Nature)

During the cell cycle, centriole duplication is initiated at the transition from G1 to S phase by the nucleation of a newly formed procentriole attached to each pre-existing centriole in a perpendicular configuration (Fig. 3). This process is controlled by Polo-like kinase 4 (PLK4)-dependent recruitment of the cartwheel component SAS6 (Nakazawa *et al.*, 2007; Park *et al.*, 2019), presumably

via phosphorylation and inactivation of the E3-ubiquitin ligase SCF-FBXW5 by PLK4, thus stabilizing SAS6 at the centrioles (Puklowski et al., 2011). Interestingly, one critical parameter of centriole duplication is PLK4 activity itself, as overexpression of PLK4 results in supernumerary centrioles, in contrast to reduced centriole numbers upon PLK4 depletion or inhibition (Habedanck et al., 2005). Therefore, PLK4 levels are tightly controlled through ubiquitination-dependent degradation via SCFβTrCP (Cunha-Ferreira et al., 2009; Guderian et al., 2010). Following nucleation, procentrioles elongate during S and G2 phases in a process that is dependent on several proteins, such as SAS4, POC5, OFD1, and CP110 (Azimzadeh et al., 2009; Schmidt et al., 2009; Tang et al., 2009; Singla et al., 2010). In addition, former daughter centrioles acquire their DAs and SDAs reaching full centriolar maturation one and a half centrosome cycles after their initial nucleation (Nigg & Stearns, 2011). At the G2 to M phase transition, the two centrosomes mature by PCM expansion and separate to form the spindle poles (Fig. 3). The expansion of pericentriolar material, favoring an increased microtubule nucleation capacity required for mitosis, depends on PLK1 activity triggering a positive feedback loop promoting PCM expansion around the mother centrioles (Lane & Nigg, 1996; Woodruff et al., 2015; Alvarez-Rodrigo et al., 2019). Since it is suggested that the PCM arises from liquid-liquid phase separation, further studies indicate that this might happen via an autocatalytic condensation process (Zwicker et al., 2014; Tiwary & Zheng, 2019). For the formation of the spindle poles, the two centrosomes separate upon dissociation of the Rootletinbased protein linker by Nek2 and PLK1 (Fry et al., 1998; Bahe et al., 2005). Finally, during mitotic exit or early G1 phase, centriole disengagement takes place (Fig. 3). Centriole disengagement, a crucial final step in centriole duplication, involves the PLK1- and separase-mediated dissolution of the linker that tethers the newly formed daughter centriole to its parental centriole during mitosis. This process is essential for centrosomal licensing, thereby enabling another round of centriole duplication (Tsou & Stearns, 2006; Tsou et al., 2009; Agircan et al., 2014). Importantly, one has to note that this tether is fundamentally different from the above-described Rootletin-based linker that ensures centrosome cohesion and centrosome function as a singular MTOC.

1.2.3 CENTROSOME FUNCTION

One of the most well-known functions of the centrosome is its central role in organizing microtubule arrays as a microtubule organizing center (MTOC). The different proteins that are locally concentrated in the PCM facilitate the nucleation, anchorage, and release of microtubules. One of them, y-tubulin as part of the y-TuRC is a key molecular player of microtubule nucleation (Zheng et al., 1995). However, further studies have shown that multiple additional factors, typically also residing at the centrosome, are able to regulate the γ-TuRC microtubule-nucleating activity (Petry & Vale, 2015). In its role as MTOC, the centrosome is needed for organelle positioning, ranging from the nucleus to endosomes, or functions as a signaling hub during DNA damage response, as well as organizes actin filaments (Conduit et al., 2015; Farina et al., 2016; Mullee & Morrison, 2016; Kroll & Renkawitz, 2024). Of note, the centrosome does not represent the only microtubule organizing center, as the Golgi apparatus functions as a second major MTOC in mammalian cells, including the ability to nucleate and anchor microtubules (Chabin-Brion et al., 2001). For instance, retinal epithelium cells (RPE1 cells) nucleate nearly half of their microtubules from the Golgi apparatus (Efimov et al., 2007). Often, Golgi membranes in mammalian cells are localized to the centrosome via dynein-mediated transport, and microtubules nucleated from the Golgi apparatus were shown to help organizing Golgi stacks after mitosis (Corthésy-Theulaz et al., 1992; Miller et al., 2009). In addition, microtubule nucleation from the nuclear envelope can be observed in some differentiated cell types like muscle cells (Petry & Vale, 2015).

Besides its role as a microtubule organizing center, the centrosome is essential for the formation of flagella and cilia, where it is needed to form the basal body (Bettencourt-Dias & Glover, 2007). Interestingly, in vertebrates, only the mother centriole carrying the distal appendages can give rise to cilia, as deletion of the appendage marker Odf2 and subsequent DA depletion resulted in centrioles that could not form cilia (Vorobjev & Chentsov, 1982; Ishikawa *et al.*, 2005). Defects in ciliogenesis can give rise to different diseases such as the Bardet-Biedl syndrome, which is characterized by retinal degeneration, chronic kidney cysts, and obesity amongst others (Badano *et al.*, 2005). Similarly, Alstrom syndrome, which is accompanied by retinitis pigmentosa and perceptive deafness, is associated with deficient ciliogenesis (Badano *et al.*, 2005).

Typically, centrosomes form the spindle poles during mitosis. Interestingly, they were shown to be not essential for spindle formation, as spindles can be nucleated by chromosomes (Khodjakov & Rieder, 2001; Uetake *et al.*, 2007), and are generally absent during female meiosis (So *et al.*, 2022). However, the importance of centrosomes for the formation of spindle poles seems to highly vary between different species and among different cell types, as sometimes mitotic fidelity and spindle orientation depend on centrosomes and centrosome loss can lead to G1 arrest (Hinchcliffe *et al.*, 2001; Khodjakov & Rieder, 2001). Of note, dysregulated centrosome structure and numbers are frequently observed in many human cancers (Remo *et al.*, 2020). For instance, mutations of the centrosome linker protein Rootletin found in aggressive colorectal cancer subtypes are associated with mitotic errors and chromosome instability (Remo *et al.*, 2018). Furthermore, excess centrosomes are frequently found in cancer cells (Godinho *et al.*, 2009). Although cells evolved coping mechanisms to ensure efficient chromosome segregation to two spindle poles by clustering of supernumerary centrosomes as pseudo-bipolar spindle, impairment of this process gives rise to multipolar anaphase spindles resulting in chromosome mis-segregation and apoptosis (Godinho *et al.*, 2009).

1.3 THE PROTEIN KINASE DYRK3

1.3.1 DYRK KINASES

The members of the DYRK ('dual-specificity tyrosine (Y) phosphorylation-regulated kinase') protein kinase family are best characterized by their ability to recognize and phosphorylate tyrosine as well as serine and threonine residues of their substrate (Becker *et al.*, 1998). For activation, DYRKs do not depend on external phosphorylation by other protein kinases but obtain full catalytic activity through autophosphorylation of the second tyrosine residue of a conserved YxY motif in their activation loop (Kim *et al.*, 2018). In mammals, the five DYRKs can be categorized into class I (Dyrk1a and Dyrk1b) mainly localizing to the nucleus, and class II (Dyrk2, Dyrk3, and Dyrk4) with a predominantly cytosolic localization (Zhang *et al.*, 2005; Aranda *et al.*, 2011). The class I DYRKs Dyrk1a and Dyrk1b are mainly associated with negative cell cycle regulation, but also with DNA damage repair, transcriptional control, and splicing (Di Vona *et al.*, 2015; Lu *et al.*, 2018; Guard *et al.*, 2019; Menon *et al.*, 2019; Dong *et al.*, 2020). While the class II DYRK Dyrk2 is also implicated with cell cycle control (Taira *et al.*, 2007; Pérez *et al.*, 2012; Taira *et al.*, 2012), Dyrk3 plays a role in various contexts (Wippich *et al.*, 2013; Rai *et al.*, 2018; Mediani *et al.*, 2021; Gallo *et al.*, 2023; Ramella *et al.*, 2024), and little is known about the function of Dyrk4 (Aranda *et al.*, 2011).

1.3.2 DYRK3 FUNCTION

Dyrk3 plays an important role in many processes. During cellular stress responses, such as oxidative stress, heat, virus infection, or osmotic stress, mRNAs can be transcriptionally silenced and accumulate in so-called stress granules (Anderson & Kedersha, 2008, 2009; Buchan & Parker, 2009; Kedersha et al., 2013). These stress granules are cytoplasmic aggregates of RNAs as well as different proteins, and compartmentalize via liquid phase separation (Hyman & Simons, 2012; Kato et al., 2012), meaning without a surrounding membrane, and are therefore also classified as membraneless organelles. Liquid phase separation is driven by weak multivalent interactions and intrinsically disordered protein domains (Brangwynne, 2013; Banani et al., 2017; Shin & Brangwynne, 2017). Under normal conditions, Dyrk3 is able to dynamically cycle between stress granules and the cytosol via its N-terminal low complexity domain and its kinase activity. When Dyrk3 is inactive, the dissolution of stress granules is prevented and also mTORC1 is sequestered in stress granules, thereby abolishing mTORC1 signaling (Takahara & Maeda, 2012; Wippich et al., 2013). In contrast, upon Dyrk3 activation, mTORC1 activity is promoted by stress granule dissolution and subsequent mTORC1 release, as well as via direct phosphorylation and inactivation of the negative mTORC regulator PRAS40 by Dyrk3 (Vander Haar et al., 2007; Wippich et al., 2013). Consequently, Dyrk3 regulates stress granule stability and therefore also mTORC1 signaling (Wippich et al., 2013).

Interestingly, Dyrk3 was shown to be bound and stabilized by the molecular chaperone Hsp90 while being available in the cytosol, in agreement with previous studies identifying Hsp90 alpha (HSP90AA1) and Hsp90 beta (HSP90AB1) as Dyrk3 interactors (Wippich *et al.*, 2013; Mediani *et al.*, 2021). Inhibition of Hsp90 ATPase activity results in Dyrk3 inactivation and subsequent degradation via the 26S proteasome (Mediani *et al.*, 2021). However, localization to biomolecular condensates such as stress granules or mitotic SC35 bodies protects Dyrk3 from degradation upon Hsp90 inhibition, albeit leading to aggregation of inactive Dyrk3 within the condensates (Mediani *et al.*, 2021). Under steady-state conditions, Hsp90 interacts with Dyrk3 at the boundaries or outside of such condensates, presumably to facilitate Dyrk3 activation and therefore condensate disassembly (Mediani *et al.*, 2021).

Furthermore, Dyrk3 interacts with ER exit site (ERES) proteins, thereby regulating the integrity and biophysical properties of ERESs by maintaining a liquid-like state of SEC16A that is essential for ERES function (Gallo *et al.*, 2023). ERES formation is driven by SEC16A phase separation (Watson *et al.*, 2006; Bhattacharyya & Glick, 2007; Hughes *et al.*, 2009), forming liquid droplets on the ER surface. Short-term inhibition of Dyrk3 for one hour results in ER growth, while prolonged inhibition of Dyrk3 for three hours or more leads to an overall disappearance of ERES, which is accompanied by mislocalization of ERES proteins to the perinuclear region (Gallo *et al.*, 2023). This mislocalization can be attributed to the severe defects in organization and protein trafficking through the early secretory pathway, as Dyrk3 inhibition disrupts the ER-Golgi interface. Secretory trafficking depends on the liquid-like state of SEC16A maintained by Dyrk3, as efficient cargo trafficking is impaired by modulating the material properties of ERESs to a more gel-like state (Gallo *et al.*, 2023).

Besides maintaining a proper RNA and protein homeostasis, Dyrk3 is also implicated in the regulation of migration of breast cancer cells *in vitro* (Ramella *et al.*, 2024). In these mesenchymal migrating cells, alterations of Dyrk3 levels result in reduced migration and decreased invasiveness. While rendering Dyrk3 non-functional only leads to reduced migration in otherwise unaffected breast cancer cells, overexpression of Dyrk3 is also accompanied by reduced lamellipodial stabil-

ity caused by disturbed plasma membrane-associated platform (PMAP) protein localization (Ramella et~al., 2024). PMAPs are dynamic assemblies of scaffold proteins including ERC1 and Liprin- $\alpha 1$ forming near integrin-mediated focal adhesions or invadosomes at the cell front of migrating cells and supporting cell motility (Astro et~al., 2014; Astro & Curtis, 2015; Sala et~al., 2018). The overexpression of Dyrk3 leads to increased phosphorylation and therefore inhibition of Liprin- $\alpha 1$, thereby impairing PMAP formation and subsequently the stability of focal adhesions and lamellipodia (Ramella et~al., 2024).

Importantly, Dyrk3 is not only important for cell homeostasis during interphase, but also plays a crucial role during mitosis where it acts as an essential dissolvase for multiple membraneless organelles (Rai et al., 2018). Such membraneless organelles like splicing speckles, P-bodies, or Cajal bodies, amongst others, are known to disappear during cell division, independently from whether their localization is cytosolic or nuclear (Spector & Smith, 1986; Dammermann & Merdes, 2002; Sivan et al., 2007). In addition, the formation of some membraneless organelles like stress granules cannot be initiated upon cell entry into mitosis (Sivan et al., 2007). Though, inhibition of Dyrk3 in mitotic cells was shown to prevent the dissolution of splicing speckles or stress granules, resulting in the formation of aberrant hybrid-like aggregates that consist of a mixture of different membraneless organelles as well as RNA and inhibited Dyrk3 itself (Rai et al., 2018). In contrast, the dissolution of P-bodies, Cajal bodies, and nucleoli remains unaffected by Dyrk3 inhibition. The formation of these hybrid structures is accompanied by a delay or even mitotic arrest, as not only multipolar spindles arise from gamma-tubulin foci, but also mitotic regulators are sequestered in the liquid unmixed compartments (Rai et al., 2018). The underlying mechanism of Dyrk3-induced dissolution of membraneless organelles is threshold-based and driven by a tightly controlled Dyrk3-to-substrate ratio, as the breakdown of the nuclear envelope at the onset of mitosis leads to an intracellular dilution of Dyrk3 substrates, thereby favoring a higher kinase-to-substrate ratio. Similarly, overexpression of Dyrk3 in interphase cells leads to condensate dissolution of nonmitotic cells in a kinase-activity-dependent manner. In order to facilitate recondensation at the end of mitosis, Dyrk3 ubiquitination and subsequent degradation is mediated by the anaphasepromoting complex/cyclosome (APC/C) (Merbl & Kirschner, 2009; Rai et al., 2018).

Overall, the importance of Dyrk3 as a phase condensate dissolvase for maintaining cellular functionality under homeostasis during interphase, as well as during mitosis and cellular stress, has been highlighted in various aspects. While a role for Dyrk3 in the migration of adhesive cancer cells has recently been discovered, it remains elusive whether Dyrk3 also plays a more general role in cell migration.

1.4 AIMS OF THE THESIS

Fast-migrating amoeboid cells like immune cells show frequent and highly dynamic shape changes while migrating through complex microenvironments of heterogenous composition (Lämmermann & Sixt, 2009). Efficiently navigating these complex environments necessitates the sensing and processing of different guidance cues (Kameritsch & Renkawitz, 2020). Therefore, amoeboid migrating cells typically generate multiple exploratory protrusions simultaneously, which undergo frequent cycles of protrusion formation and retraction. The mechanisms by which amoeboid cells coordinate these dynamic shape changes are becoming increasingly clear (Lämmermann *et al.*, 2009; Harada *et al.*, 2012; Leithner *et al.*, 2016; Fritz-Laylin *et al.*, 2017; Kopf *et al.*, 2020). The centrosome represents one major orchestrator of cellular coordination, as it functions as a primary microtubule organizing center in many mammalian cells, nucleating and anchoring microtubules (Bettencourt-Dias & Glover, 2007). Yet, how membraneless organelles such

as the centrosome withstand extra- and intracellular forces exerted by the surrounding microenvironment itself as well as by dynamic cell shape changes, thereby compressing and bending microtubules, has remained elusive.

In order to address this knowledge gap, I employed dendritic cells expressing Centrin2-GFP (CETN2-GFP) as centriole marker to characterize centrosomal dynamics during dendritic cell migration in microenvironments of varying complexity. To further elucidate the mechanisms underlying the maintenance of centrosome cohesion upon mechanical forces, transcriptome analysis of dendritic cells migrating in collagen matrices of increasing complexity was performed. This revealed that the dual-specificity tyrosine phosphorylation-regulated kinase 3 (Dyrk3) is upregulated in response to increasing microenvironmental complexity. Using pharmacological inhibitors and expression of a dominant-negative kinase-dead point mutant of Dyrk3 (K218M), I investigated the role of Dyrk3 for immune cell motility by impairing Dyrk3 function (Wippich et al., 2013; Rai et al., 2018). Rendering Dyrk3 non-functional resulted in decreased centrosomal stability, ultimately leading to centrosome fracturing and reduced migration velocities in complex microenvironments. To broaden these findings, I additionally utilized a Hoxb8 cell line depleted of a centriolar linker component to validate the impact of microenvironment-dependent mechanical stress on centrosome stability. Furthermore, I employed various pharmacological inhibitors such as Latrunculin A for actin polymerization and para-nitroblebbistatin for myosin-II contractility to identify the underlying mechanism of intracellular force generation acting on the centrosome. By performing immunofluorescence staining of different MTOC components including α-tubulin, γtubulin, or ninein, I elucidated the impact of centrosome fracturing on centrosome-dependent microtubule-organizing center (MTOC) organization. Finally, to further explore the functional consequences of centrosome fracturing on cellular pathfinding, I utilized fluorescently labeled Hoxb8 cell lines in diverse microenvironments to investigate cellular polarity, coordination, and decision-making processes upon centrosome fracturing.

2 MATERIAL AND METHODS

2.1 MATERIAL

2.1.1 Media, buffers, and reagents

Table 1: Media and buffers.

Media and buffers	Supplementing Reagents	Supplier (Cat. #)
R10 medium	RPMI1640	Gibco (21875091)
	10 % FCS (v/v)	Gibco (10270098)
	100 U/ml penicillin	Sigma-Aldrich (P0781)
	100 mg/ml streptomycin	Sigma-Aldrich (P0781)
	0.1 mM 2-mercaptoethanol	Gibco (31350010)
R20 medium	RPMI1640, phenol-free	Gibco (11835105)
	20 % FCS (v/v)	Gibco (10270098)
	100 U/ml penicillin	Sigma-Aldrich (P0781)
	100 mg/ml streptomycin	Sigma-Aldrich (P0781)
	0.1 mM 2-mercaptoethanol	Gibco (31350010)
LX-293 medium	DMEM (low glucose)	Gibco (31885)
	10 % FCS (v/v)	Gibco (10270098)
	100 U/ml penicillin	Sigma-Aldrich (P0781)
	100 mg/ml streptomycin	Sigma-Aldrich (P0781)
	0.1 mM 2-mercaptoethanol	Gibco (31350010)
Freezing medium	90 % FCS (v/v)	Gibco (10270098)
	10 % DMSO (v/v)	Fisher Scientific (10397841)
Imaging medium	RPMI1640, phenol-free	Gibco (11835105)
	10 % FCS (v/v)	Gibco (10270098)
	100 U/ml penicillin	Sigma-Aldrich (P0781)
	100 mg/ml streptomycin	Sigma-Aldrich (P0781)
	0.1 mM 2-mercaptoethanol	Gibco (31350010)
	50 μM L-ascorbic acid	Sigma-Aldrich (A92902)
FACS buffer	1x PBS	Pharmacy LMU Hospital
	1 % bovine serum albumin (BSA) (w/v)	AppliChem GmbH (A1391)
	2 mM EDTA	Sigma-Aldrich (EDS-500g)
Cell sorting buffer	1x PBS	Pharmacy LMU Hospital
	0.5 % BSA (w/v)	AppliChem GmbH (A1391)
	2 mM EDTA	Sigma-Aldrich (EDS-500g)
	25 mM HEPES	Gibco (15630056)
1x SAPO	1x PBS	Pharmacy LMU Hospital
	0.2 % BSA (w/v)	AppliChem GmbH (A1391)
	0.05 % saponin	Sigma-Aldrich (SAE0073)
Microtubule stabilizing	80 mM K-PIPES, pH 6.8	Thermo Fisher (J60300.AK)
buffer (MTSB)	1 mM MgCl ₂	Invitrogen (AM9530G)
, ,	5 mM EGTA	Sigma-Aldrich (E3889)
	in ddH_2O , pH adjusted to 6.8 with KOH	
Quenching solution	1x PBS	Pharmacy LMU Hospital
	0.1 % NaBH ₄ (w/v)	Sigma-Aldrich (71320)

 $Table\ 2: Pharmacological\ inhibitors.$

Inhibitor	Concentration	Supplier	Catalogue #
GSK-626616	1-10 μΜ	Tocris	6638
Harmine	10-100 μΜ	Sigma-Aldrich	286044
Latrunculin A	50 nM	Sigma-Aldrich	428026
para-nitroblebbistatin	25 μΜ	Motorpharma	-
Centrinone	500 nM	bio-techne	5690

Table 3: Enzymes.

Name	Supplier	Catalogue #
Q5® High-Fidelity Polymerase	New England Biolabs	M0491
BsrGI-HF®	New England Biolabs	R3575
EcoRI-HF®	New England Biolabs	R3101
Quick Ligation™ Kit	New England Biolabs	M2200

Table 4: Kits.

Name	Supplier	Catalogue #
GeneJET Plasmid-Miniprep-Kit	Thermo Fisher	K0503
PureLink™ Expi Endotoxin-Free Maxi Plasmid Purification Kit	Invitrogen	A31231
Monarch DNA Gel Extraction Kit	New England Biolabs	T1020S
Neon™ Transfection Kit	Invitrogen	MPK1025

Table 5: Reagents.

Name	Supplier	Catalogue #
β-Estradiol	Sigma-Aldrich	E2758
Lipopolysaccharide (E. coli O26:B6)	Sigma-Aldrich	L2654
Blasticidin S-hydrochlorid	Thermo Fisher	R21001
Puromycin-dihydrochloride	Thermo Fisher	A1113803
Doxycycline-hydrochloride	Sigma-Aldrich	D3072
NEB® Stable Competent E. coli	New England Biolabs	С3040Н
Polybrene	Merck-Millipore	TR-1003-G
Sylgard 184	Biesterfeld	5498840000
CCL19	Bio-Techne	440-M3-025
CXCL12	Bio-Techne	350-NS-050
UltraPure agarose	Invitrogen	16500500
Polybeads®	Polysciences	07312-5
PureCol, bovine collagen	Cellsystems	5005-100ml
10x MEM	Thermo Fisher	21430020
NaHCO ₃	Sigma-Aldrich	S8761-100ml

Paraformaldehyde	Merck-Millipore	818708
Glutaraldehyde	Sigma-Aldrich	G6257
Fluoromount-G	Invitrogen	00-4958-02

2.1.2 CELL LINES

Table 6: Cell lines.

Name	Provider
Hoxb8 WT	Renkawitz Lab
Hoxb8 CETN2-GFP	Eva Kiermaier (LIMES institute, Bonn, Germany) (Weier <i>et al.</i> , 2022)
Hoxb8 CETN2-GFP indCas9 sgC-NAP1	Peter Konopka (LIMES institute, Bonn, Germany)
Hoxb8 EB3-mCherry	Michael Sixt (IST, Vienna, Austria) (Kopf <i>et al.</i> , 2020)
Hoxb8 Lifeact-GFP	Michael Sixt (IST, Vienna, Austria)
Hoxb8 PCNT-dTomato	this study
Hoxb8 CETN2-GFP PH-Akt-dTomato	this study
Hoxb8 Lifeact-GFP EMTB-mCherry	this study
Jurkat T cells	Jan Schwarz
LX293T cells	Michael Sixt (IST, Vienna, Austria)

2.1.3 PLASMIDS

Table 7: Plasmids.

Name	Provider	Addgene #	
psPAX2	Didier Trono	#12260	
pMD2.G	Didier Trono	#12259	
PH-Akt-GFP	Tamas Balla (Várnai & Balla, 1998)	#51465	
pLenti-V6.3 Ultra-Chili	Ewa Snaar-Jagalska	#106173	
hCEP120-EGFP	Tang Tang (Lin <i>et al.</i> , 2013)	#50382	
pLenti-V6.3 EB3-mCherry	Michael Sixt (IST, Vienna, Austria)	-	
pLenti-V6.3 EMTB-mCherry	Michael Sixt (IST, Vienna, Austria)	-	
pCAG-mAkna-EGFP	-mAkna-EGFP Magdalena Götz (Institute for Physiological Genomics, Munich, Germany)		
RFP-Pericentrin	Melina Heuze (Heuzé <i>et al.,</i> 2019)	-	
pcDNA5-Dyrk3-WT-GFP	Lucas Pelkmans & Dorothee Dormann (Rai <i>et al.</i> , 2018)	-	

pcDNA5-Dyrk3-K218M-GFP	Lucas Pelkmans & Dorothee Dormann (Rai <i>et al.</i> , 2018)	-
pcDNA5/ FRT/ TO- GFP	Harm Kampinga (Hageman & Kampinga, 2009)	#19444
mCherry-Centrin2-N-10	Michael Davidson	#55018
pLenti-V6.3 Ultra-Chili-PCNT	this study	-
pLenti-V6.3 Ultra-Chili-PH-Akt	this study	-

2.1.4 OLIGONUCLEOTIDES

Table 8: Oligonucleotides.

Primer	Sequence (5' -3')	Tm (°C)
Pericentrin-forward	CGAGCTGTACAAGGGTGGTTCTGGTGAGCAAAAGC	72
Pericentrin-reverse	GGAACGAATTCCTACTGTTTAATCATCGGGTGGC	72
PH-Akt-forward	CGAGCTGTACAAGGGTGGTTCTGGTAGCGACGTGG	72
PH-Akt-reverse	GGAACGAATTCCTAGGTGGCGACCGGTGG	72
Sequencing	AGCTGGACATCACCTCCCACAACG	-

2.1.5 ANTIBODIES AND STAINING REAGENTS

Table 9: Antibodies and staining reagents.

Specificity/ staining reagent	Host and conjugation	Dilution	Supplier	Catalogue #
Anti-mouse CD16/32	rat unconjugated	5 μg/ml	Invitrogen	14-0161-85
Anti-mouse CD11c	armenian hamster APC	0.67 μg/ml	Invitrogen	17-0114-82
Anti-mouse MHCII	rat eFluor™ 450	0.67 μg/ml	Invitrogen	48-5321-82
Anti -mouse/human α-tubulin	rat unconjugated	2 μg/ml	Invitrogen	MA1-80017
Anti -mouse/human Ninein	rabbit unconjugated	0.25 μg/ml	Invitrogen	PA5-82224
Anti -mouse/human γ-tubulin	mouse unconjugated	4.25 μg/ml	Sigma-Aldrich	Т6557
Anti-mouse AKNA	mouse unconjugated	1:25	in-house production (gift from Magdalena Götz, Institute for Physiological Genomics, Munich, Germany)	
Anti -mouse/human Ccdc88b	rabbit unconjugated	0.8 μg/ml	Atlas Antibodies	HPA026652

Anti-human AKNA	rabbit unconjugated	1 μg/ml	Atlas Antibodies	HPA052367
Rat IgG (H+L)	goat Alexa Fluor® Plus 647	4 μg/ml	Invitrogen	A48265
Rabbit IgG (H+L)	donkey Alexa Fluor® Plus 647	4 μg/ml	Invitrogen	A32795
Mouse IgG (H+L)	goat Alexa Fluor® 555	2 μg/ml	abcam	ab150114
Rat IgG (H+L)	goat Alexa Fluor® Plus 594	4 μg/ml	Invitrogen	A11007
DAPI	-	1:1000	Thermo Fisher	62248
NucBlue	Hoechst33342	-	Invitrogen	R37605

2.2 METHODS

2.2.1 CELL CULTURE

All cells were grown and maintained at 37 °C in a humidified incubator with 5 % CO_2 . Cells were either used directly or stored frozen in liquid nitrogen until further usage. For freezing, cells were centrifuged at 300xg for 5 min, and cell pellets were resuspended in freezing medium (Table 1) at cell densities of 2.5-5x10 6 cells/ml. To prevent cell damage, cells were initially frozen at -80 °C and transferred to liquid nitrogen at least two days later.

Hoxb8 cell culture

Immortalized hematopoietic precursor cell lines (Hoxb8 cells) (Redecke *et al.*, 2013) were grown and maintained in R10 medium (Table 1) supplemented with 5 % Flt3l-containing cell culture supernatant (in-house production) and 1 μ M β -estradiol. CETN2-GFP+indCas9 sgC-NAP1 Hoxb8 cells were grown and maintained in a conditioned medium additionally supplemented with 10 μ g/ml blasticidin and 3 μ g/ml puromycin.

Dendritic cell differentiation

Dendritic cells were differentiated either from Hoxb8 precursor cell lines (Table 6) or from bone marrow isolated from male C57Bl6/J wildtype mice (aged 8-12 weeks). For Hoxb8-derived dendritic cells, Hoxb8 cells were washed twice with 1x PBS to remove remaining Flt3l and β -estradiol. Afterwards, Hoxb8 cells were seeded in R10 medium (Table 1) supplemented with 10 % granulocyte–macrophage colony-stimulating factor (GM-CSF) hybridoma supernatant in a 10 cm cell culture dish at a density of $0.1x10^6$ cells for WT cells, $0.4x10^6$ cells for CETN2-GFP+indCas9 sgC-NAP1 Hoxb8 cells, and $0.3x10^6$ cells for all other Hoxb8 lines used in this study. On differentiation day 3, fresh R10 medium supplemented with 20 % GM-CSF was added. On differentiation day 6, half of the medium was exchanged for fresh R10 medium supplemented with 20 % GM-CSF. Cas9 expression in dendritic cells expressing CETN2-GFP+indCas9 sgC-NAP1 was induced by the addition of 1 μ g/ml doxycycline on differentiation day 0 and continued by the addition of 2 μ g/ml doxycycline on differentiation days 3 and 6. For centriole depletion experiments, differentiating dendritic

cells expressing CETN2-GFP were treated with a final concentration of 500 nM Centrinone on differentiation days 2, 3, 6, 7, and 8. For bone marrow-derived dendritic cells, isolated hematopoietic precursor cells were seeded at a density of 2.5×10^6 cells/culture dish and subsequently cultured as described above. For migration experiments, either fresh or thawed dendritic cells (differentiation day 8) were stimulated by adding 200 ng/ml lipopolysaccharide (LPS) for 24 h to induce cell maturation.

Jurkat T cell culture

Jurkat T cells were cultured and maintained in R10 medium at a cell density of 0.1– 1.5×10^6 cells/ml.

Lenti-X 293T culture

Lenti-X 293T cells (LX293T cells), derived from HEK293 cells, were used for lentivirus production. Cells were maintained in LX-293 medium (Table 1) at 70-80 % confluency until further usage.

2.2.2 FLOW CYTOMETRY ANALYSIS

Dendritic cell maturation was routinely checked for surface expression of CD11c and MHCII. After Fc receptor blockage using an anti-mouse CD16/32 antibody diluted in FACS buffer (Table 1) as indicated in Table 9, cells were stained with anti-mouse CD11c and anti-mouse MHCII antibodies (Table 9). Flow cytometry analysis was performed on a Cytoflex S flow cytometer (Beckmann-Coulter).

2.2.3 MICE

All animals were housed in the Core Facility Animal Models at the Biomedical Centre (Ludwig-Maximilians-Universität) and animal procedures and experiments were in accordance with the ministry of animal welfare of the region of Oberbayern and with the German law of animal welfare.

2.2.4 GENERATION OF FLUORESCENT REPORTER CONSTRUCTS

Insert amplification

Generation of a N- terminal dTomato fusion construct of Pericentrin was performed by amplifying Pericentrin from an RFP-Pericentrin encoding plasmid (Table 3) using a BsrGI restriction site containing forward and an EcoRI restriction site containing reverse primer pair (Table 8). N-terminal dTomato fusions constructs of PH-Akt were generated by amplifying PH-Akt from a PH-Akt-GFP encoding plasmid (Table 7) using a BsrGI restriction site containing forward and an EcoRI restriction site containing reverse primer pair (Table 8). To ensure reliable insert amplification, Q5® High-Fidelity DNA polymerase was employed according to the manufacturer's instructions. Optimal primer annealing temperatures were determined using the NEB Tm calculator. Typically, 35 cycles of PCR amplification would yield a sufficient amount of PCR product for downstream processing.

Gel purification

Following PCR amplification, PCR products were purified on a 1 % agarose gel. For this purpose, 1 % agarose (w/v) was heated in 1x TAE buffer (Thermo Fisher) until fully dissolved, and Midori Green (Nippon Genetics) was added for subsequent DNA visualization. After solidification, gel electrophoresis was performed at 100 V. DNA bands of correct size were cut, and subsequent DNA extraction was performed using the Monarch DNA Gel Extraction Kit according to the manufacturer's instructions.

Restriction digest and ligation

PCNT and PH-Akt inserts, as well as the pLenti-V6.3 Ultra-Chili plasmid serving as lentiviral backbone were digested with BsrGI and EcoRI according to the manufacturer's instructions. Afterwards, DNA fragments were gel purified as described above. The purified DNA fragments were ligated using the Quick Ligation $^{\text{TM}}$ Kit as recommended by the manufacturer.

Transformation and plasmid isolation

Ligation reactions were transformed into chemically competent *E. coli* according to the manufacturer's instructions. Successfully transformed clones were used to inoculate liquid bacterial cultures for downstream plasmid isolation using the GeneJET Plasmid-Miniprep-Kit as recommended by the manufacturer, and isolated plasmid DNA was sent for sequencing. To avoid immune cell activation upon lentiviral transfection, plasmid isolation of verified clones intended for lentivirus production was performed with the PureLink™ Expi Endotoxin-Free Maxi Plasmid Purification Kit according to manufacturer's instructions.

Sequencing

The correct sequence and orientation of clones were verified by sequencing with the Mix2Seq service as recommended by the sequencing company (Eurofins).

2.2.5 TRANSGENE DELIVERY

Lentiviral transfection

For stable expression of fluorescent reporter constructs, lentiviral transduction of Hoxb8 cells was performed. For lentivirus production, 5x106 LX293T cells were seeded in antibiotic-free LX293T-medium (Table 1). On the next day, cells were co-transfected with the respective fusion construct encoding plasmid in combination with pMD2.G (envelope expressing plasmid), and psPAX2 (packaging plasmid). For this purpose, 4.53 µg construct encoding plasmid, 1.13 µg pMD2.G and 2.27 μg psSPAX2 were incubated with 65 μl PEI solution and DMEM for 10 minutes at room temperature, before being added to the LX293T cells. After 48 hours, the supernatant of lentivirus-producing cells was harvested, and either used directly for lentiviral transduction or stored at -80 °C until further usage. For lentiviral infection, 0.1x106 Hoxb8 cells for WT background and 0.3x106 for LifeactGFP and CETN2-GFP background were seeded in R10 medium (Table 1) supplemented with Flt3l and β-estradiol as described above. Following lentiviral infection in the presence of 3 µg/ml polybrene, medium was replaced after one day to reduce polybrene concentration. After three days, Hoxb8 cells were selected for stable virus insertion using 10 µg/ml blasticidin for at least one week until the non-transduced selection control cells were dead. Following cell expansion, Hoxb8 cells were collected and resuspended in cell sorting buffer (Table 1). Hoxb8 cells expressing fluorescent reporter constructs were sorted using fluorescenceactivated cell sorting on a FACSAriaFusion (BD) equipped with 4 lasers (405, 488, 561, 640 nm). Live fluorescent Hoxb8 cells were directly sorted into 25 mM HEPES-buffered R10 medium (Table 1) supplemented with Flt3l and β -estradiol as described above, and used for downstream cell culture.

Transient transfection

For transient expression of fluorescent reporter constructs, Jurkat T cells were electroporated with plasmids encoding the respective constructs 16 hours prior to the experiment using the Neon Transfection system (Invitrogen). For this purpose, $1x10^6$ Jurkat T cells were washed with 1x PBS and resuspended in Resuspension Buffer T according to the manufacturer's instructions. After addition of 1 μ g plasmid DNA, cells were electroporated with 3 pulses at 1600 V for 10 ms each. For recovery, cells were incubated in R10 medium (Table 1).

Dyrk3 localization was analyzed by co-electroporating Jurkat T cells with pcDNA5-Dyrk3-WT-GFP and mCherry-Centrin2-N-10 as described above. The next day, cells were injected in an underagarose migration assay as described below and mCherry+ GFP+ cells were selected for imaging. For validation of Dyrk3 inhibition mediated effects on migration, Jurkat T cells were electroporated as described above, either with pcDNA5/FRT/TO-GFP as control, or pcDNA5-Dyrk3-K218M-GFP encoding for a dominant-negative point-mutant Dyrk3, respectively. The next day, cells were collected and resuspended in cell sorting buffer (Table 1) to prepare for fluorescence-activated cell sorting on a FACSAriaFusion (BD) equipped with 4 lasers (405, 488, 561, 640 nm). Live GFP+ cells were directly sorted into R10 medium buffered with 25 mM HEPES. After 1 hour of recovery in the incubator, cells were used for downstream migration assays as described below.

2.2.6 MICRO-FABRICATED DEVICES

Micro-fabricated devices were prepared as described previously (Renkawitz *et al.*, 2018; Kroll *et al.*, 2022). Briefly, micro-structures were replicated from custom-made wafers produced by photolithography or epoxy replicates as templates, with defined width, height, length, and pore sizes. The height of the micro-structures ranged between 4-5 μ m to allow cell confinement from top and bottom. Wide straight channels had a width of 50 μ m. Narrow straight channels, channels with constrictions, 3-way pathfinding channels, and 6-way pathfinding channels had a width of 8 μ m, thereby confining cells from all sides. The distance between two 6-way crossings was 90 μ m. The pore size of microchannels with constrictions was 2 μ m.

Polydimethylsiloxane (PDMS, Sylgard 184) was prepared by mixing elastomer base and elastomer curing agent in a 10:1 ratio (w/w) in a Thinky Mixer in mixing mode for 2 minutes, followed by centrifugation in defoaming mode for another 2 minutes. Subsequently, the PDMS mixture was poured onto the template structures to generate replica of the micro-structures. Air bubbles were removed with a desiccator. After solidification at 80 °C overnight, PDMS was carefully removed from the templates and cut into pieces according to the respective design size. Holes for cell and chemokine loading were punched in a distance of 1-2 mm. Using a plasma cleaner, the PDMS device was bonded to glass coverslips, that were cleaned with isopropanol and ethanol in an ultrasound water bath. PDMS devices were then placed on a heating plate set to 120 °C for 10 min, followed by overnight incubation at 80 °C to permanently bond them to the glass surface. The devices were then either directly glued into 6-well plates with drilled holes using non-toxic aquarium glue or stored at room temperature until further usage.

2.2.7 MIGRATION ASSAYS

For live cell imaging, cell nuclei were visualized by incubating cells for at least 30 min with NucBlue diluted in imaging medium according to the manufacturer's instructions, followed by washing. For pharmacological inhibition experiments, final concentrations of inhibitors were used as indicated in Table 2 and the figure legends. All inhibitors were dissolved in DMSO, and control samples were treated with DMSO in the corresponding dilution.

Microchannel migration assay

Prior to the experiment, PDMS devices were flushed with imaging medium (Table 1) supplemented inhibitors if needed according to the experimental setup. For this purpose, PDMS devices were placed in a plasma cleaner for surface activation. Afterwards, medium was added to both loading holes. After incubation at 37 °C, 5 % CO₂ in a cell culture incubator for at least 1 hour to ensure a uniform liquid distribution and to avoid liquid flow, devices were used for downstream experiments. Then, 0.625 $\mu g/ml$ CCL19 (DCs) or 1.25 $\mu g/ml$ CXCL12 (Jurkat T cells) were loaded into the chemokine loading hole to establish a chemokine gradient, followed by addition of 0.3-0.5x10⁵ cells into the second loading hole. Microchannel migration assays were placed in the incubator, and cell behavior was regularly checked for migration initiation. Live-cell imaging was typically started at approximately 30 minutes after cell loading and performed as described below.

Under-agarose migration assay

Under-agarose migration assays without bead obstacles were prepared as described previously (Renkawitz et al., 2009). Briefly, 1 % agarose was prepared by dissolving 4 % UltraPure agarose (w/v) in sterile water. Then, the liquid 4 % agarose was mixed with R20 medium (Table 1) premixed with Hanks buffered salt solution pH 7.3 and prewarmed to 55 °C, in a 1:3 ratio to a final agarose concentration of 1 %. For experiments including inhibitors, the 1 % agarose mixture was let cool down to 37 °C before adding the inhibitor to the respective final concentration to avoid heat-induced inhibitor inactivation. 300 µl of agarose mixture per well was poured into imagingsuitable 8-well slides (Ibidi), polymerized for 1 hour at room temperature and was then transferred to the incubator for 1 hour for equilibration. For under-agarose migration assays including bead obstacles, 8-well slides were pre-coated with Polybeads® (6 µm diameter). Typically, two drops of Polybeads® were washed in 10 ml phenol-free R10 medium and resuspended in 100 μl of phenol-free R10 medium. For coating, the well glass surface was activated with oxygen plasma and 10 µl of beads were added, followed by incubation at room temperature for 30 minutes to ensure stable bead attachment. Afterwards, the agarose mixture was prepared and carefully added as described above. For both, under agarose with and without bead obstacles, 2 mm wide holes were generated using tissue biopsy punchers after agarose solidification and equilibration. Then, CCL19 (2.5 μg/ ml; DCs) or CXCL12 (5 μg/ml; Jurkat T cells) in imaging medium (Table 1) were loaded as chemotactic stimulus. 0.2x105 cells were injected between the glass surface and agarose layer in a distance of 2-3 mm to the chemokine loading hole. For live-imaging, assays were placed in the incubator for 1 hour to allow induction of directional migration towards the chemokine source before imaging.

Collagen migration assay

In order to study cell migration in a more physiological environment, collagen migration assays were performed as described previously (Sixt & Lämmermann, 2011; Kroll *et al.*, 2022). Briefly,

for DC collagen migration assays, a collagen gel mixture was prepared by mixing 225 μ l PureCol with 30 μ l 10x minimum essential medium (MEM) and 15 μ l 7.5 % sodium bicarbonate (NaHCO₃). This collagen mixture was carefully mixed with 3x10⁵ cells in R10 medium at a 2:1 ratio, resulting in gels with a final collagen concentration of 1.7 mg/ml. Collagen-cell mixtures were cast in custom-made migration chambers with a diameter of 18 mm and a height of approx. 1 mm. After polymerization of collagen fibers at 37 °C, 5 % CO₂ in a cell culture incubator for 75 min, 80 μ l CCL19 (0.625 μ g/ml) was added to the top of the chamber. For Jurkat T cell collagen migration assays, PureCol stock solution was diluted with 1x PBS, resulting in a final collagen concentration of 1.3 mg/ml mixed with 2x10⁵ cells in R10 at a 2:1 ratio. After polymerization at 37 °C, 5 % CO₂, in a cell culture incubator for 75 min, 80 μ l CXCL12 (1.25 μ g/ml) was added to the top of the chamber. For inhibition experiments, inhibitors were added to the collagen-cell mixture as well as to the chemokine solution at the indicated concentrations.

2.2.8 IMMUNOFLUORESCENCE STAINING

Immunofluorescence staining

For immunofluorescence staining, under-agarose migration assays were prepared as described above. Following cell migration for 2-4 hours to allow stable chemokine gradient generation and directed cell migration, 300 μ l 3.7 % paraformaldehyde (PFA) diluted in 1x PBS and prewarmed to 37 °C was added on top of the agarose and incubated for 1 hour at 37 °C, 5 % CO₂. After fixation the agarose block was carefully removed, and cells were washed three times with 1x PBS. Afterwards, cells were permeabilized with 1x SAPO buffer for 30 minutes at room temperature. Following permeabilization, blocking was performed with 5 % BSA diluted in 1x SAPO buffer for another 30 minutes at room temperature. Primary antibodies were diluted in 1x SAPO buffer as indicated in Table 9, and incubated overnight at 4 °C. The next day, primary antibodies were removed, and cells were washed three times with 1x PBS for 5 minutes each. Secondary antibodies and DAPI were diluted in 1x SAPO as indicated in Table 9, and incubated at room temperature for 1 hour, protected from light. After washing three times with 1x PBS for 5 minutes each, cells were mounted using Fluoromount-G.

Immunofluorescence staining for STED imaging

For super-resolution imaging of microtubules, under-agarose migration assays were performed as described above. Following migration for 2-4 hours, 3.7 % PFA was additionally supplemented with 0.5 % glutaraldehyde and diluted in microtubule-stabilizing buffer to ensure microtubule structure preservation and prevent microtubule disintegration, which would result in a beads-on-a-string-like appearance in STED imaging. 300 μ l of fixation solution prewarmed to 37 °C was added on top of the agarose block. After fixation for 30 minutes at 37 °C, 5 % CO₂, the agarose block was carefully removed, and quenching solution was added to reduce glutaraldehyde-induced background fluorescence and incubated for 8 min at room temperature. Afterwards, permeabilization, blocking, and anti- α -tubulin primary antibody incubation were performed as described above. The next day, the primary antibody was removed, and cells were washed three times with 1x PBS for 5 minutes each. The secondary antibody was diluted in 1x SAPO as indicated in Table 9, and incubated at room temperature, protected from light. Importantly, the secondary antibody was conjugated with Alexa Fluor® Plus 594 as STED-suitable fluorophore. Afterwards, washing and mounting was performed as described above.

2.2.9 IMAGING

Widefield microscopy

Live-cell imaging was performed at 37 °C, and supplementation with 5 % CO_2 in a humidified chamber if needed. Cell migration was recorded using conventional inverted wide-field DMi8 microscopes (Leica) using HC PL FLUOTAR $4\times/0.5$ PH0 air, HC PL FLUOTAR L20x/0.40 PH1 air, HC PL APO $40\times/0.9$ PH3 air and HC PL APO 100x/1.40 oil objectives. Microscopes were equipped with a Lumencor or pE-4000 light source (395, 475, 555, and 635 nm) and an incubation chamber, heated stage, and a CO_2 mixer (Pecon). Cells migrating in collagen networks were imaged for 5 hours in 1 minute time intervals. Microchannel migration assays were recorded for at least 5 hours every minute. Centriole separation dynamics were imaged every 10 seconds. For evaluation of microtubule nucleation dynamics, EB3-mCherry expressing DCs were imaged at 5 s intervals. Acquisition of immunofluorescence samples was performed on an inverted wide-field DMi8 microscope (Leica) equipped with an HC PL APO 100x/1.47 oil objective.

Fluorescence recovery after photobleaching

Fluorescence recovery after photobleaching (FRAP) experiments were performed at the Core Facility Bioimaging of the Biomedical Center with an inverted Leica TCS SP8X STED 3X equipped with two photomultiplier tubes (PMTs) and three hybrid detectors (HyDs), Argon laser, WLL2 laser (470 - 670 nm), acusto-optical beam splitter and 592 nm and 660 nm continuous wave and 775 nm pulsed depletion lasers. Cells were recorded at 37 °C and 5 % CO₂. Images were acquired in unidirectional scanning mode with an HC PL APO CS2 40x/1.30 OIL objective, with an image pixel size of 142.6 nm and a pixel dwell time of 4.8 μ s. The following fluorescence settings were used: GFP (excitation: 488 nm (Argon laser); emission 500-570 nm) or RFP (514 nm; 536-661 nm), both being recorded with conventional PMTs. 5 pre-bleach frames at a frame rate of 1 s were recorded, followed by bleaching at full laser power in zoom-in mode for two times. Initial signal recovery was recorded for 10 frames at a frame rate of 1 s, followed by extended post-bleach recording in 5 s time intervals for at least 2 min.

Stimulated emission depletion

Stimulated emission depletion (STED) microscopy was performed at the Core Facility Bioimaging of the Biomedical Center with an inverted Leica TCS SP8X STED 3X equipped with two PMTs and three hybrid detectors (HyDs), Argon laser, WLL2 laser (470 - 670 nm), acusto-optical beam splitter and 592 nm and 660 nm continuous wave and 775 nm pulsed depletion lasers. Images were acquired in unidirectional scanning mode with an HC PL APO CS2 100x/1.40 OIL STED WHITE objective, with an image pixel size of 25 nm and an accumulated pixel dwell time of 29.3 μ s. For conventional confocal imaging of the CETN2-GFP signal, the following fluorescence settings were used: GFP (WLL2 pulsed excitation 489 nm; emission 500-570 nm; PMT). For STED microscopy of microtubules stained with anti- α -tubulin, the following settings were used: AlexaFluor 594 (WLL2 pulsed excitation 590 nm; emission 600-670 nm; depletion in 2D mode with a 775 nm pulsed laser). The signal was recorded with a hybrid detector in photon counting mode with time gating set to 0.5-6 ns and the corresponding reference wavelength of 590 nm. The recording was sequentially to avoid signal bleed-through.

2.2.10 IMAGE ANALYSIS

Fiji / ImageJ (Schneider *et al.*, 2012), ilastik (Berg *et al.*, 2019) and Imaris (Bitplane) were used for image processing. In general, only single, non-interacting cells were included for analysis to avoid effects of neighboring cells on cell path, cell speed and centriolar dynamics. Centrosome fracturing was classified as a distance above 1.5 μ m between the two individual centrioles in a centriolar pair (Weier *et al.*, 2022).

Migration analysis in microchannel migration assays

Velocity of migrating DCs and Jurkat T cells along unidirectional paths (narrow straight, wide straight microchannels) was analyzed using the tracking function of Imaris v9.7.2. For DC migration, cell nuclei were tracked with the following settings: object diameter 12 μm , manually adjusted quality threshold, autoregressive motion tracking algorithm (max. distance 25 μm , gap size =3), min. track duration 15 min. For Jurkat T cell migration the following settings were applied: object diameter 15 μm , manually adjusted quality threshold, autoregressive motion tracking algorithm (max. distance 15 μm , gap size=3), min. track duration 15 min. Pore translocation time and junction passing time, as well as centriolar distances were manually quantified in Fiji. The competing protrusion length was measured by Mauricio Ruiz Fernandez using ImageJ by determining the maximal length for each protrusion during a productive path decision. The longest of those protrusions was defined as the main competing protrusion.

Migration analysis in collagen migration assays

Dendritic cell migration in collagen matrices was analyzed using a custom-made cell tracking tool for ImageJ (Leithner *et al.*, 2016) . In brief, cell migration image sequences were background corrected by subtracting the average of the entire sequence. Particle filtering was used to discard objects smaller or larger than the cells. Then, for each image in the sequence the lateral displacement that optimizes its overlap with the previous frame was determined. Finally, the migration velocity towards the chemokine source was calculated from the y-displacement and the time between two consecutive frames. To analyze Jurkat T cell migration, cells were manually tracked in Fiji / ImageJ using the manual tracking plugin. Migration speed, accumulated distance and directionality were calculated using the Ibidi chemotaxis and migration tool (Zantl & Horn, 2011). The first 30 minutes of the recordings were excluded from analysis due to initial image drift.

Cell shape analysis of dendritic cells and Jurkat T cells was performed by manually outlining randomly selected cells after 200 minutes of recording to ensure a well-established chemokine gradient across the entire field of view, and thus directionally migrating cells. Afterwards, cell shape descriptors were measured and exported from ImageJ.

Centrosome characterization

Characterization of intact centrosomes was performed by measuring mean fluorescence intensities of two circular regions of interest (radius $0.35~\mu m$) each centered to one centriole in summed Z-projections. Next, the ratio between both measured values was calculated choosing the higher value as divisor.

For characterization of fractured centrosomes by immunofluorescence staining, recorded cells were analyzed by categorizing fluorescence signal patterns as indicated. Dyrk3 localization was evaluated by measuring fluorescence intensity profiles along a 5 μ m long line determined by the centriolar axis using the Plot profile function in Fiji. Then, fluorescence values were normalized to the mean intensity value of the first and last four measured values, respectively.

FRAP analysis

FRAP analysis was performed using ImageJ. Per cell, three ROIs were chosen, and mean fluorescence intensity values were measured for every time point and every ROI: I) the bleached region, II) a non-bleached reference region within the cell, and III) a non-bleached region outside the cell to determine background detector noise. The signal recovery rate was calculated by first subtracting the unspecific background detector noise and then normalizing the mean fluorescence intensity of the bleached region to the non-bleached reference region inside the cell. Then, the recovery rate was normalized to the mean pre-bleach level.

EB3 comet analysis

Analysis of EB3 comets was performed by Dr. Robert Hauschild (IST, Vienna, Austria). For analysis of microtubule nucleation rate and speed, cells that were well separated from other cells were randomly selected and cut out from raw movies. The EB3 comets within these cells were then tracked in Fiji using TrackMate v7.9.2 (Tinevez *et al.*, 2017) with the following settings: LoG detector (object diameter: 0.65 μ m), manually adjusted quality threshold and min. intensity filters, Kalman tracker: search radii 7,10 μ m, no frame gap). The resulting tracks were exported and the presented statistics were derived with a custom Matlab script.

Pericentriolar material shape analysis

For PCM shape analysis, I manually selected directionally migrating cells with a stable fluorescence signal in the focal plane, on a random basis. Downstream segmentation was performed by Dr. Robert Hauschild (IST, Vienna, Austria). The fluorescence signal associated with the PCM was segmented using ilastik's pixel classifier workflow. In Fiji, movies related to a single experimental condition were combined, and the y-branching area of each channel was aligned using the "3D drift correct" plugin. Subsequently, the PCM was filtered based on size, and shape analysis was conducted using the particle analyzer. The PCM was then skeletonized. Shape parameters, along with skeleton length, were extracted for further analysis.

PH-Akt polarity analysis

The PH-Akt signal gradient was analyzed by Mauricio Ruiz Fernandez in DCs migrating under agarose towards a chemokine gradient consistently for at least 30 min. Cells were imaged every 5 minutes, results were averaged over 6-20 time points for each cell. Fluorescence intensities of all pixels were extracted with a custom-made ImageJ script from images of cells segmented based on threshold and manual input. Using a custom-made R script (RStudio version 2022.12.0.353, R version 4.22, and the package tidyverse version 2.0.0) (Wickham *et al.*, 2019; R Core Team, 2021), the PH-Akt-dTomato to CETN2-GFP ratio was calculated from back to front of the cell: To normalize cells with different PH-Akt-dTomato and CETN2-GFP intensities, the respective fluorescence intensity was normalized to the intensity averaged over all time points of one cell, excluding a 1.5 µm area around each centriole for the entire analysis. Pixels were grouped in 50 (from 0 'back' to 1 'front', see Fig 22B) or 2 ('back' and 'front', see Fig 22C) equally long segments, based on the distance to the rear of the cell in the direction of migration, normalized to the respective cell length. The ratio of the normalized PH-Akt to CETN2 signal was averaged for each of those segments, first in each time point and then over all time points for each cell.

2.2.11 STATISTICAL ANALYSIS

All data that show individual cellular data points derived from cells from at least three independent biological replicates. All replicates were validated independently and pooled only when all showed similar results. Statistical analysis was conducted using GraphPad Prism Version 10 (GraphPad Software) using the appropriate tests according to normal or non-normal data distribution.

3 RESULTS

3.1 Cell motility forces deform the centrosome

As a model to investigate centrosomal dynamics during migration, I employed highly motile mouse dendritic cells (DCs) as these cells are terminally differentiated (Worbs et al., 2017; Weier et al., 2022), thereby excluding any mitosis-related effects. Furthermore, dendritic cells centrally nucleate microtubules from the centrosome as their only microtubule organizing center (MTOC) (Kopf et al., 2020). The centrosome was visualized via stable expression of Centrin2-GFP (CETN2-GFP) as a fluorescent reporter construct marking the two centrioles (Weier et al., 2022). Centriolar distances were analyzed upon dendritic cell migration towards a CCL19 chemokine source in different microchannel designs of different complexity. Using live-cell imaging with short time intervals of 1 minute enabled the analysis of centriole dynamics at a high temporal resolution. Since the microchannel devices typically contain many parallel channels, a large number of migrating cells could be recorded simultaneously. Dendritic cells migrating in narrow straight channels, thereby being confined from all sides, showed centriolar pairs that remained in stable proximity to each other (Fig. 4, A and B). Similarly, dendritic cells migrating in wide linear paths allowing a less predefined migration path showed continuously close centriolar distances (Fig. 4, D and E). In both microenvironments, centrioles showed minor distance fluctuations between 0.5 and 1 micrometer, consistent with permanent, yet flexible centrosome cohesion in non-dividing cells (Nigg & Stearns, 2011). In contrast, when dendritic cells encountered a path junction during their migration path, requiring a decision for one of two path options for onward migration, centrioles considerably stretched at the path junction compared to before entering the junction from 0.5 -1.0 μm to 1.0 - 1.5 μm (Fig. 4, C, F, and G). However, the stretching was only transient, as the initial centriolar distance was restored once the cells fully passed the junction (Fig. 4C). Interestingly, centriolar stretching could only be observed when cells entered the path junction with two competitive cell fronts simultaneously exploring the two path options (Fig. 4, C, F, and G). When cells entered the path junction with only one protrusion and immediately decided for one path option, centrioles stably remained in close proximity before, during, and after path decisions (Fig. 4, H, I, and J). Thus, these findings indicate that the centrosome in motile cells is subject to mechanical deformations by formation of two competing protrusions. Furthermore, the ability of cells to restore the original centriolar distance after stretching indicates that cells have probably developed mechanisms to counteract these mechanical deformations.

3.2 CENTROSOMES FRACTURE IN THE ABSENCE OF DYRK3 ACTIVITY

3.2.1 IMMUNE CELL MOTILITY REQUIRES FUNCTIONAL DYRK3

In order to screen for potential mechanisms, transcriptome analysis of dendritic cells migrating along a chemotactic CCL19 gradient in collagen matrices of varying density and therefore with differently sized pores and varying complexity (Fig. 5A) was performed by Prof. Jörg Renkawitz in collaboration with Dr. Thomas Penz, and Prof. Christoph Bock (CeMM Research Center for Molecular Medicine of the Austrian Academy of Sciences, Vienna, Austria), based on the rationale that cells form a higher number of competing protrusions in more complex collagen matrices. As controls, dendritic cells in suspension with and without a CCL19 stimulus were included to control

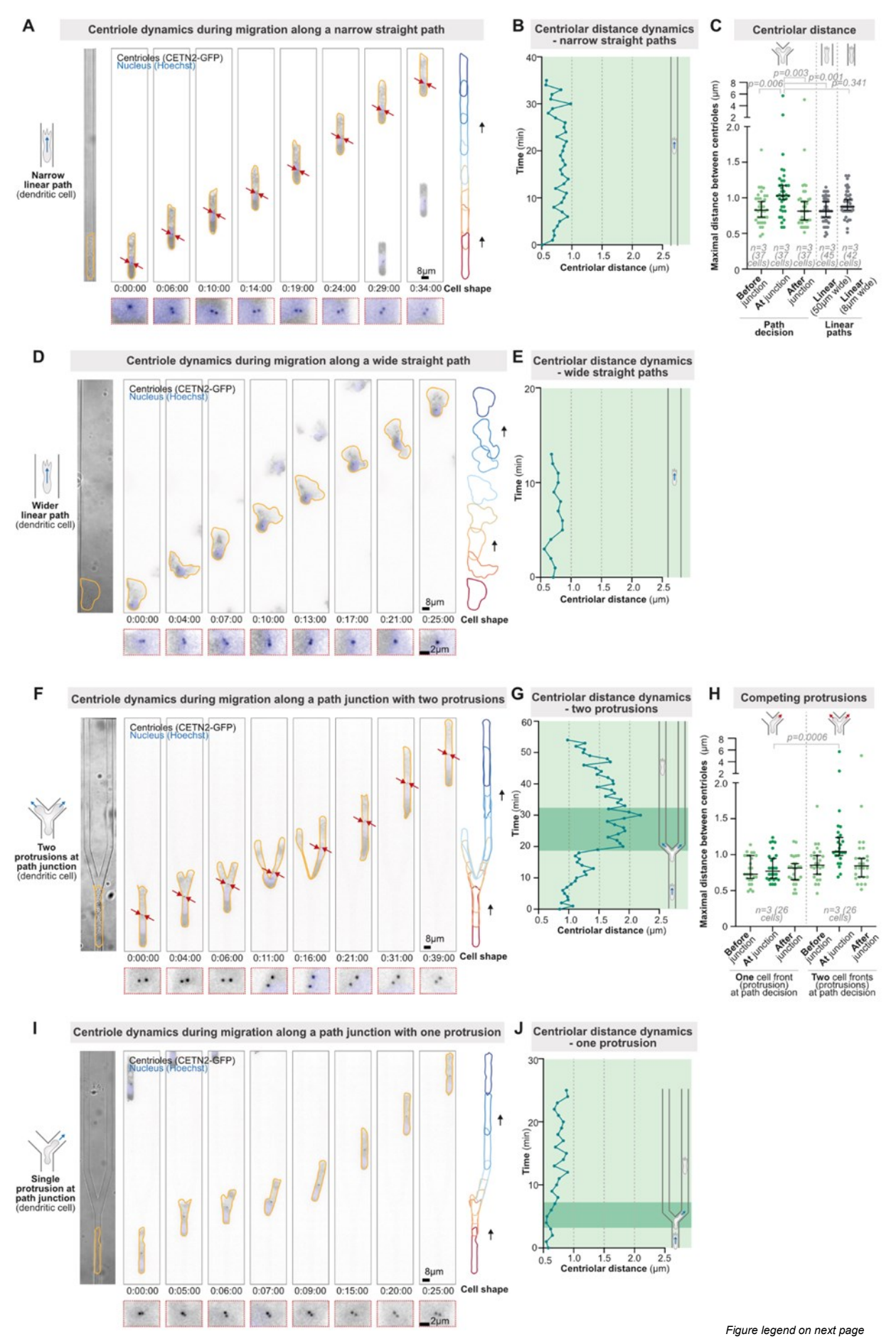


Figure 4: Mechanical centrosome deformations in motile cells. (A) Representative CETN2-GFP (centriole pair; black; enlargement in red dashed boxes) expressing dendritic cell (DC) stained with Hoechst (nucleus; blue) migrating along a unidirectional straight path (linear microchannel). (B) Centriolar distance dynamics during migration along a unidirectional straight path. (C) Quantification of centriolar distances before, during, and after migration through path junctions, as well as during migration along narrow and wide linear paths. Data represent median ± 95 % CI, Kruskal-Wallis with Dunn's multiple comparison test. (D) Representative CETN2-GFP (centriole pair; black; enlargement in red dashed boxes) expressing dendritic cell (DC) stained with Hoechst (nucleus; blue) migrating along a unidirectional 50 µm wide straight path. (E) Centriolar distance dynamics during migration as depicted in (D). (F) Representative CETN2-GFP (centriole pair: black; enlargement in red dashed boxes) expressing DC stained with Hoechst (nucleus; blue) migrating through a path junction (Y microchannel) with two cell fronts exploring the alternative paths. (G) Centriolar distance dynamics during a path decision; note the transiently increased distance between the individual centrioles. (H) Quantification of centriolar distances of cells that pass the junction either with two simultaneous explorative protrusions or DCs that immediately decide for one path alternative with one protrusion. Data represent median ± 95 % CI, Kruskal-Wallis with Dunn's multiple comparison test. (1) Representative CETN2-GFP (centriole pair; black; enlargement in red dashed boxes) expressing DC stained with Hoechst (nucleus; blue) migrating through a path junction (Y microchannel). Note that this specific cell has only one cell front at the path junction, and directly follows this cell protrusion into one of the two alternative paths. (J) Centriolar distance dynamics during migration through a path junction with one cell front; note the stable proximity of the individual centrioles. All data show representative cells from at least three independent biological replicates. Time is indicated as h:min:s.

for CCL19- and confinement-induced transcriptome changes. Initial cluster analysis of differentially regulated genes performed by Maximillian Götz, and Dr. Tobias Straub (Bioinformatics Unit, BMC, Munich, Germany) revealed that dendritic cells indeed adapt to migration in more complex environments on transcriptome level (Fig. 5B), including genes that are upregulated in response to more dense collagen networks (Fig. 5C). Among those genes, the dual-specificity tyrosine phosphorylation-regulated kinase 3 (Dyrk3) was identified (Fig. 5D). Dyrk3 was already described as a biomolecular condensate dissolvase including its activity at the centrosome (Wippich *et al.*, 2013; Rai *et al.*, 2018), and since the centrosome has biomolecular condensate-like features (Woodruff *et al.*, 2017), I further investigated the role of Dyrk3 during cell migration and centrosome deformations.

For this purpose, I first evaluated whether rendering Dyrk3 non-functional has an effect on cell migration in general by analyzing migration velocities of dendritic cells migrating within collagen networks. This approach not only facilitates the assessment of Dyrk3's function in migration with a well-established readout but also within collagen networks, which closely resemble *in vivo* environments. Thus, dendritic cell migration through collagen matrices in the presence of GSK-626616, a well-described small compound inhibitor of Dyrk3 (Wippich *et al.*, 2013; Rai *et al.*, 2018), was analyzed using an automated custom-made ImageJ script (Fig. 6, A and B) (Leithner *et al.*, 2016). Migration velocities were reduced upon Dyrk3 inhibition, showing a dose-dependent decrease with increasing inhibitor concentrations (Fig. 6C). Similarly, when inhibited with harmine, another well-known Dyrk inhibitor, dendritic cells displayed reduced migration velocities (Fig. 6D), indicating that Dyrk3 indeed plays a role for dendritic cell locomotion.

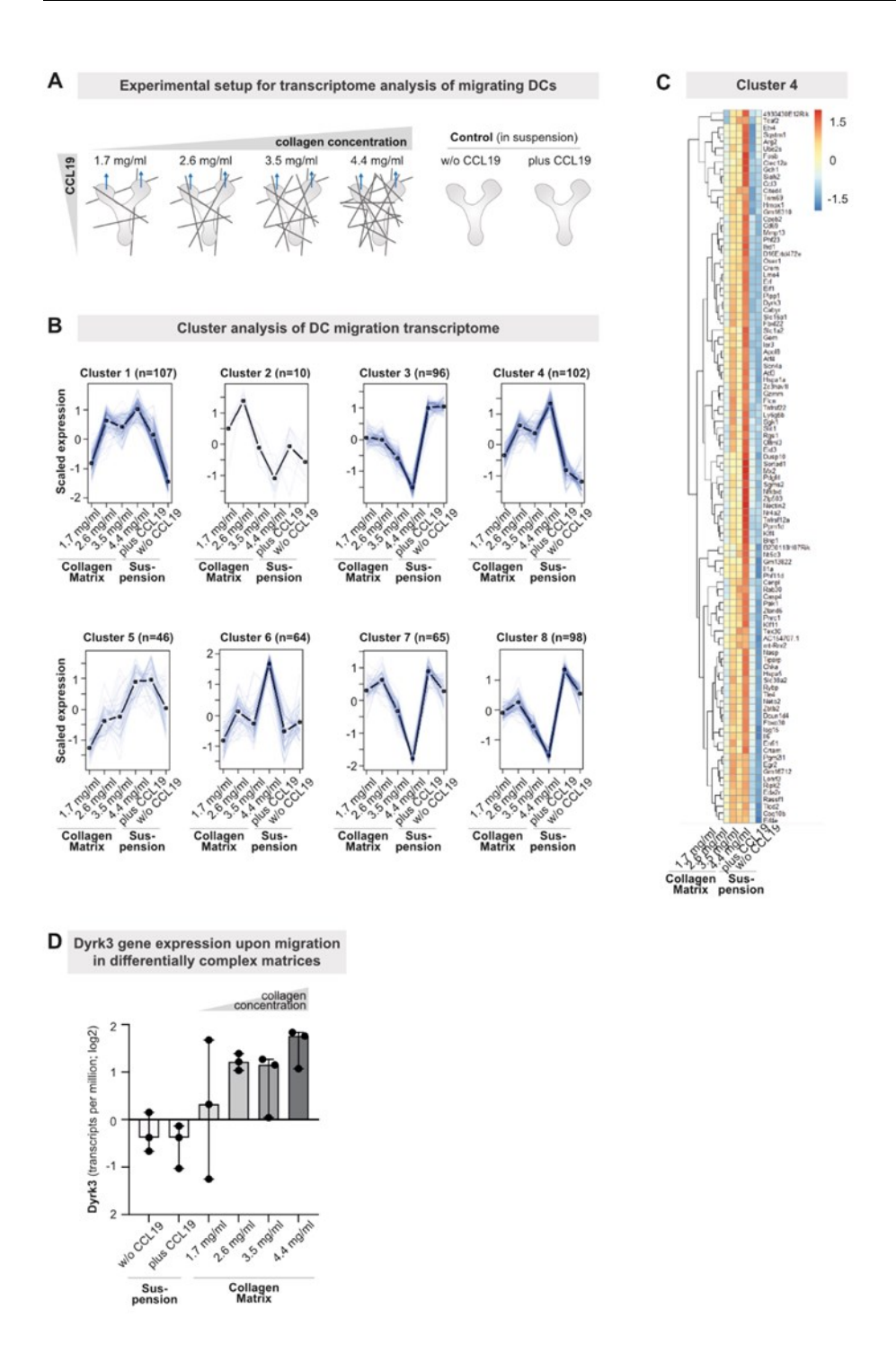


Figure 5: Transcriptome analysis of migrating dendritic cells. (A) Scheme of the experimental setup to investigate the transcriptome of migrating dendritic cells in differentially complex collagen matrices. In brief, dendritic cells migrated within collagen networks of collagen densities ranging from 1.7 mg/ml over 2.6 mg/ml and 3.5 mg/ml to 4.4 mg/ml along a chemotactic CCL19 stimulus. As controls, suspension cells with and without CCL19 stimulus were included (see 'Material and Methods' for details). **(B)** Cluster analysis of differentially expressed genes derived from (A). **(C)** Close up view of genes in cluster 4, which upregulate their gene expression in more complex collagen matrices. **(D)** Differential gene expression of Dyrk3. Data represent median ± 95 % CI, n=3 biological replicates.

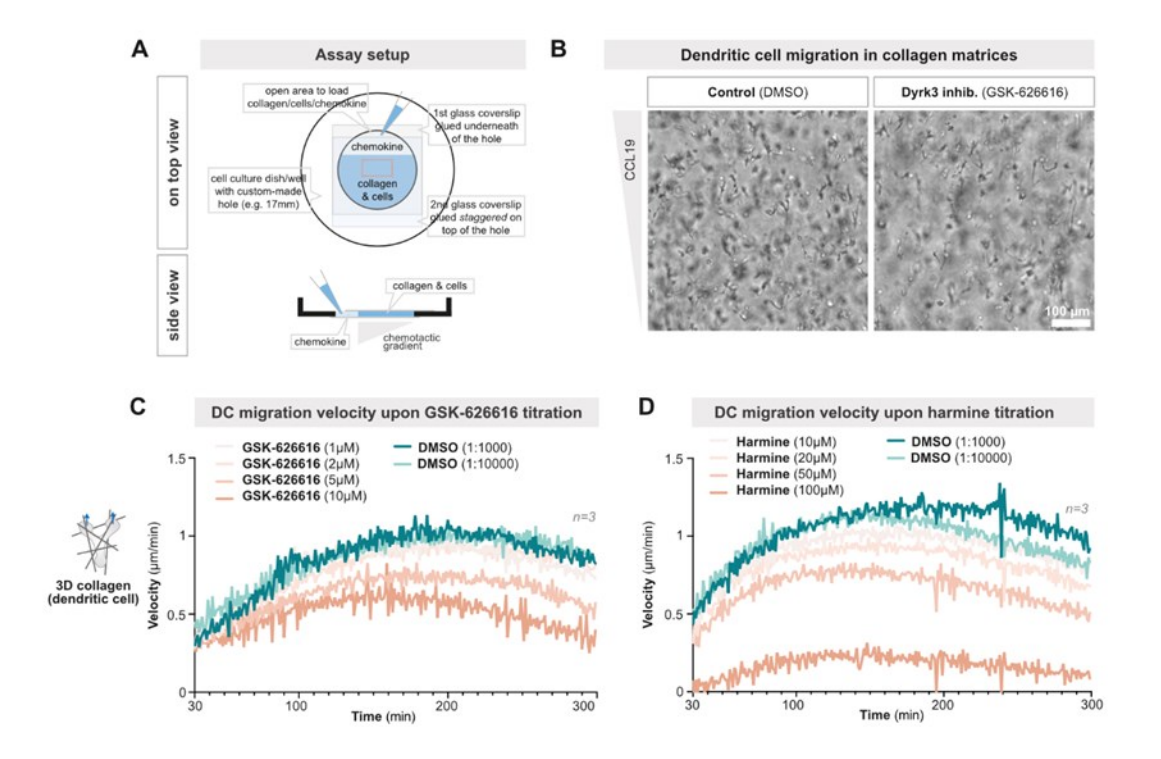


Figure 6: Pharmacological inhibition of Dyrk3 during dendritic cell migration. (A) Scheme of the experimental setup to analyze cell migration within collagen networks by live-cell imaging. (B) Representative dendritic cells migrating in 3D collagen matrices (1.7 mg/ml collagen) along a CCL19 chemokine gradient in the presence of DMSO (control) or $5 \mu M$ GSK-626616 (Dyrk3 inhibition). (C) Dendritic cell migration in three-dimensional (3D) collagen matrices (1.7 mg/ml collagen) along a CCL19 chemokine gradient in the presence of different concentrations of GSK-626616 (Dyrk3 inhibitor) or DMSO (control). Data are mean, n=3 biological replicates. (D) Dendritic cell migration in three-dimensional (3D) collagen matrices (1.7 mg/ml collagen) along a CCL19 chemokine gradient in the presence of different concentrations of Harmine (Dyrk inhibitor) or DMSO (control). Data are mean, n=3 biological replicates.

To test whether Dyrk3 is also important for migration of other immune cell types, Jurkat T cells, an immortalized human T cell line, were employed. Automated script analysis revealed that also Jurkat migration velocities in collagen networks towards a CXCL12 source were reduced upon Dyrk3 inhibition using GSK-626616 (Fig. 7A). Additional manual tracking showed that the reduced migration velocities were also accompanied by a reduced accumulated distance that was traveled (Fig. 7B), while directionality towards the chemotactic cue remained unaffected (Fig. 7C). In order to confirm these findings on a genetic level, a dominant-negative kinase-dead variant of Dyrk3 (K218M) was transiently expressed in Jurkat T cells (Rai *et al.*, 2018). Similarly, migration velocities, as well as the accumulated distance, were reduced by rendering Dyrk3 non-functional compared to cells that were transfected with a control plasmid lacking the K218M construct (Fig. 7D), without affecting the cells' ability to directionally migrate towards a chemotactic cue (Fig. 7C). Overall, these experiments show that Dyrk3 is not only upregulated on expression level in response to migration in a complex collagen network but is also required for immune cell locomotion.

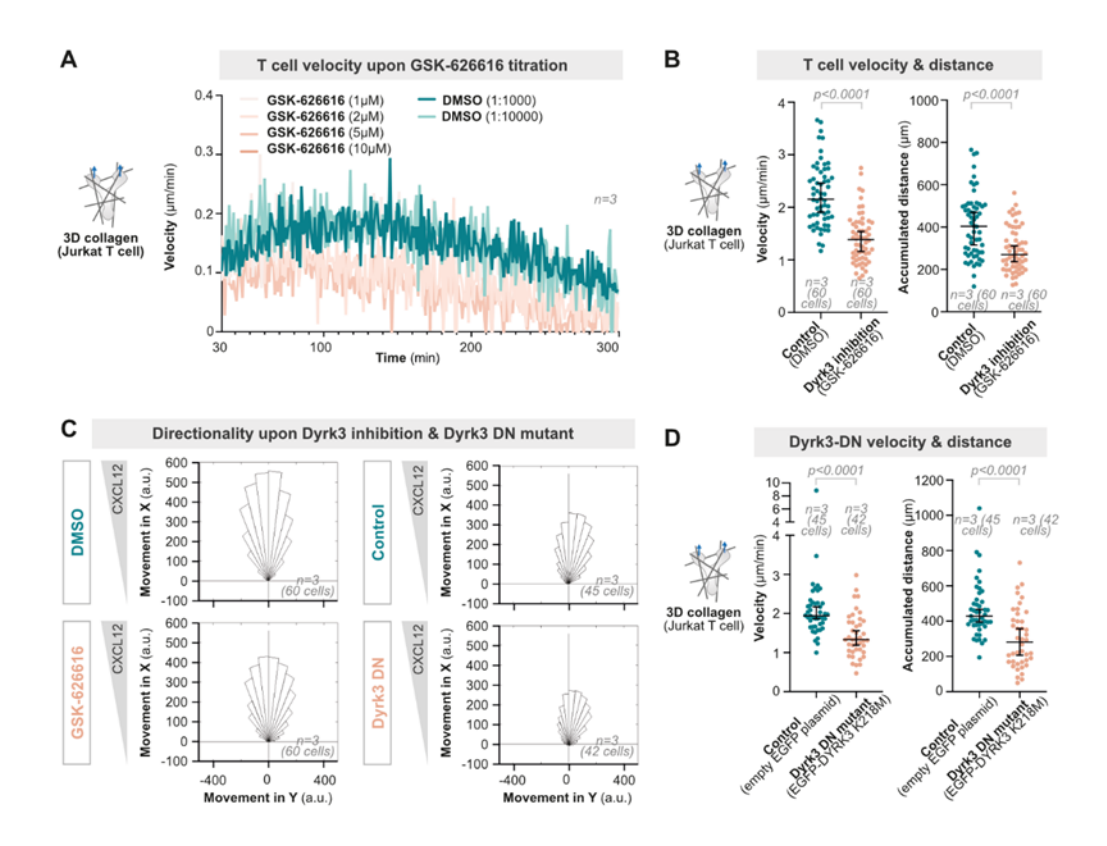


Figure 7: Pharmacological inhibition and expression of a kinase-dead point mutant of Dyrk3 during Jurkat T cell migration. (A) Jurkat T cell migration in three-dimensional (3D) collagen matrices (1.3 mg/ml collagen) along a CXCL12 chemokine gradient in the presence of different concentrations of GSK-626616 (Dyrk3 inhibitor) or DMSO (control). Data are mean, n=3 biological replicates. (B) Velocity and migrated distance of Jurkat T cells migrating in 3D collagen matrices (1.3 mg/ml) along a CXCL12 chemokine gradient in the presence of 5 μ M GSK-626616 or DMSO (control). Data represent median \pm 95 % CI, Mann-Whitney. (C) Directionality along a chemotactic gradient (CXCL12) of Jurkat T cells upon rendering Dyrk3 non-functional. (D) Velocity and migrated distance of Jurkat T cells migrating in 3D collagen matrices (1.3 mg/ml) along a CXCL12 chemokine gradient expressing a dominant-negative (DN) EGFP-Dyrk3 K218M mutant or the corresponding empty EGFP plasmid. Data represent median \pm 95 % CI, Mann-Whitney. All data derive from at least three independent biological replicates.

3.2.2 DYRK3 KINASE IS ACTIVE AT THE CENTROSOME

In the next step, Dyrk3 localization inside the cell and its relation to the centrosome was further characterized to identify a potential link between Dyrk3 function and centrosome cohesion. For this purpose, I performed simultaneous transient overexpression of Dyrk3 (WT)-EGFP and Centrin2-mCherry via electroporation of Jurkat T cells, given that dendritic cells are difficult to transfect. Live-cell imaging after 16 hours using an under-agarose assay, thereby generating a highly confining environment with flattened cells, revealed that Dyrk3 accumulated in a cloud-like structure within the cytoplasm that co-localized with the two centrioles (Fig. 8A). Fluorescence intensity measurements along a 5 μ m long line that was centered to the centriole pair showed that the Dyrk3-EGFP signal was mainly distributed within a 2 μ m radius around the centrioles (Fig. 8B), indicating that Dyrk3 might directly act at the centrosome.

In order to investigate whether the protein kinase Dyrk3 directly acts on targets at the centrosome, phospho-proteome analysis of dendritic cells migrating in collagen networks under control conditions or upon Dyrk3 inhibition was performed by Dr. Petra Kameritsch (Walter Brendel Cen-

ter of Experimental Medicine, Munich, Germany) and Jingyuan Cheng (Institute of Innate Immunity, Bonn, Germany). For this purpose, custom-made migration chambers with a diameter of 10 cm were used to initiate simultaneous migration of 10 million bone marrow-derived dendritic cells embedded in a thin collagen layer towards a CCL19 source (Fig. 8C). Following phosphopeptide enrichment and depletion of the non-phosphorylated collagen, peptides were desalted, and phosphorylation was measured using mass spectrometry (MS) (Humphrey *et al.*, 2018; Kitata *et al.*, 2021). MS data analysis revealed various proteins to be differentially phosphorylated upon Dyrk3 inhibition compared to untreated controls.

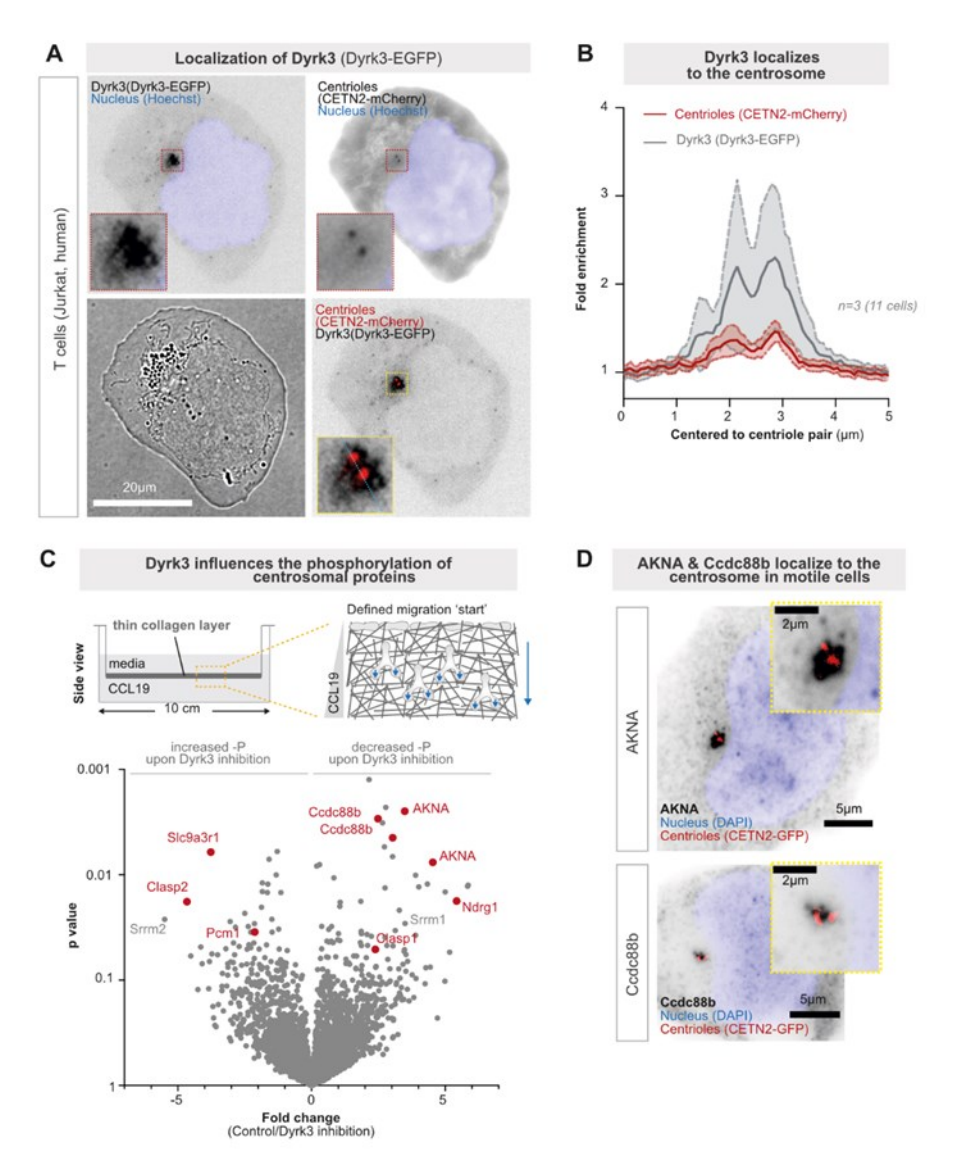


Figure 8: Dyrk3 localization and phosphoproteome analysis of migrating dendritic cells upon Dyrk3 inhibition. (A) Representative CETN2-mCherry (centriole pair; black and red; enlargement in yellow dashed box) Dyrk3-EGFP (black; enlargement in yellow dashed box) expressing Jurkat T cell stained with Hoechst (nucleus; blue) (B) Quantification of Dyrk3 localization by measuring the fluorescent intensity along a 5 μ m line (blue dotted line in A) centered to the centriole pair. Data represent mean \pm 95 % CI. (C) Scheme of the experimental setup for phosphoproteome analysis of migrating dendritic cells. Phosphoproteomics of migrating dendritic cells in collagen matrices (1.7 mg/ml collagen) along a CCL19 chemokine gradient in the presence of 5 μ M GSK-626616 or DMSO (control). Centrosomal proteins are highlighted in red. (D) Immunofluorescence staining of a representative CETN2-GFP (centriole pair; red) expressing Jurkat T cell stained with DAPI (nucleus; blue) and with AKNA or Ccdc88b (black), respectively. All data show representative cells from at least three independent biological replicates.

Among those, well-known Dyrk3 target proteins such as the splicing-associated proteins Serine/arginine repetitive matrix protein 1 (SRRM1) and Serine/arginine repetitive matrix protein 2 (SRRM2) were identified, confirming the effectiveness of the approach (Wippich *et al.*, 2013). In addition, several centrosomal proteins were found to be differentially phosphorylated when Dyrk3 was rendered non-functional, such as Pericentriolar material protein 1 (PCM1) which is required for centrosome assembly and function, as well as for recruitment of other centrosomal proteins (Dammermann & Merdes, 2002; Hames *et al.*, 2005). Similarly, the microtubule plus-end tracking proteins CLIP-associating protein 1 (CLASP1) and CLIP-associating protein 2 (CLASP2) that were shown to stabilize dynamic microtubules as well as the kinetochore during mitosis, could be identified (Lawrence *et al.*, 2020). Beside other more recently identified centrosomal proteins like AKNA and Ndrg1 (Kalaydjieva *et al.*, 2000; Kim *et al.*, 2004; Camargo Ortega *et al.*, 2019), proteins with annotated centrosomal localization like SLC9A3R1 and Ccdc88b (Cho *et al.*, 2022) were differentially phosphorylated upon Dyrk3 inhibition (Fig. 8C).

In order to confirm the centrosomal localization of Dyrk3-associated target proteins in motile cells, immunofluorescence staining for AKNA and Ccdc88b was performed in Jurkat T cells, that transiently expressed Centrin2-GFP as a marker for the two centrioles. Similar to Dyrk3 itself, both proteins exhibited a cloud-like centrosomal localization around the centriolar pair (Fig. 8D). Altogether, phospho-proteome analysis of migrating dendritic cells revealed that Dyrk3 not only localizes to the centrosome but also directly influences the phosphorylation of different centrosomal proteins in motile cells.

3.2.3 DYRK3 IMPAIRMENT ALTERS DIFFUSION DYNAMICS OF CENTROSOMAL PROTEINS

Given the role of Dyrk3 as a biomolecular condensate dissolvase and the condensate-like nature of the pericentriolar material (PCM) (Wippich *et al.*, 2013; Woodruff *et al.*, 2017; Rai *et al.*, 2018), I next tested whether Dyrk3 also regulates the physical properties of the centrosome. For this purpose, fluorescence recovery after photobleaching (FRAP) of different centrosomal proteins was performed to measure protein diffusion properties. In general, individual molecules of liquid condensates are more dynamic and show more internal rearrangement as well as more external exchange with the surrounding solution. In contrast, the more solid-like condensates become, the more they lack this dynamic behavior (Banani *et al.*, 2017; Shin & Brangwynne, 2017). For FRAP experiments, a fluorescently tagged protein is fully bleached within a defined area, followed by measurement of fluorescence signal recovery over time afterwards. More dynamic proteins show faster and higher rates of signal recovery, indicating faster diffusion, whereas proteins with lower diffusion rates display reduced internal and cytosolic exchange, and therefore also lower recovery rates.

To investigate whether Dyrk3 regulates the biophysical properties of the centrosome, Jurkat T cells were transiently transfected via electroporation with fluorescently labeled constructs encoding CEP120, Dyrk3, Pericentrin (PCNT), and Akna. After 16 hours upon electroporation, allowing sufficient time for the expression of the fluorescently tagged proteins, FRAP experiments were conducted under control conditions or in the presence of the Dyrk3 inhibitor GSK-626616. For this purpose, the initial fluorescence intensity was measured before completely bleaching the entire centrosomal area. Subsequently, signal recovery was recorded every second initially, and then every five seconds until a plateau was reached. Fluorescence signal recovery, and therefore diffusion properties, of the less diffusive proteins PCNT (Fig. 9A), which acts as scaffold protein of the pericentriolar material (Lawo *et al.*, 2012; Mennella *et al.*, 2012), and AKNA (Fig. 9B) remained unaffected when Dyrk3 was rendered non-functional (Fig. 9, A, B, and E). In contrast, the rather

quick diffusion properties of Dyrk3 itself in a range of 80 % signal recovery after 60 seconds under control conditions, were decreased when Dyrk3 function was inhibited, although accompanied by Dyrk3 accumulation around the centrosome compared to controls (Fig. 9, C and E). Similarly, CEP120 which was selected due to its well-known fast diffusion properties (Cheng *et al.*, 2023), showed significantly reduced diffusion, from 50 % signal recovery after two minutes to approximately 30 % recovery upon rendering Dyrk3 non-functional (Fig. 9, D and E). Together, these results indicate that Dyrk3 inhibition leads to reduced diffusion of PCM-associated proteins, thus suggesting altered centrosomal material properties and a potential shift to a more solid-like state.

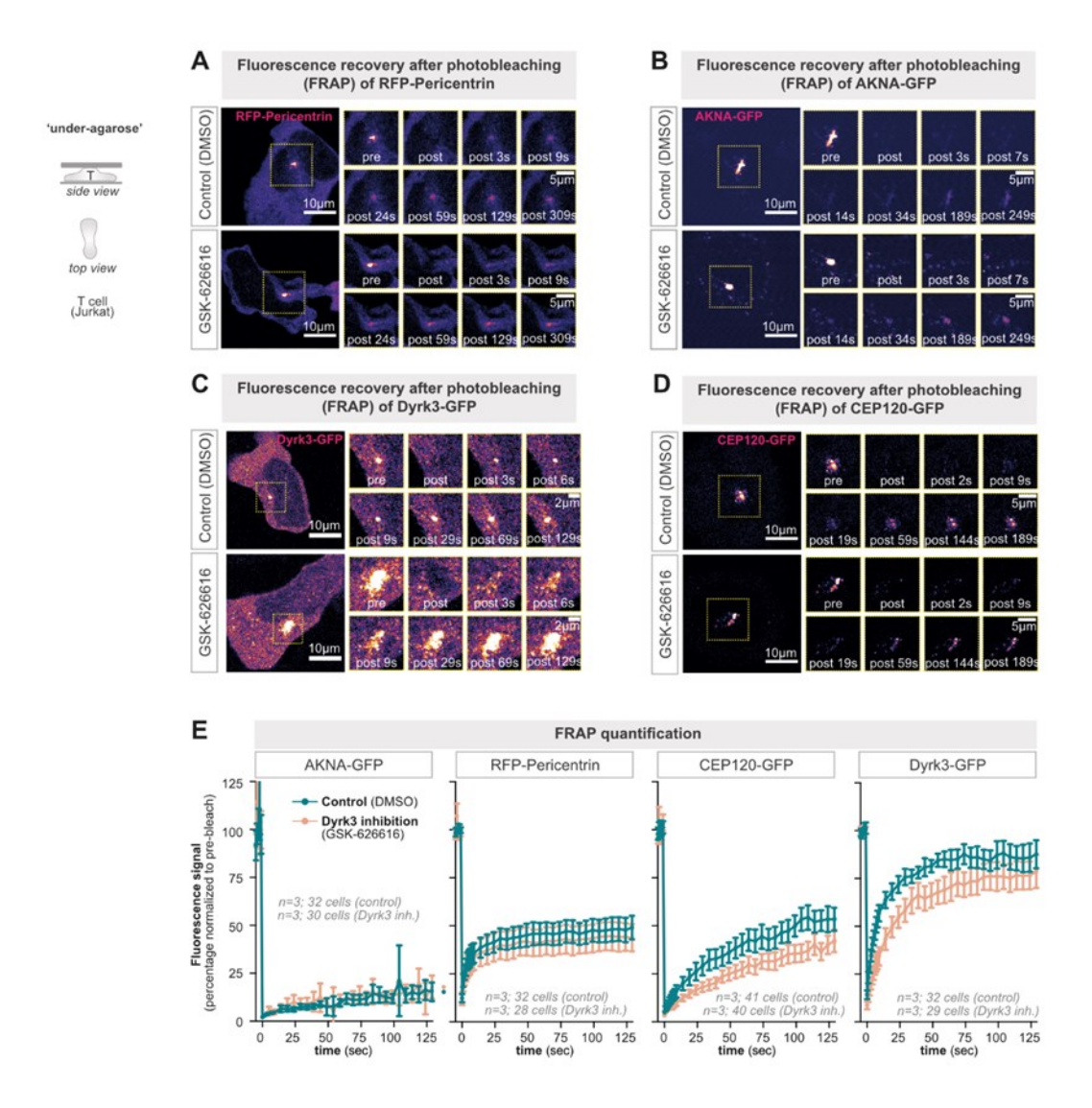


Figure 9: Fluorescence recovery after photobleaching (FRAP) of centrosomal proteins. (A) Representative RFP-Pericentrin (fire-color coded; enlargement in yellow dashed boxes) expressing Jurkat T cells before, immediately after, and for an extended time after bleaching of the Pericentrin signal in the presence of 5 μ M GSK-626616 or DMSO (control). (B) Representative AKNA-GFP (fire-color coded; enlargement in yellow dashed boxes) expressing Jurkat T cells before, immediately after, and for an extended time after bleaching of the AKNA signal in the presence of 5 μ M GSK-626616 or DMSO (control). (C) Representative Dyrk3-GFP (fire-color coded; enlargement in yellow dashed boxes) expressing Jurkat T cells before, immediately after, and for an extended time after bleaching of the Dyrk3 signal in the presence of 5 μ M GSK-626616 or DMSO (control). (D) Representative CEP120-GFP (fire-color coded; enlargement in yellow dashed boxes) expressing Jurkat T cells before, immediately after, and for an extended time after bleaching of the CEP120 signal in the presence of 5 μ M GSK-626616 or DMSO (control). (E) Quantification of fluorescence signal recovery after photobleaching as shown in (A-D). Data represent mean ± 95 % CI. All data derive from at least three independent biological replicates.

3.2.4 THE CENTROSOME FRACTURES DURING CELLULAR PATHFINDING IN THE ABSENCE OF DYRK3 ACTIVITY

Based on the idea that Dyrk3 regulates the molecular as well as physical properties of the centrosome, I next hypothesized that Dyrk3 might be critical for maintaining centrosome stability when experiencing cellular motility forces. Therefore, CETN2-GFP-expressing dendritic cells were liveimaged during migration in microchannels with different designs under control conditions or in the presence of the Dyrk3 inhibitor GSK-626616. As a control for facing low motility forces, migrating DCs were imaged in wide straight paths that do not require the formation of multiple cell fronts or extensive cell navigation. Regardless of rendering Dyrk3 non-functional, centrioles remained in close proximity of around one micrometer and moved synchronously during migration along the unidirectional paths (Fig. 10A). Similarly, centriolar pairs of dendritic cells migrating in more complex channel designs with path junctions, where cells would experience higher motility forces, were typically located in close proximity before cells entered the path junctions. However, once Dyrk3-inhibited cells encountered multiple path options, where they would typically explore most of the available paths with multiple protrusions at the same time, the centriolar pair frequently broke into far-distantly located and individually moving centrioles when Dyrk3 was nonfunctional (Fig. 10B). Centrosome breakage was sudden and fast, with separation velocities in the range of around 6 micrometers per minute, indicating strong opposing forces that fracture the centrosome (Fig. 10C). Based on previous publications, I considered centrosome fracturing in the following for a centriolar distance of more than 1.5 µm. Occasional centrosome fracturing was also observed in two cases for control cells in path junctions, yet the frequency of such events barely reached 0.5 events/hour, and maximal measured centriole distances were four and ten micrometers, respectively (Fig. 10, D and E). In contrast, the fracturing frequency was significantly increased upon Dyrk3 inhibition to 0.8 to 1.5 events/hour, and maximal centriole distances ranged up to almost 60 micrometers in some cases (Fig. 10, D and E). For dendritic cells migrating along unidirectional paths, a single event of centrosome fracturing with a centriolar distance of around 2 micrometers was detected under control conditions (Fig. 10E), indicating that inactive Dyrk3 did not cause major effects on the integrity of the centrosome in this less complex microenvironment. Altogether, these findings show that centrosomes are prone to mechanical breakage when Dyrk3 is not active and dendritic cells navigate their path in complex microenvironments.

3.3 Mechanical centrosome fracturing

3.3.1 THE CENTROSOMAL LINKER PROTEIN C-NAP1 IS REQUIRED FOR CENTROSOME COHESION DURING CELLULAR PATHFINDING

The centriolar pair at the center of the centrosome is well-known to be connected via a protein-based linker. This linker is composed of a network of intertwined Rootletin/CEP68 filaments attached to C-Nap1 that acts as a filament anchor at the proximal end of centrioles (Fry et al., 1998; Mayor et al., 2000; Bahe et al., 2005; Graser et al., 2007; Vlijm et al., 2018). Additional, less well-characterized proteins that are implicated in centrosome cohesion are LRRC45 and CEP215 (Graser et al., 2007; He et al., 2013). To investigate whether this protein-based linker mechanism is also involved in maintaining centrosome integrity under mechanical motility forces, a conditional CRISPR/Cas9-based knockout of C-NAP1 (CEP250) in CETN2-GFP-expressing dendritic cells was generated by Peter Konopka and Prof. Eva Kiermaier (LIMES Institute, Bonn, Germany).

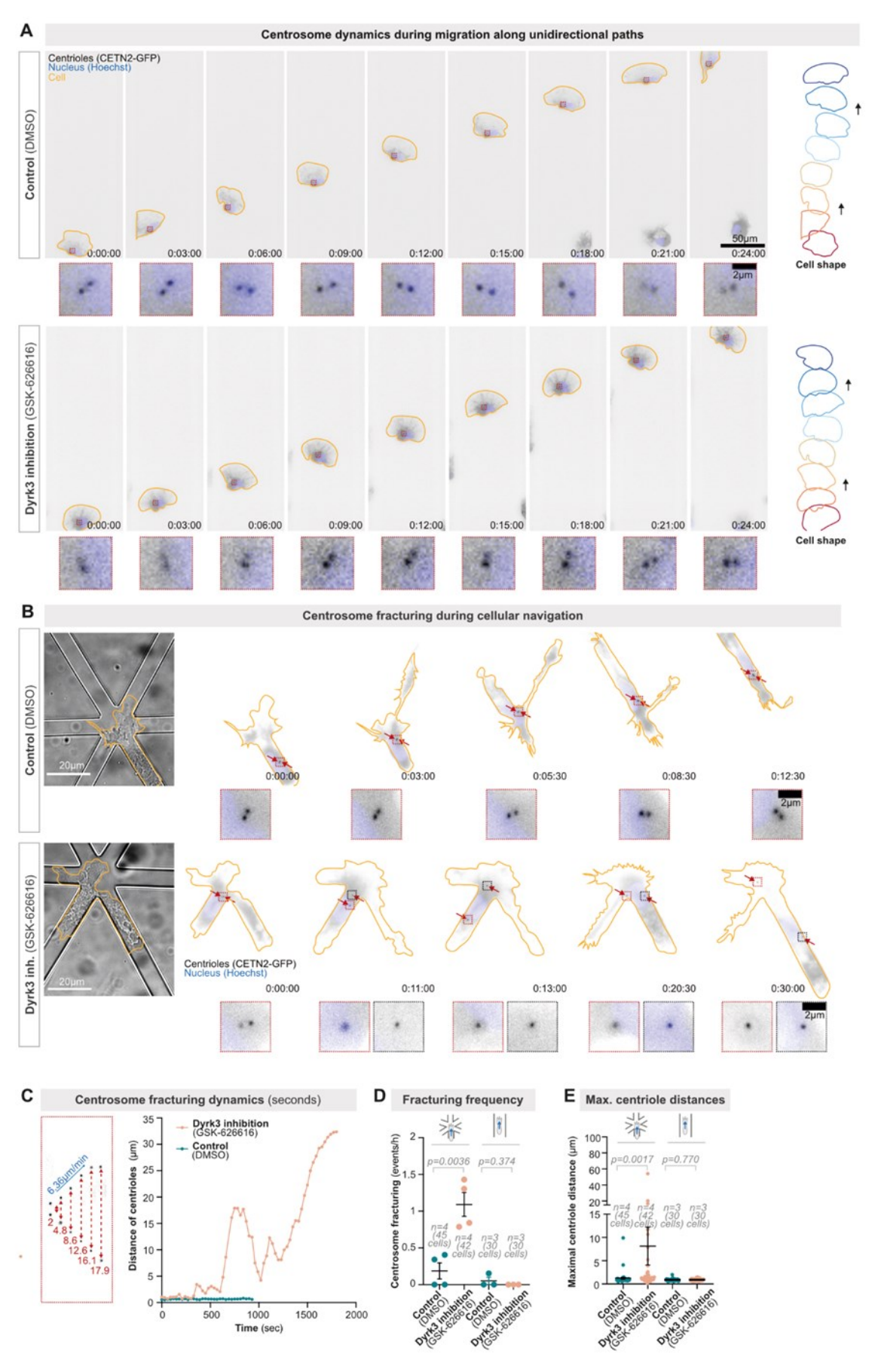


Figure legend on next page

Figure 10: Centrosome deformation dynamics and fracturing frequency during dendritic cell migration upon Dyrk3 inhibition. (A) Representative CETN2-GFP (centriole pair; black; indicated by red arrows; enlargement in red dashed boxes) expressing dendritic cells (DCs) stained with Hoechst (nucleus; blue) migrating along a wide unidirectional straight path (linear microchannel) in the presence of 5 μ M GSK-626616 or DMSO (control). (B) Representative CETN2-GFP (centriole pair; black; enlargement in red dashed boxes) expressing dendritic cells (DCs) stained with Hoechst (nucleus; blue) migrating along a 6-way path junction in the presence of 5 μ M GSK-626616 or DMSO (control). Note the far-distant separation of the two centrioles in the presence of 5 μ M GSK-626616. (C) Representative quantification of centrosome fracturing, showing the detailed velocity of the separation of the centriole pair. (D) Quantification of the centrosome fracturing frequency during dendritic cell migration along 6-way path junctions or wide unidirectional straight paths in the presence of 5 μ M GSK-626616 or DMSO (control). Data represent mean \pm SEM, unpaired test. (E) Quantification of the maximal distance between individual centrioles during dendritic cell migration along 6-way path junctions or wide unidirectional straight paths in the presence of 5 μ M GSK-626616 or DMSO (control). Data represent mean \pm SEM, Mann-Whitney. All data show representative cells from at least three independent biological replicates. Time is indicated as h:min:s.

Upon addition of doxycycline during cell differentiation, Cas9 expression under the control of a Tet-on operator was induced, and due to stable expression of a CEP250-sgRNA also subsequent Cas9 targeting of the CEP250 locus. Therefore, I live-imaged C-Nap1-depleted as well as Dyrk3-inhibited CETN2-GFP expressing dendritic cells during migration in path junctions (Fig. 11A). Analysis of centriole dynamics revealed an increased distance between the two centrioles already during migration in the linear path before cells entered the path junctions. Upon transition of the path junction, centriolar distance was significantly increased. Similarly, the fracturing frequency of Dyrk3-inhibited cells was more pronounced when cells entered a path junction compared to before the junction (Fig. 11B).

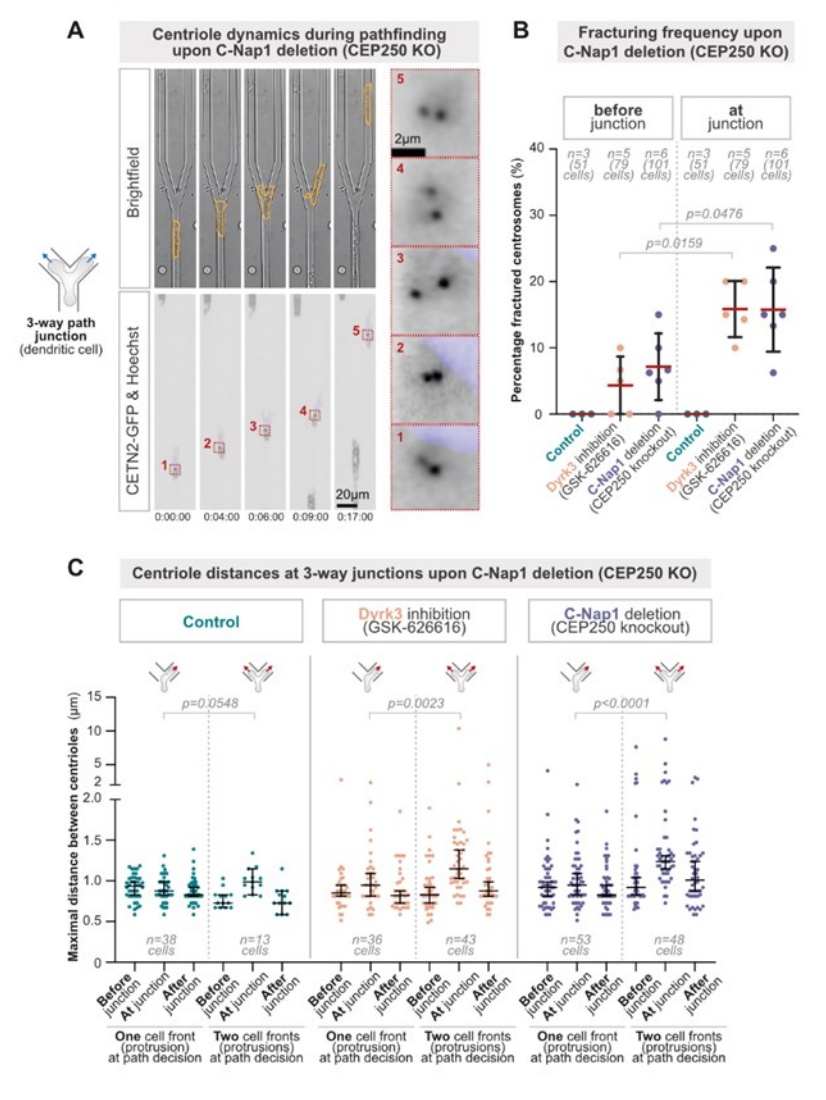


Figure 11: Centrosome deformation dynamics and fracturing frequency during dendritic cell migration upon C-Nap1 deletion. (A) Representative CETN2-GFP (centriole pair; black; enlargement in red dashed boxes) expressing C-Nap1-deficient dendritic cells (DCs) stained with Hoechst (nucleus; blue) migrating along a 3-way path junction. (B) Quantification of the centrosome breakage frequency during dendritic cell migration before and during passing a 3-way path junction in the presence of 5 μ M GSK-626616 or control (DMSO), or upon C-Nap1 deletion. Data represent median \pm 95 % CI, Mann-Whitney. (C) Quantification of the maximal distance between individual centrioles before, during, and after migration through path junctions of cells that pass the junction either with two simultaneous explorative protrusions or dendritic cells that immediately decide for one path alternative with one protrusion, in the presence of 5 μ M GSK-626616 or control (DMSO), or upon C-Nap1 deletion. Data represent median \pm 95 % CI, Mann-Whitney. All data show representative cells from at least three independent biological replicates. Time is indicated as h:min:s.

Next, I investigated whether this centrosome fracturing in C-Nap1-depleted cells was due to motility forces generated by two competing cellular protrusions during path navigation. For this purpose, centriolar fracturing rates were analyzed in C-Nap1-depleted and Dyrk3-inhibited cells that migrated either with one or two protrusions through the path junctions. Again, specifically C-Nap1-depleted cells that explored the path junctions with two competing protrusions showed increased centriolar distances and fracturing rates during path navigation. In contrast, C-Nap1-depleted cells migrating with one cell front showed stable centriole distances around one micrometer before, at, and after the path junction (Fig. 11C). Similar to the rates of centrosome breakage, Dyrk3-inhibited cells showed a similar behavior as C-Nap1-depleted cells, with an increase in centriolar distances only when cells encountered a path junction with two competing cell fronts. (Fig. 11C) Together, these data demonstrate that C-Nap1 is required to maintain the mechanical stability of the centrosome during cellular pathfinding. In addition, the role of Dyrk3 for centrosome cohesion during migration in complex environments was confirmed.

3.3.2 ACTOMYOSIN FORCES FRACTURE THE CENTROSOME

In order to identify the source of intracellular forces causing centrosome breakage, I next focused on the actomyosin cytoskeleton. Actin is known to be located at the centrosome of lymphocytes and dendritic cells, where the centrosome organizes a local network of actin filaments which, in turn, are inversely correlated with the number of centrosomal microtubules (Farina et al., 2016; Inoue et al., 2019; Weier et al., 2022). Furthermore, actomyosin forces have been shown to be implicated in centriole separation during cell cycle progression by modulating direction, distance, and time of centriole separation, as well as PLK4 recruitment to the centrosome (Vitiello et al., 2019). Therefore, I treated CETN2-GFP expressing dendritic cells migrating through path junctions either with the myosin inhibitor para-nitroblebbistatin (Képiró et al., 2014) or the actin inhibitor Latrunculin A upon Dyrk3 inhibition or C-Nap1 depletion, respectively (Fig. 12, A and B). Of note, treatment with low doses of Latrunculin A still allows cell migration. Notably, centrosome fracturing rates were clearly reduced from 16 % in only Dyrk3-inhibited cells to approximately 3 % upon myosin inhibition in cells without functional Dyrk3. Interestingly, this effect was even more striking when actin polymerization was blocked using Latrunculin A, thereby completely preventing any centrosomal breakage in Dyrk3-inhibited cells (Fig. 12C). Additionally, inhibition of myosin contractility in C-Nap1-depleted cells led to a decrease in centriolar fracturing rates. However, this effect was considerably less pronounced compared to Dyrk3 inhibited cells. Yet, inhibition of actin polymerization in the presence of Latrunculin A strongly reduced centrosome fracturing from around 17 % under control conditions to approximately 2 % upon actin inhibition during cellular pathfinding of C-Nap1-depleted cells (Fig. 12C). Thus, these data suggest that forces from the actomyosin cytoskeleton can lead to centrosome fracturing.

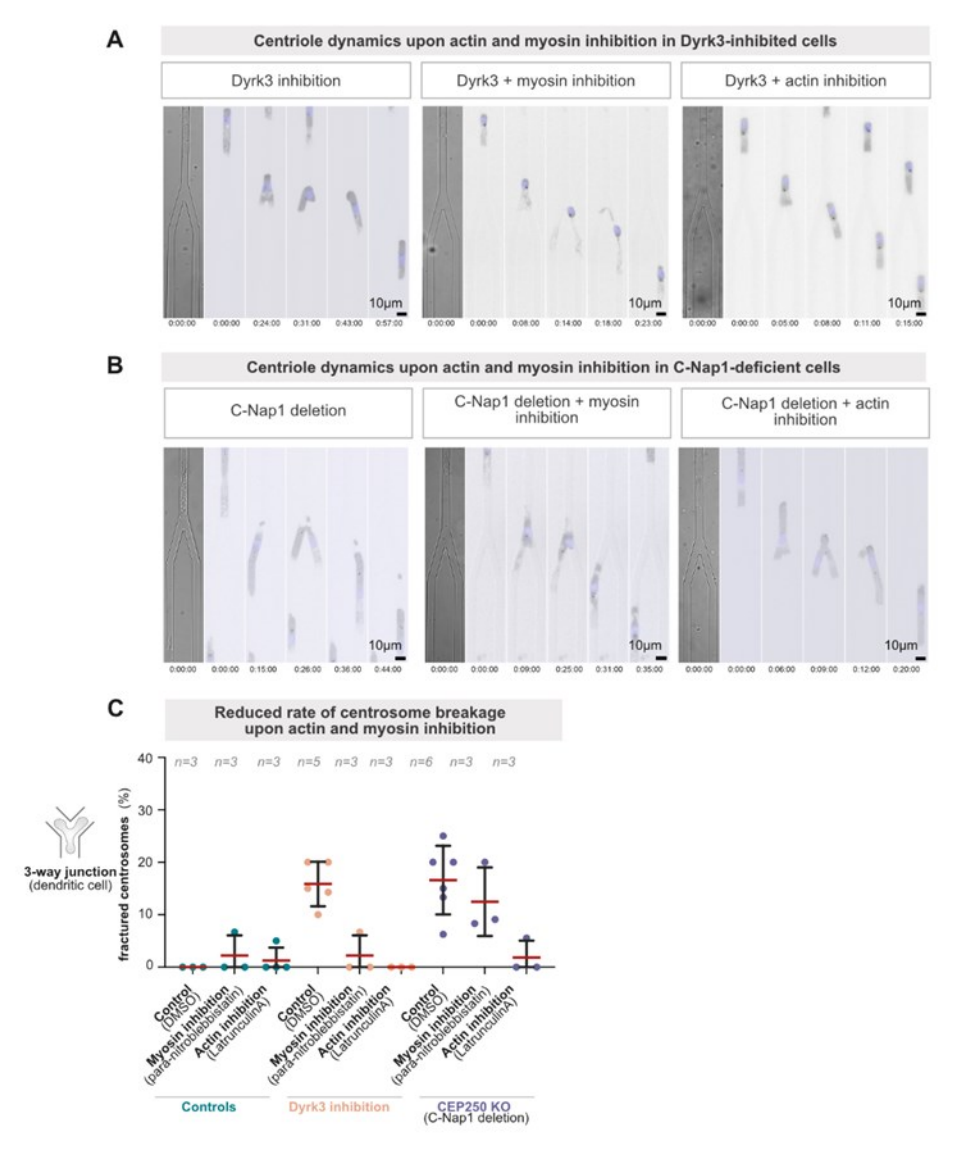


Figure 12: Inhibition of actomyosin forces upon centrosome fracturing. (A) Representative CETN2-GFP (centriole pair; black) expressing dendritic cells (DCs) stained with Hoechst (nucleus; blue) migrating along a 3-way path junction in the presence of 5 μM GSK-626616 and 25 μM para-nitroblebbistatin (myosin-II inhibition) or 5 μM GSK-626616 and 50 nM Latrunculin A (actin inhibition). **(B)** Representative CETN2-GFP (centriole pair; black) expressing C-Nap1-deficient DCs stained with Hoechst (nucleus; blue) migrating along a 3-way path junction in the presence of 25 μM para-nitroblebbistatin (myosin-II inhibition) or 50 nM Latrunculin A (actin inhibition). **(C)** Quantification of the centrosome breakage frequency during dendritic cell migration along a 3-way path junction in the presence of 5 μM GSK-626616 or control (DMSO), or upon C-Nap1 deletion, and in co-presence of 25 μM para-nitroblebbistatin, 50 nM Latrunculin A, or control (DMSO). Data represent mean \pm SD. All data show representative cells from at least three independent biological replicates. Time is indicated as h:min:s.

Next, I investigated whether these actomyosin-based forces do not only affect the centriolar pair but also on the surrounding pericentriolar material (PCM). For this purpose, I generated dendritic cells that stably expressed the PCM marker Pericentrin-dTomato and PCM shape was analyzed during cellular pathfinding through path junctions either under control conditions or upon inhibition of actin polymerization using Latrunculin A (Fig. 13A). For PCM shape analysis, the Pericentrin-dTomato signal was segmented using the machine-learning-based image analysis software ilastik (Berg *et al.*, 2019), followed by extraction and cell position-based mapping of different shape descriptors during migration along a path junction in collaboration with Dr. Robert Hauschild (IST, Vienna, Austria) (Fig. 13B). This revealed that the different shape descriptor values were overall fluctuating during cellular locomotion along the linear path, which is consistent

with a deformable and deforming biomolecular condensate. However, circularity, solidity, and roundness were specifically decreased at the path junction, whereas the skeleton length was increased under control conditions. Since the PCM was less round and more elongated at the path junction, these data suggest that the PCM is particularly subject to deformations during cell navigation through path junctions. Yet, this specific decrease of circularity and roundness, and increase of elongation, respectively, was only transient, as the initial shape was restored once cells fully passed the junction (Fig. 13B). In contrast, upon actin inhibition, cells showed an increased circularity, solidity, and roundness, as well as an unaffected skeleton length compared to controls when cells entered the path junction, suggesting that the PCM was not specifically deformed anymore during pathfinding when actin polymerization was inhibited (Fig. 13B). Overall, these data indicate that the forces exerted by the actomyosin cytoskeleton can not only cause centrosome fracturing but are also able to deform the surrounding pericentriolar material.

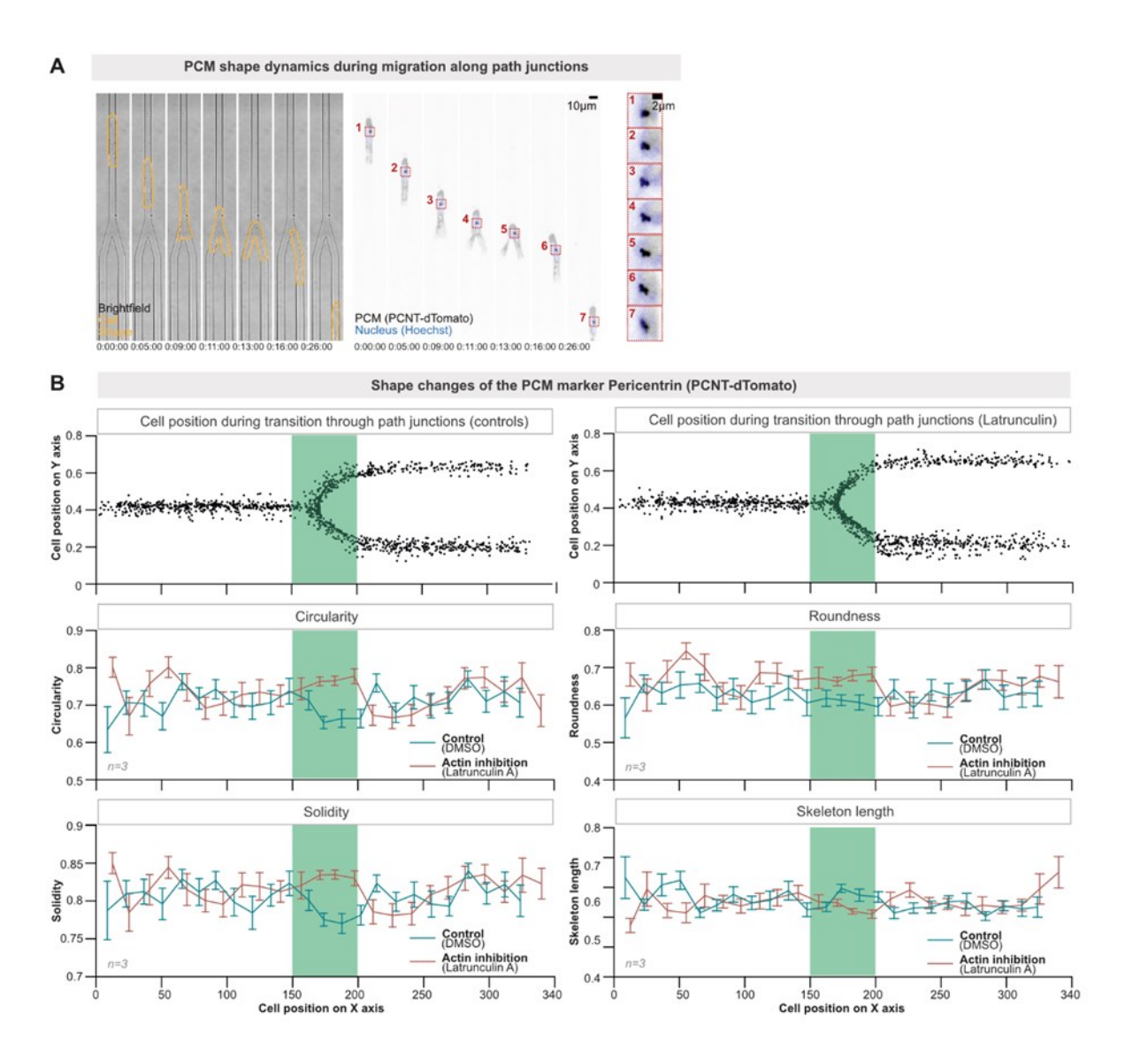


Figure 13: Pericentriolar material shape deformations during dendritic cell migration. (A) Representative Pericentrin-dTomato (pericentriolar material (PCM); black; enlargement in red dashed boxes) expressing dendritic cells (DCs) stained with Hoechst (nucleus; blue) migrating along a 3-way path junction. Note the frequent PCM shape deformations during migration. **(B)** Quantification of PCM shape changes during dendritic cell migration along 3-way path junctions in the presence of 50 nM Latrunculin A or DMSO (control). Data represent mean ± SD. All data show representative cells from at least three independent biological replicates. Time is indicated as h:min:s.

3.4 CENTROSOME FRACTURING GENERATES COEXISTING MTOCS

Permanent centrosome depletion often results in surprisingly mild cellular phenotypes, as other organelles such as the Golgi membrane are able to function as alternative microtubule organizing centers (MTOCs) (Chabin-Brion et al., 2001). The findings of centrosome fracturing raised the possibility that the consequences of fractured centrosomes are entirely different from the consequences of the non-functionality of the entire centrosome. In order to investigate this possibility, the basic features of intact centrosomes were first characterized using immunofluorescence staining for alpha-tubulin (α -tubulin) marking the microtubule filaments, gamma-tubulin (γ -tubulin) as a well-established PCM marker, and the microtubule-anchoring protein (Piel et al., 2000; Bornens, 2002). For this purpose, I established a stimulated-emission depletion (STED)-suitable immunofluorescence staining protocol for microtubules, that preserved microtubule integrity and prevented filament disintegration. Super-resolution-based STED microscopy of microtubules revealed that the centriolar pair localized to the center of the microtubule asters (Fig. 14A). To analyze the symmetry of the signal distribution of α -tubulin, γ -tubulin, and ninein around the individual centrioles of one pair, fluorescence intensities in a defined area around the centrioles were measured and set in relation to each other. While α - and γ -tubulin were only slightly more present around one centriole compared to the other, the microtubule anchoring protein ninein asymmetrically localized more to one of the centrioles (Fig. 14B), which is consistent with ninein being described as a marker for mother centrioles (Piel et al., 2000).

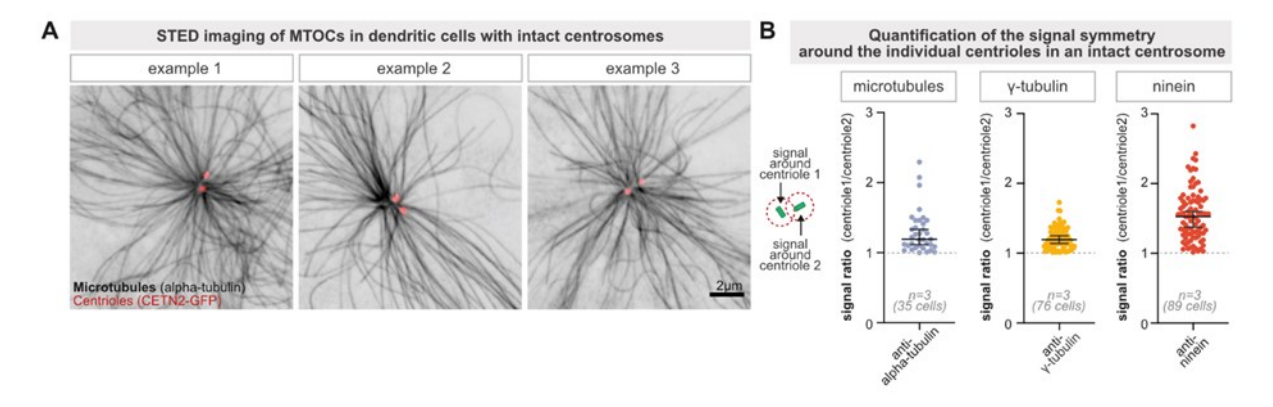


Figure 14: Characterization of intact centrosomes in dendritic cells. (A) Representative stimulated emission depletion (STED) images of microtubules stained with alpha-tubulin (black) in CETN2-GFP (centriole pair; red) expressing dendritic cells (DCs) with intact centrosomes. (B) Quantification of signal symmetry of microtubules, the microtubule nucleator gamma-tubulin, and the microtubule anchoring protein ninein around individual centrioles in intact centrosomes. Data represent median \pm 95 % CI. All data show representative cells from at least three independent biological replicates.

Next, the microtubule nucleation capacities of intact centrosomes were further analyzed by live-cell imaging of dendritic cells stably expressing the microtubule plus-end marker EB3, thereby visualizing the growing microtubule tips (Fig. 15A) (Efimov *et al.*, 2007; Renkawitz *et al.*, 2019; Kopf *et al.*, 2020). Tracking of the EB3-positive microtubule plus-ends in collaboration with Dr. Robert Hauschild (IST, Vienna, Austria) revealed efficient microtubule nucleation under control conditions. Under control conditions, the number of EB3 comets ranged between 100 to 150 comets per cell (Fig. 15B), while the velocity of these comets was approximately 25 micrometers per minute (Fig. 15C). Neither EB3 comet number nor comet velocity were affected by Dyrk3 inhibition (Fig. 15, B and C), indicating that Dyrk3 does not influence the microtubule nucleation capacities of intact centrosomes.

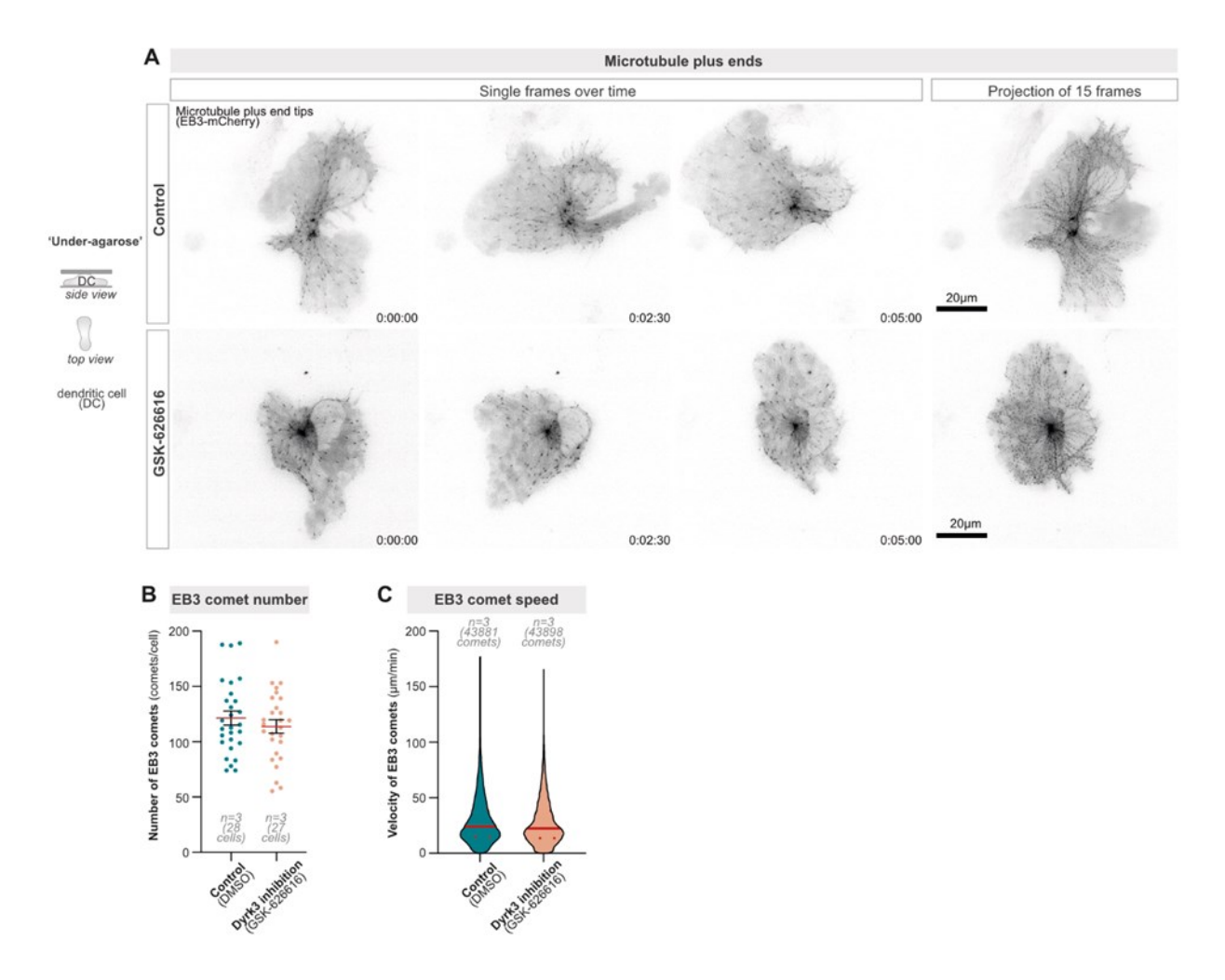


Figure 15: Microtubule nucleation in intact centrosomes. (A) Live-cell imaging examples of representative EB3-mCherry (microtubule-plus end tip marker; black) expressing DCs in the presence of 5 μ M GSK-626616 or DMSO (control). (B) Quantification of EB3 comet numbers (microtubule plus ends) as shown in (D). Data represent mean \pm SEM. (C) Quantification of EB3 comet velocity. Data represent median and interquartile range. All data show representative cells from at least three independent biological replicates. Time is indicated as h:min:s.

To investigate the effect of centrosome fracturing on the centrosome's function as microtubule organizing center (MTOC), I visualized the microtubule cytoskeleton of fractured centrosomes in CETN2-GFP expressing dendritic cells using immunofluorescence staining (Fig. 16A). For this purpose, the under-agarose migration assay was modified by embedding small six micrometer-sized beads as path obstacles between the layer of agarose and the glass coverslip, thereby generating a confined environment requiring cells to navigate around the bead obstacles and favoring centrosome fracturing. Surprisingly, upon centrosome fracturing, single distant centrioles formed two separate MTOCs, from which microtubules radially distributed in an aster-like manner, in approximately 90 % of cells, whereas only in 10 % of cells a single MTOC was detected. If a further distinction was also drawn between equally sized and unequally sized MTOCs, two equally sized MTOCs were found in 60 %, and one larger together with one smaller MTOC were found in 30 % of cells. Of note, no cell that entirely lost its capacity to nucleate microtubules was identified (Fig. 16B). Together, these results suggested the intriguing possibility that individual centrioles can form two coexisting functional MTOCs within one motile cell upon centrosome fracturing.

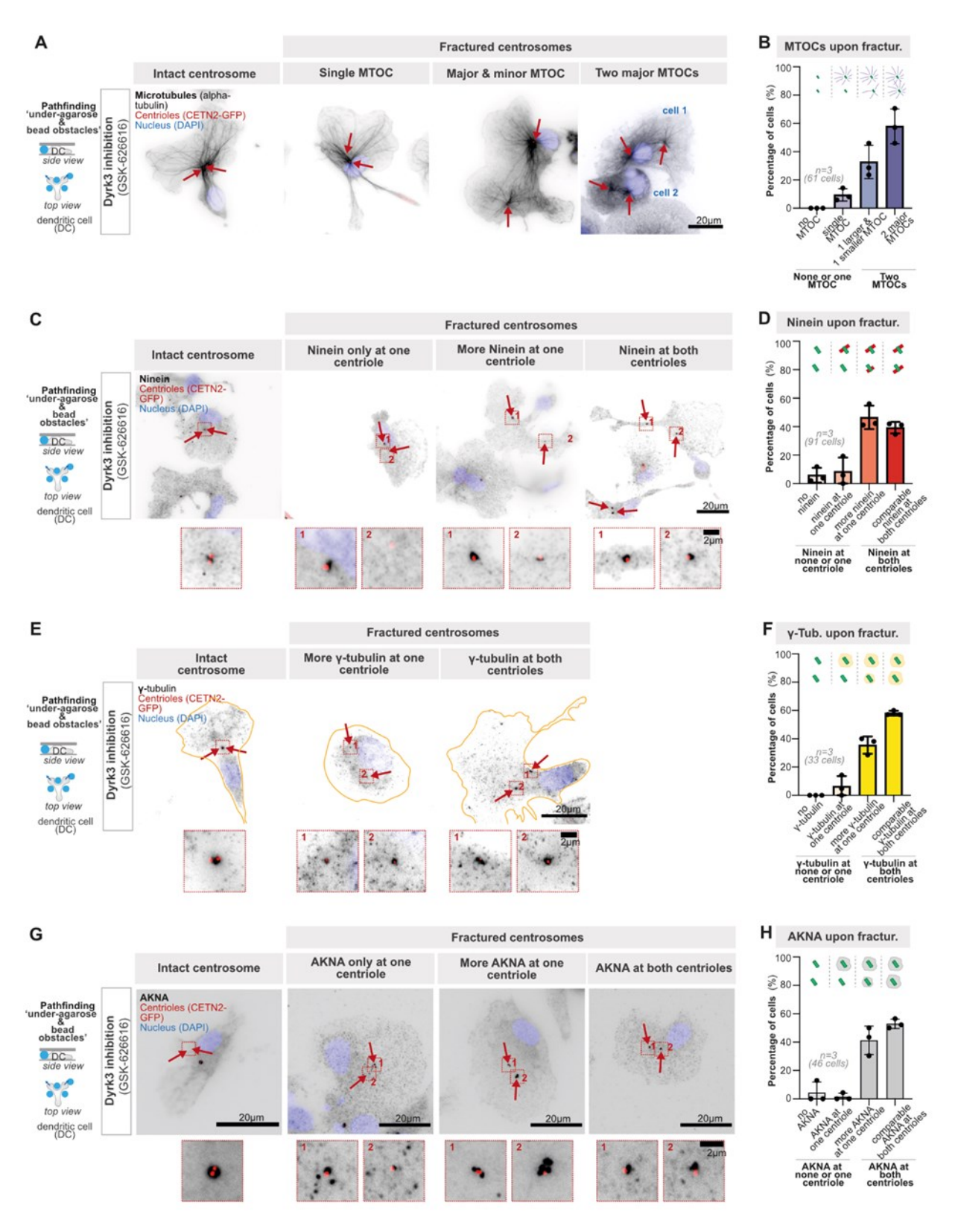


Figure 16: Characterization of individual centrioles upon centrosome fracturing. (A) Immunofluorescence staining of representative CETN2-GFP (centriole pair; red; indicated by red arrows) expressing dendritic cells (DCs) stained with DAPI (nucleus; blue) and with anti-alpha-tubulin (black) in the presence of 5 μ M GSK-626616. (B) Quantification of microtubule aster formation upon centrosome fracturing as shown in (A). Data represent mean \pm SD. (C) Immunofluorescence staining of representative CETN2-GFP (centriole pair; red; indicated by red arrows; enlargement in red dashed boxes) expressing dendritic cells (DCs) stained with DAPI (nucleus; blue) and with anti-ninein (black) in the presence of 5 μ M GSK-626616. (D) Quantification of the microtubule anchoring protein ninein upon centrosome fracturing as shown in (C). Data represent mean \pm SD. (E) Immunofluorescence staining of representative CETN2-GFP (centriole pair) as shown in (C).

triole pair; red; indicated by red arrows; enlargement in red dashed boxes) expressing dendritic cells (DCs) stained with DAPI (nucleus; blue) and with anti-gamma-tubulin (black) in the presence of 5 μ M GSK-626616. **(F)** Quantification of the microtubule nucleator gamma-tubulin upon centrosome fracturing as shown in (E). Data represent mean \pm SD. (G) Immunofluorescence staining of representative CETN2-GFP (centriole pair; red; indicated by red arrows; enlargement in red dashed boxes) expressing dendritic cells (DCs) stained with DAPI (nucleus; blue) and with anti-AKNA (black) in the presence of 5 μ M GSK-626616. **(H)** Quantification of the centrosome-associated protein AKNA upon centrosome fracturing as shown in (G). Data represent mean \pm SD. All data show representative cells from at least three independent biological replicates.

By immunofluorescence staining of additional MTOC markers, the functionality of these coexisting MTOCs was further characterized. To test their microtubule anchoring capacity, ninein was imaged as a major microtubule anchoring protein at the centrioles (Fig. 16C), revealing that ninein mostly localized to both centrioles upon fracturing. In 40 % of cells, a comparable amount of ninein was found at both centrioles, and in addition approximately 50 % of cells showed a ninein signal at both single centrioles with being more present at one centriole. In contrast, no ninein signal or ninein at only one centriole were detected in less than 10 % of cells with fractured centrosomes (Fig. 16D). Overall, the distribution of ninein upon centrosome breakage shows a functional microtubule anchoring capacity of both coexisting MTOCs. Similarly, the PCM component and microtubule nucleator γ-tubulin frequently localized to both centrioles upon fracturing in around 60 % of cells. In more than 30 % of cells, γ-tubulin was more prominent at one centriole compared to the other, and in less than 10 %, y-tubulin could be detected at only one centriole. Again, no cells without y-tubulin, and therefore presumably without PCM were found, indicating that upon centrosomal breakage, both centrioles typically retain pericentriolar material (Fig. 16, E and F). In addition, the microtubule organizing protein AKNA, that has been identified more recently (Camargo Ortega et al., 2019) and is less phosphorylated upon Dyrk3 inhibition (Fig. 8C), is also localized equally to both centrioles in more than 50 % of cells, and more pronounced to one centriole in approximately 40 % of cells. In less than 10 % of cells, no AKNA signal could be detected following centrosome breakage (Fig. 16, G and H).

Altogether, these data show that in the majority of cells upon centrosome fracturing, the single centrioles are not only able to nucleate microtubules but also to efficiently anchor them. Furthermore, they are equipped with their own pericentriolar material and typical centrosome-associated proteins. Thus, the fracturing of the centrosome leads to the emergence of two simultaneously coexisting functional microtubule organizing centers within a single cell.

3.5 CENTROSOME FRACTURING IMPEDES CELLULAR NAVIGATION

3.5.1 MECHANICALLY UNSTABLE CENTROSOMES IMPAIR CELLULAR PATHFINDING

Singular microtubule organizing centers function as steering organelles during cellular locomotion, for instance by facilitating microtubule-based cell shape control upon migration in complex microenvironments, thereby preventing cellular entanglement and cell body fragmentation (Kopf et al., 2020). Therefore, I next investigated the functional consequences of two coexisting MTOCs upon centrosome fracturing within a single cell for cellular movement. For this purpose, dendritic cell migration velocities were analyzed during migration in microchannel designs of varying complexity either under control conditions or upon rendering Dyrk3 non-functional, thus rendering the centrosome prone to breakage. During migration along wide unidirectional paths that do not require cellular navigation and formation of multiple protrusions (Fig. 17A), and thus do not spe-

cifically favor centrosomal fracturing, dendritic cell migration velocities of approximately 8 micrometers per minute were unaffected by inhibition of Dyrk3 (Fig. 17C). Similarly, rendering Dyrk3 non-functional upon migration along narrow straight paths did not affect migration velocities of 5 micrometers per minute (Fig. 17, B and C). The overall lower migration velocities upon migration in 8 micrometer-wide compared to 50 micrometer-wide unidirectional paths could presumably be induced by the higher degree of confinement that cells are experiencing in more narrow microchannel designs.

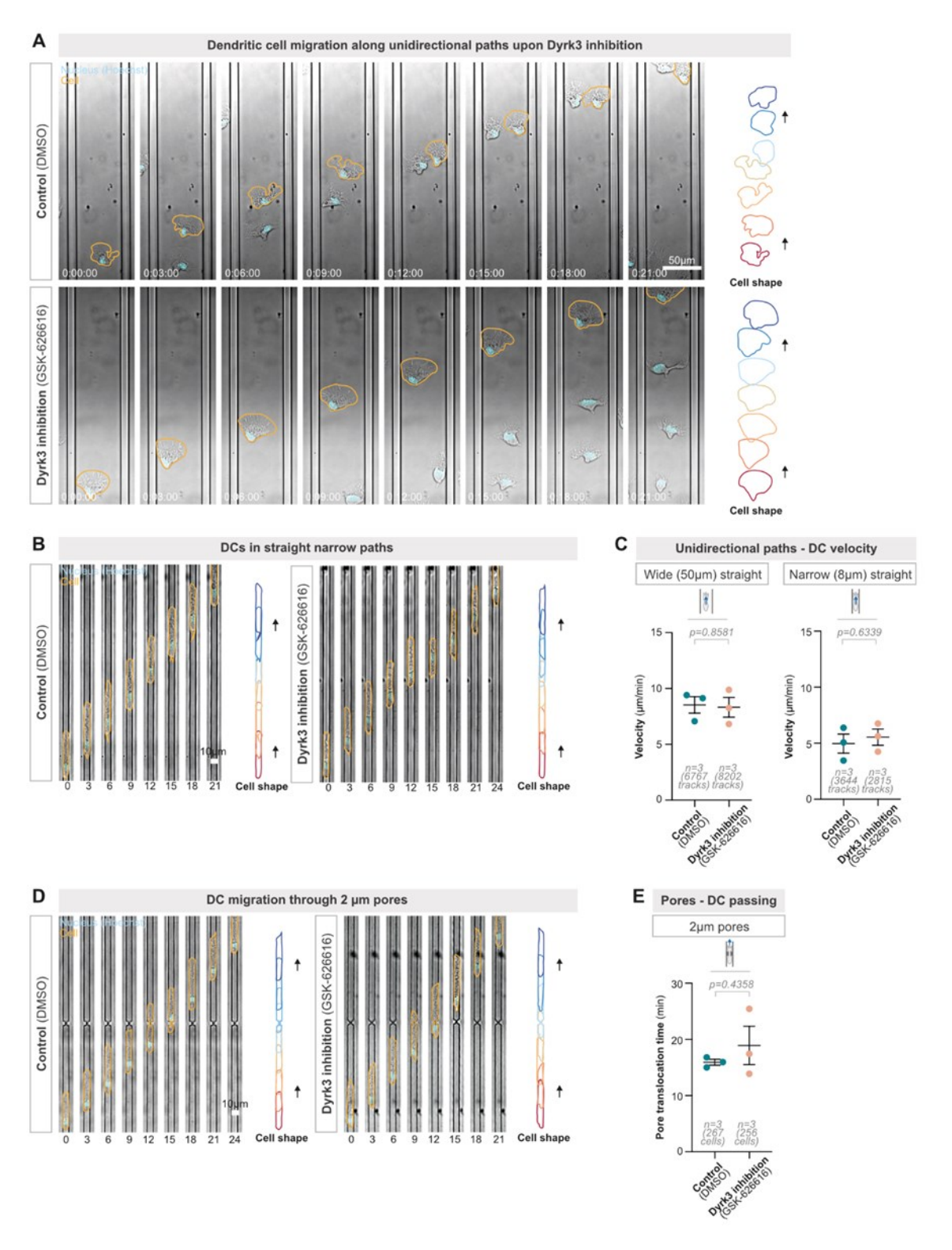


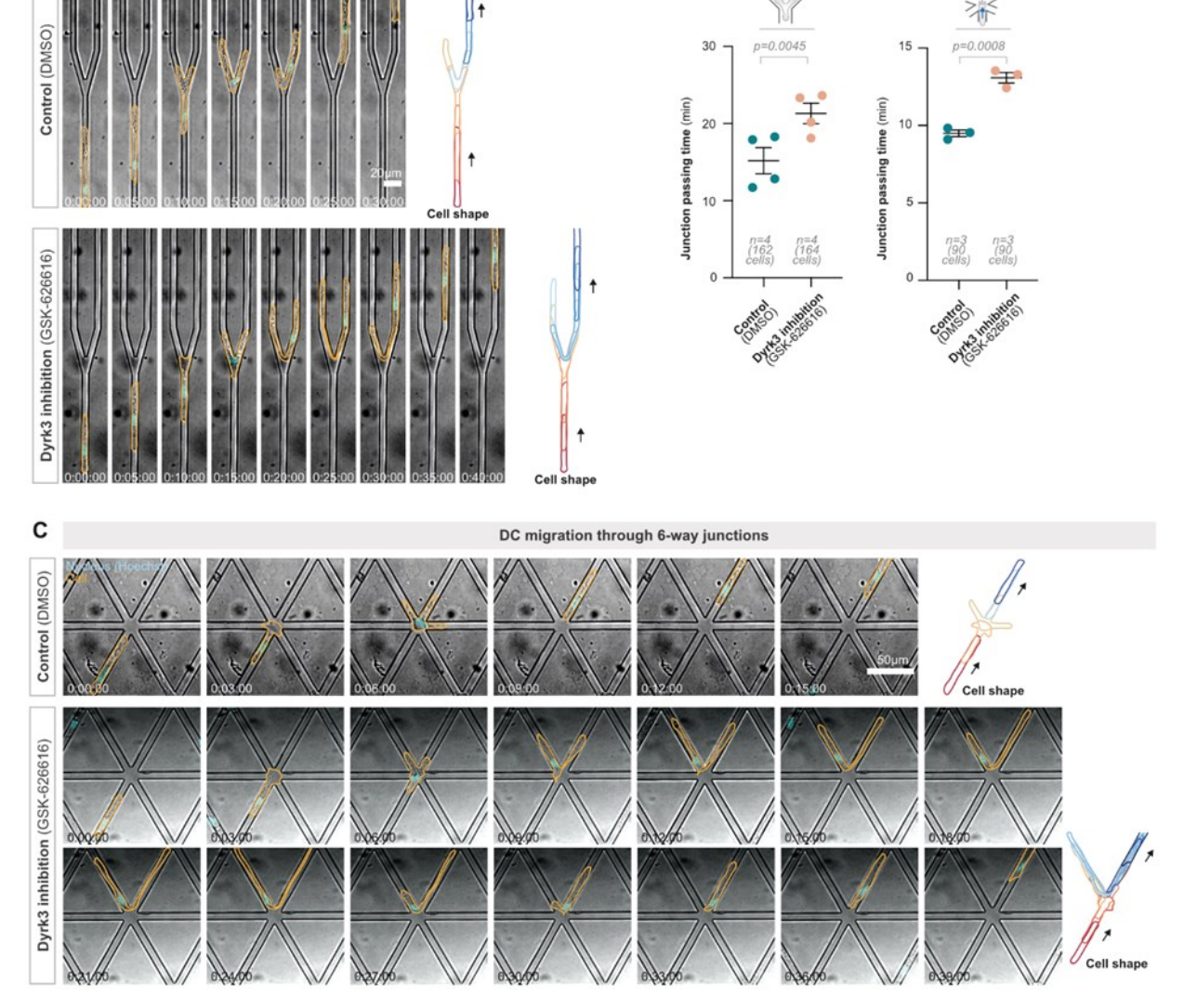
Figure legend on next page

Figure 17: Dendritic cell migration in less complex environments in the presence of mechanically unstable centrosomes. (A) Representative dendritic cells (DCs) migrating along a unidirectional straight path (wide linear microchannel) in the presence of 5 μ M GSK-626616 or DMSO (control). (B) Representative dendritic cells (DCs) migrating along a unidirectional straight path (narrow linear microchannel) in the presence of 5 μ M GSK-626616 or DMSO (control). (C) Quantification of migration velocities along wide and narrow unidirectional paths in the presence of 5 μ M GSK-626616 or DMSO (control). Data represent mean \pm SEM, unpaired t-test. (D) Representative dendritic cells (DCs) migrating through a 2 μ m pore in the presence of 5 μ M GSK-626616 or DMSO (control). (E) Quantification of migration velocities through 2 μ m pores in the presence of 5 μ M GSK-626616 or DMSO (control). Data represent mean \pm SEM, unpaired t-test. All data show representative cells from at least three independent biological replicates. Time is indicated as h:min:s.

Since dendritic cell migration under physiological conditions does not only require cellular navigation in the context of protrusion coordination but also the translocation through narrow pores within the extracellular matrix or upon entering the lymphatic capillaries (Kameritsch & Renkawitz, 2020), the capability of cells to squeeze through narrow microenvironmental pores, in particular during translocation through two-micrometer constrictions, in the presence of GSK-626616 was further investigated (Fig. 17D). Interestingly, the translocation time through narrow pores remained unchanged upon Dyrk3 inhibition, showing that squeezing is not affected by a less stable centrosome, at least during a singular squeezing event (Fig. 17E). Overall, these findings are consistent with microtubules being dispensable for unidirectional cellular movement, as the actin cytoskeleton is the driving force for cellular forward locomotion (Yamada & Sixt, 2019). My previous data already demonstrated that less stable centrosomes show higher rates of centrosomal fracturing particularly in more complex microenvironments necessitating a higher degree of cellular navigation (Fig. 10D). Therefore, cell migration upon Dyrk3 inhibition in more complex microenvironments, thus favoring the presence of two coexisting MTOCs, was analyzed next. In contrast to migration along unidirectional paths, dendritic cells moving through microchannels with more complex 3-way path junctions needed significantly longer to productively perform path decisions upon rendering Dyrk3 non-functional (Fig. 18, A and B). This effect was even more pronounced when dendritic cells without functional Dyrk3 migrated in 6-way path junctions, where cells typically explored a higher number of possible path options with multiple protrusions at the same time (Fig. 18, B and C), indicating that a higher rate of fracturing correlates with prolonged path decisions. Together, these data suggest that the emergence of two co-existing MTOCs upon centrosome fracturing impairs the ability of cells to efficiently navigate during pathfinding. To test the generality of these findings, I again employed human Jurkat T cells as another cellular model for fast cell migration and measured migration properties upon Dyrk3 inhibition using GSK-626616. Similar to dendritic cells, rendering Dyrk3 non-functional in Jurkat T cells did not show an effect on migration velocities of around 7 micrometers per minute upon migration along unidirectional paths (Fig. 19, A and C). In contrast, inhibition of Dyrk3 in Jurkat T cells migrating in complex 6-way path junctions resulted in a significantly prolonged decision time required to perform a productive path decision (Fig. 19, B and C).

DC migration through 3-way junctions

A



В

Path junctions - DC transition time

6-way junction

3-way junction

Figure 18: Dendritic cell migration in complex environments in the presence of mechanically unstable centrosomes. (A) Representative dendritic cells (DCs) migrating along a 3-way path junction in the presence of 5 μ M GSK-626616 or DMSO (control). (B) Quantification of dendritic cell passing time along 3-way or 6-way path junctions in the presence of 5 μ M GSK-626616 or DMSO (control). Data represent mean \pm SEM, unpaired t-test. (C) Representative dendritic cells (DCs) migrating along a 3-way path junction in the presence of 5 μ M GSK-626616 or DMSO (control). All data show representative cells from at least three independent biological replicates. Time is indicated as h:min:s.

Next, I aimed to confirm these findings on a genetic level. For this purpose, either an empty EGFP encoding plasmid as control or the dominant-negative kinase-dead point mutant of Dyrk3 (K218M) coupled to EGFP was transiently expressed in Jurkat T cells. Following FACS-based sorting for successfully transfected EGFP-positive cells, Jurkat T cell migration properties in different microenvironments were analyzed. Expression of the kinase-dead point mutant resulted in only mildly reduced migration velocities of approximately 4 micrometers per minute along unidirectional paths compared to control cells expressing the empty control vector and migrating with around 5 micrometers per minute (Fig. 20, A and C). However, the expression of Dyrk3(K218M), thus rendering Dyrk3 non-functional, led to strongly delayed passages through 6-way path junctions (Fig. 20, B and C). Altogether, these findings indicate that impaired centrosome stability caused by non-functional Dyrk3 also hinders cell migration of other immune cell types specifically during cellular navigation.

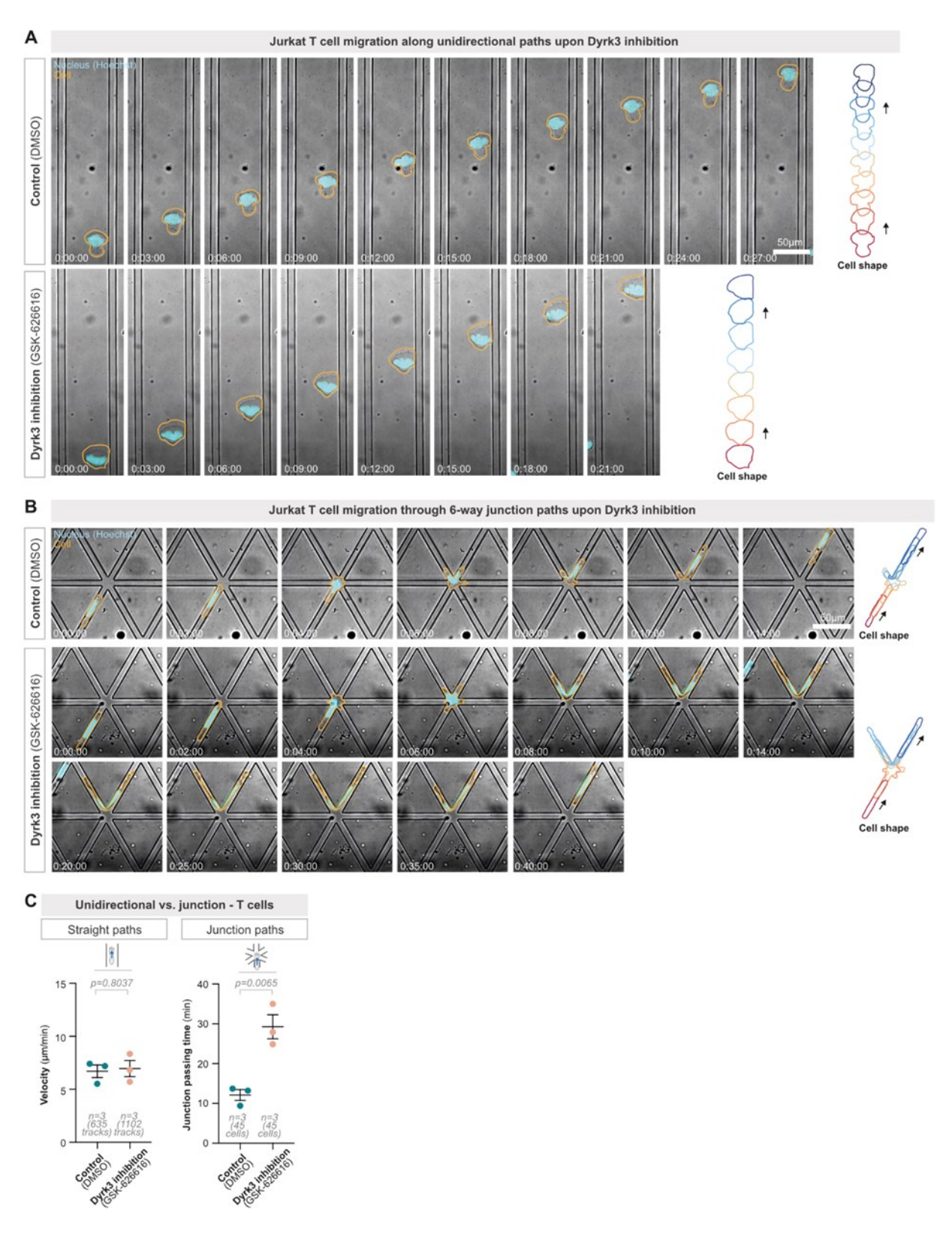


Figure 19: Jurkat T cell migration in the presence of mechanically unstable centrosomes upon Dyrk3 inhibition. (A) Representative Jurkat T cells migrating along a unidirectional straight path (wide linear microchannel) in the presence of 5 μ M GSK-626616 or DMSO (control). (B) Representative Jurkat T cells migrating along a 6-way path junction in the presence of 5 μ M GSK-626616 or DMSO (control). (C) Quantification of Jurkat T cell migration velocities along unidirectional paths or 6-way path junctions in the presence of 5 μ M GSK-626616 or DMSO (control). Data represent mean \pm SEM, unpaired t-test. All data show representative cells from at least three independent biological replicates. Time is indicated as h:min:s.

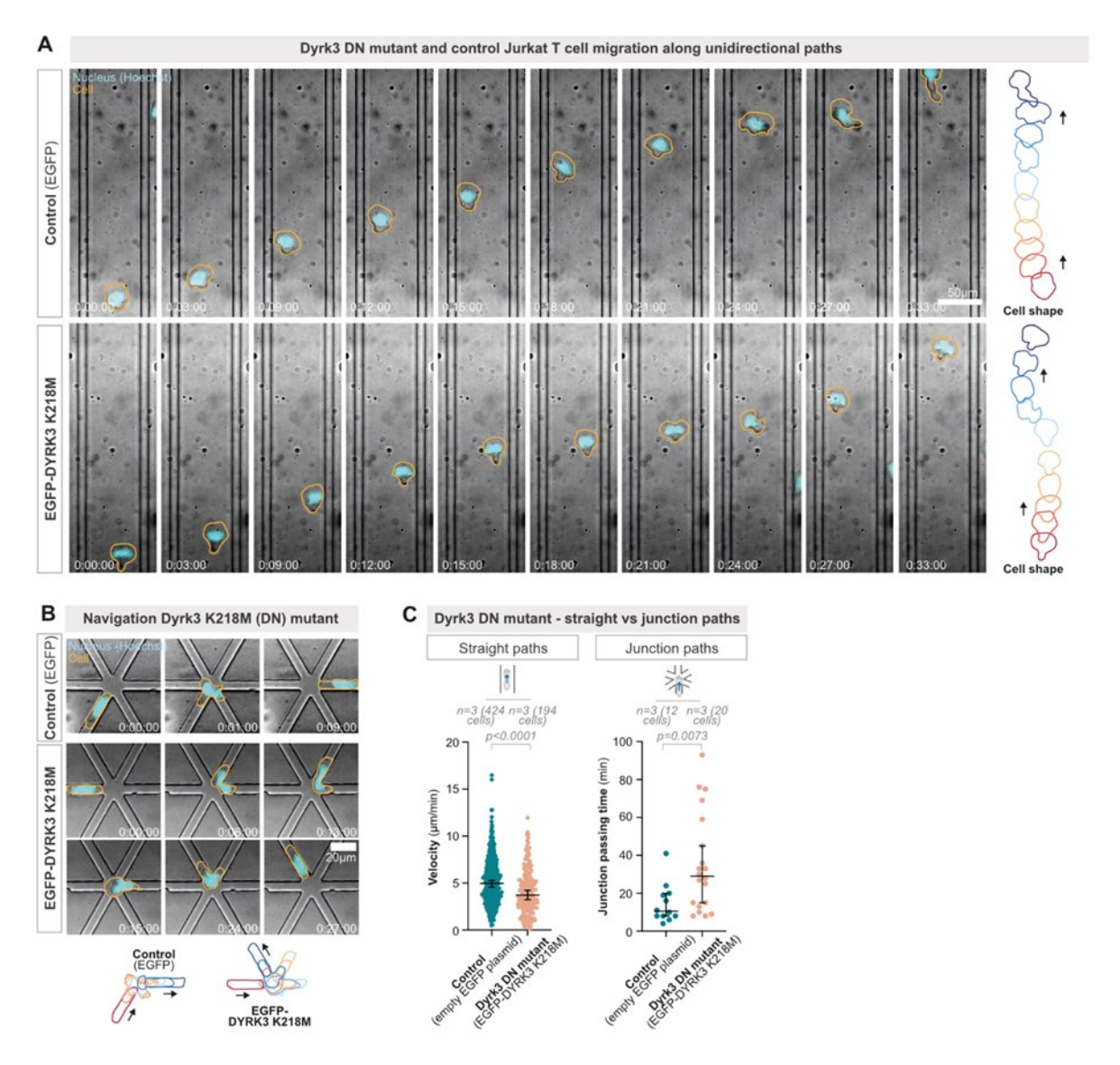


Figure 20: Jurkat T cell migration in the presence of mechanically unstable centrosomes upon expression of dominant-negative Dyrk3 (K218M). (A) Representative EGFP-Dyrk3 K218M (kinase-dead point mutant Dyrk3) or EGFP (control) expressing Jurkat T cells migrating along a unidirectional straight path (wide linear microchannel). (B) Representative EGFP-Dyrk3 K218M (dominant-negative kinase-dead point mutant Dyrk3) or the corresponding empty EGFP plasmid (control) expressing Jurkat T cells migrating along a 6-way path junction. (C) Quantification of Jurkat T cell migration velocities along unidirectional paths or 6-way path junctions upon expression of EGFP-Dyrk3 K218M (dominant-negative kinase-dead point mutant Dyrk3) or the corresponding empty EGFP plasmid (control). Data represent median ± 95 % CI, Mann-Whitney. All data show representative cells from at least three independent biological replicates. Time is indicated as h:min:s.

Of note, cells frequently seemed to exhibit prolonged protrusions and an overall elongated cell shape upon rendering Dyrk3 non-functional. To investigate this observation in more detail, the shape of cells migrating in 3D collagen matrices as a more physiological microenvironment was analyzed under control conditions or with non-active Dyrk3. For this purpose, the borders of randomly selected cells including their protrusions were manually outlined after 200 minutes of live-cell imaging to ensure a well-established chemokine gradient across the entire field of view. Subsequent extraction of shape descriptors revealed that migratory dendritic cells exhibited reduced circularity and roundness, accompanied by an increase in Feret's diameter upon Dyrk3 inhibition (Fig. 21A). These findings were consistent with an overall more elongated cell shape, as a circularity of 1.0 indicates a perfect circle, whereas circularity approaching 0.0 indicates an increasingly elongated shape.

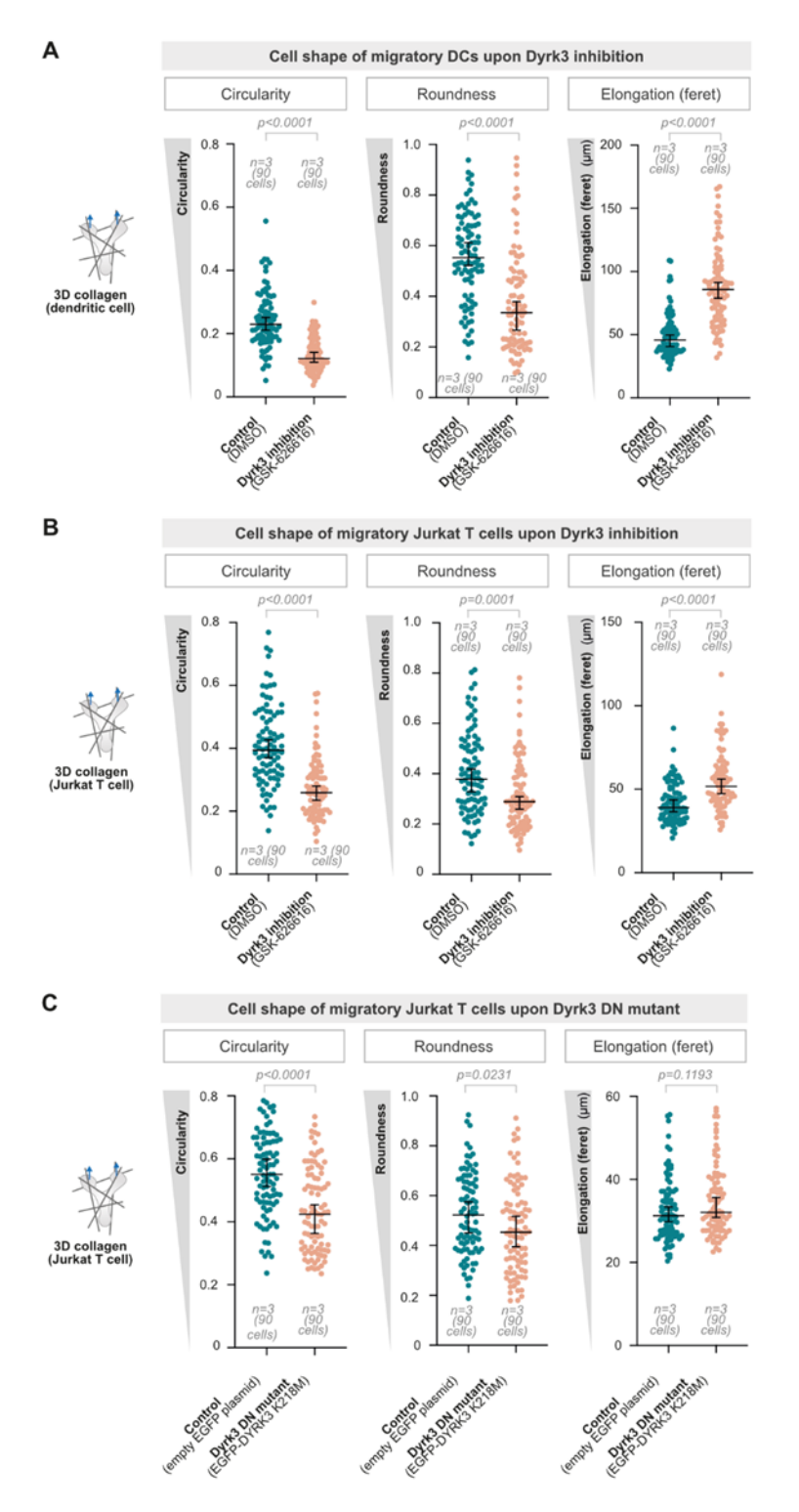


Figure 21: Dendritic cell and Jurkat T cell shapes during migration in 3D collagen matrices upon rendering Dyrk3 non-functional. (A) Circularity, roundness, and elongation of dendritic cells migrating in 3D collagen matrices (1.7 mg/ml collagen) along a CCL19 chemokine gradient in the presence of 5 μ M GSK-626616 or DMSO (control). Data represent median ± 95 % CI, Mann-Whitney. (B) Circularity, roundness, and elongation of Jurkat T cells migrating in 3D collagen matrices (1.3 mg/ml collagen) along a CXCL12 chemokine gradient in the presence of 5 μ M GSK-626616 or DMSO (control). Data represent median ± 95 % CI, Mann-Whitney. (C) Circularity, roundness, and elongation of Jurkat T cells that express a dominant-negative (DN) EGFP-Dyrk3 K218M mutant or the corresponding empty EGFP plasmid (control) migrating in 3D collagen matrices (1.3 mg/ml collagen) along a CXCL12 chemokine. Data represent median ± 95 % CI, Mann-Whitney. All data derive from at least three independent biological replicates.

Similarly, lower roundness points towards a more elongated shape. In accordance with that, Feret's diameter, which is also known as the maximum caliper or the maximum distance between two points of the selection boundary, was significantly increased suggesting a more pronounced elongation upon cell migration without active Dyrk3. In line, analysis of Jurkat T cell shapes upon Dyrk3 inhibition by GSK-626616 during migration in collagen matrices revealed more elongated and less round cell shapes. Of note, circularity was overall higher in Jurkat T cells compared to dendritic cells, which is consistent with the visual evaluation that in general Jurkat T cells displayed a more compact shape with less extensive protrusion formation during migration. However, also these cells showed significantly decreased circularity and roundness, as well as increased Feret's diameter upon Dyrk3 inhibition compared to controls (Fig. 21B). Furthermore, the shape analysis of the kinase-dead point mutant of Dyrk3 expressing Jurkat T cells confirmed these findings on a genetic level by similarly causing a more elongated, less round cell shape (Fig. 21C). Together, these data demonstrate that the mechanical fracturing of centrosomes results in an impaired migration ability that is accompanied by cell shape elongation suggestive of reduced cell shape control.

3.5.2 DENDRITIC CELLS RETAIN THEIR POLARITY UPON RENDERING DYRK3 NON-FUNCTIONAL

Given that loss of cell shape control can go hand in hand with altered cell polarity in dendritic cells, for instance, by impaired actomyosin contractility of retracting protrusions due to depletion of the RhoA exchange factor Lfc (Kopf et al., 2020), I next aimed to investigate cell polarity upon Dyrk3 inhibition. For this purpose, CETN2-GFP expressing dendritic cells were genetically engineered to stably express the PI(3,4,5)P3/PI(3,4)P2 biosensor PH-Akt which was fluorescently labeled with dTomato. PH-Akt is a well-established cellular polarity marker, consisting of the PH domain of Akt and thereby detecting the PI(3)K products PI(3,4,5)P3/PI(3,4)P2 (Várnai & Balla, 1998). In vivo zebrafish experiments revealed that PH-Akt translocates towards sites of PI(3)K activity at the leading edge of migrating neutrophils (Yoo et al., 2010). To investigate cell polarity of cells with non-active Dyrk3 and intact centrosomes, CETN2-GFP PH-Akt-dTomato expressing dendritic cells were live-imaged during migration in an under-agarose assay either under control conditions or upon Dyrk3 inhibition (Fig. 22A). For analysis performed by Mauricio Ruiz-Fernandez, directionally migrating cells with intact centrosomes were manually selected. Cytoplasmic volume changes during migration were accounted for by generating a ratio between the actual PH-Akt signal and the cytoplasmic background signal of CETN2-GFP, thus ensuring that any reduced or accumulated PH-Akt signal intensities were not artificial. Ratiometric measurement of the PH-Akt signal along the cell axis revealed a preferentially forward localization of PH-Akt towards the leading edge, whereas the signal gradually decreased towards the cell rear (Fig. 22, B and C). The frontward PH-Akt localization remained unchanged upon rendering Dyrk3 non-functional, indicating that cell polarity is not affected by Dyrk3 inhibition per se.

Configuration of the nucleus-MTOC axis was recently shown to play an important role in amoeboid cell migration, resulting in microenvironmental cellular arrest if cells fail to reorientate their nucleus in front of the MTOC during cellular pathfinding (Kroll *et al.*, 2023). Therefore, I further characterized nucleus-to-MTOC polarity as a broad polarity marker upon Dyrk3 inhibition. For this purpose, dendritic cells stably expressing the microtubule marker EMTB-mCherry that also functions as an MTOC marker, were analyzed during migration along unidirectional paths either under control conditions or in the presence of the Dyrk3 inhibitor GSK-626616 (Fig. 23A).

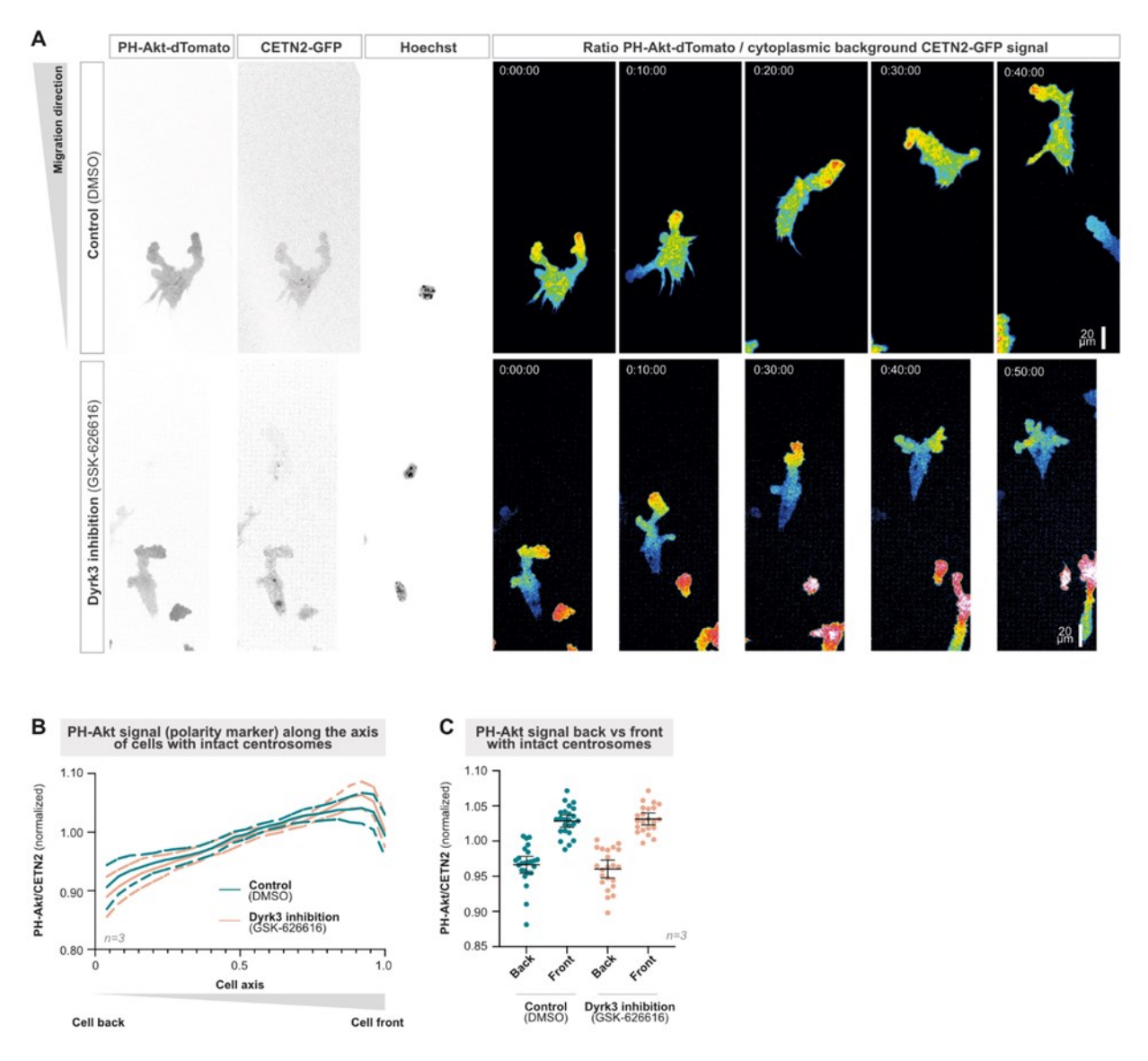


Figure 22: Dendritic cell polarity upon rendering Dyrk3 non-functional. (A) Representative CETN2-GFP (centriole pair; black) PH-Akt-dTomato (polarity marker; black) expressing dendritic cells (DCs) stained with Hoechst (nucleus; black) migrating in microenvironmental confinement ('under-agarose assay') in the presence of 5 μ M GSK-626616 or DMSO (control). Fluorescence ratio images show the PH-Akt-dTomato signal normalized to the CETN2-GFP signal (see 'Material and Methods' for details). (B) Quantification of normalized PH-Akt signal distribution along the cell axis of migrating dendritic cells with intact centrosomes as shown in (A). Data represent mean \pm 95 % CI. (C) Quantification of normalized PH-Akt signal in the front and back half of migrating dendritic cells with intact centrosomes as shown in (A). Data represent mean \pm 95 % CI. All data show representative cells from at least three independent biological replicates. Time is indicated as h:min:s.

Analysis revealed that nucleus-to-MTOC polarity remained unchanged, with around 60% of cells migrating with a nucleus-forward configuration in both control conditions and upon Dyrk3 inhibition. Similarly, approximately 30% of cells in both conditions showed an MTOC forward configuration, whereas around 10% of cells migrated with the nucleus and MTOC in parallel (Fig. 23B). Thus, these data show that altering Dyrk3 activity does not impair cellular polarity as long as the centrosome remains intact, and therefore, only one MTOC is present.

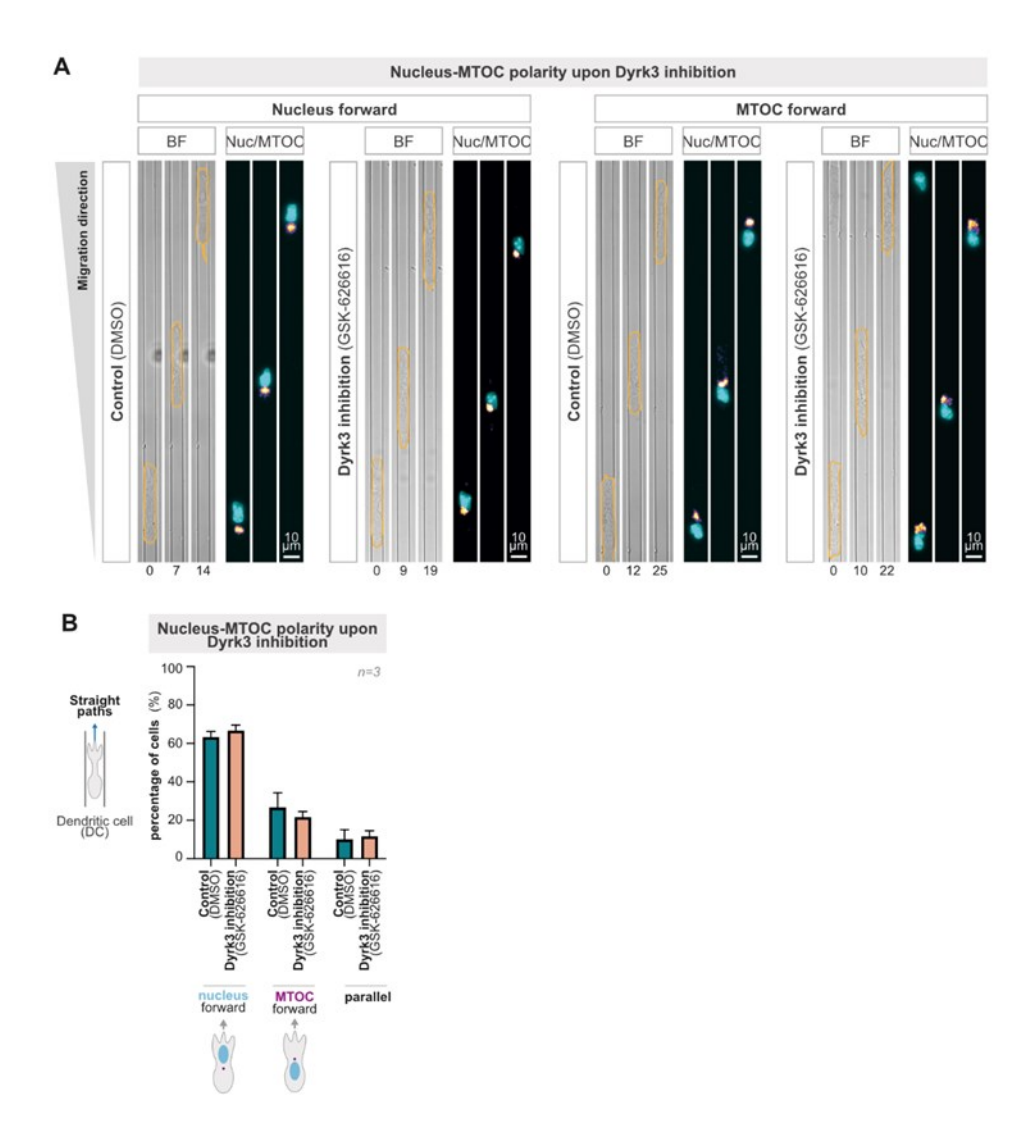


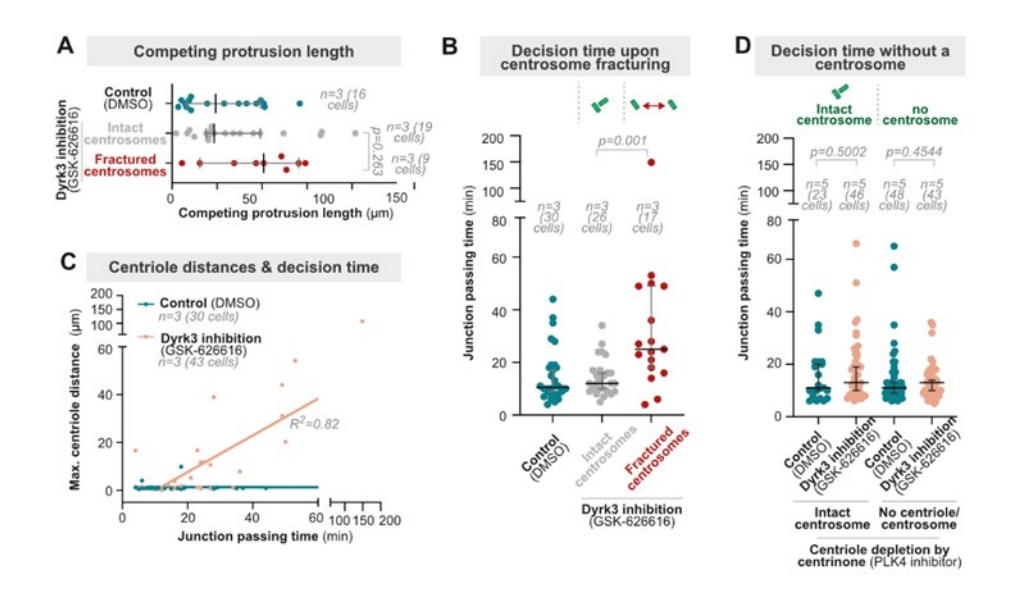
Figure 23: Dendritic cell nucleus-MTOC axis configuration upon rendering Dyrk3 non-functional. (A) Representative EMTB-mCherry (microtubule organizing center (MTOC) marker; fire-color coded) expressing dendritic cells stained with Hoechst (nucleus; cyan) migrating along a unidirectional straight path (narrow linear microchannel) in the presence of $5 \,\mu\text{M}$ GSK-626616 or DMSO (control). (B) Quantification of nucleus-MTOC-axis configuration as shown in (A). Data represent mean \pm SD. All data show representative cells from at least three independent biological replicates. Time is indicated in minutes.

3.5.3 EMERGENCE OF TWO COEXISTING MTOCS CAUSES CELLULAR ENTANGLEMENT

Since the analysis of Dyrk3-inhibited cells migrating in different microenvironments revealed a specific delay in passing complex path junctions, presumably due to the emergence of two coexisting MTOCs, I next tested the direct consequences of centrosome fracturing during migration. For this purpose, live-cell imaging of CETN2-GFP-expressing dendritic cells during complex path decisions was performed, while differentiating between Dyrk3-inhibited cells with an intact centrosome and a fractured centrosome for analysis. Interestingly, analysis performed by Mauricio Ruiz-Fernandez revealed that specifically cells with a fractured centrosome had longer competing protrusions which were characterized as the longest non-winning, thus ultimately retracted protrusions, suggesting cellular entanglement and an impaired ability to efficiently coordinate multiple protrusions at the same time. In contrast, cells with non-active Dyrk3 but intact centrosomes

formed competing protrusions with a comparable length to control conditions (Fig. 24A). Similarly, specifically cells with fractured centrosomes required significantly more time to navigate through complex path junctions upon rendering Dyrk3 non-functional. In line with the hypothesis that impairment of migration is a direct result of two coexisting MTOCs due to centrosomal breakage, Dyrk3-inhibited cells with intact centrosomes productively performed a path decision within the same time as untreated control cells (Fig. 24B). Remarkably, even the delay of path junction passage and the distance between fractured singular centrioles of Dyrk3-inhibited cells correlated with each other (Fig. 24C). These findings suggested the intriguing possibility that if impairment of cellular pathfinding upon rendering Dyrk3 non-functional was a direct consequence of the emergence of two coexisting MTOCs, then centrosome depletion would completely abolish the Dyrk3-associated migration defects. In order to test this hypothesis, I generated dendritic cells without any centrioles by treatment with the well-established Polo-like kinase 4 (PLK4) inhibitor centrinone (Wong et al., 2015). PLK4 plays a central role in centriole duplication by triggering the formation of the procentriole during S-phase and recruitment of centriole biogenesis proteins (Bettencourt-Dias et al., 2005; Habedanck et al., 2005). Consequently, PLK4 inhibition upon centrinone treatment disrupts centriole duplication during mitosis. Over the course of multiple cell divisions without centriole duplication in the presence of centrinone, daughter cells arise that did not receive any centriole from their corresponding mother cell, amongst other daughter cells that still harbor centrioles. To deplete centrioles in dendritic cells, I treated CETN2-GFP-expressing dendritic cells with centrinone starting from day 2 of cell differentiation. By the time of cell maturation, this resulted in a mixed cell population with varying numbers of centrioles, as could be observed based on the CETN2-GFP signal, including dendritic cells without any centrioles. To confirm that the Dyrk3-related impairment of cellular locomotion could solely be attributed to the emergence of two coexisting MTOCs upon centrosome fracturing, the decision time of centrioledepleted cells during navigation in complex path junctions either under control conditions or in the presence of the Dyrk3 inhibitor GSK-626616 was analyzed. As expected, cells that still retained a full centriolar pair upon centrinone treatment needed the same time to productively perform a path decision upon Dyrk3 inhibition compared to controls when their centrosome remained intact. Strikingly, cells migrating without any centrioles showed similar migration velocities as acentriolar control cells upon rendering Dyrk3 non-functional (Fig. 24, D and E), thus confirming that only the emergence of two coexisting microtubule organizing centers impairs cellular pathfinding when Dyrk3 is nonactive.

Overall, these findings show that mechanical centrosome fracturing impedes cell functionality by generating coexisting microtubule organizing centers that compete during cellular path navigation and thereby cause cellular entanglement in the microenvironmental matrix.



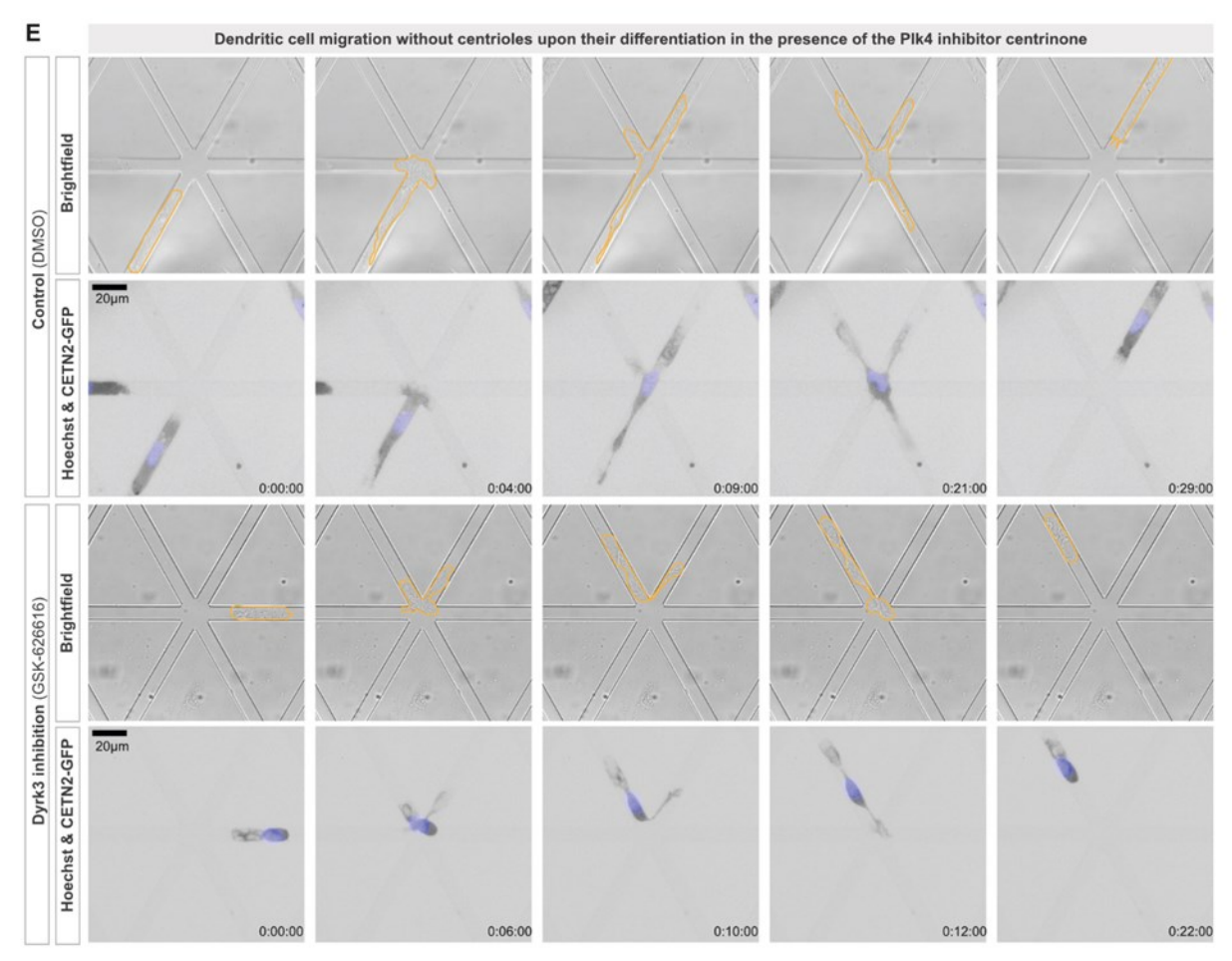


Figure 24: Consequences of centrosome fracturing on cellular navigation. (A) Length of the major competing protrusion of dendritic cells with fractured and non-fractured centrosomes migrating through 6-way path junctions in the presence of 5 μ M GSK-626616 or DMSO (control). Data represent median ± 95 % CI, Mann-Whitney. (B) Path decision time of CETN2-GFP expressing dendritic cells with fractured and non-fractured centrosomes migrating through 6-way path junctions in the presence of 5 μ M GSK-626616 or DMSO (control). Data represent median ± 95 % CI, Mann-Whitney. (C) Correlation of the cellular decision time as shown in (B) with the maximal distance between individual centrioles in the presence of 5 μ M GSK-626616 or DMSO (control). Linear regression fit. (D) Path decision time of centriole-depleted CETN2-GFP expressing dendritic cells migrating through 6-way path junctions in the presence of 5 μ M GSK-626616 or DMSO (control). Data represent median ± 95 % CI, Mann-Whitney. (E) Representative centriole-depleted CETN2-GFP (absent centriole pair; black) expressing dendritic cells stained with Hoechst (nucleus; blue) migrating along a 6-way path junction in the presence of 5 μ M GSK-626616 or DMSO (control). All data show representative cells from at least three independent biological replicates. Time is indicated as h:min:s.

4 DISCUSSION

4.1 EVALUATION OF DYRK3 FUNCTION IN VIVO

In this study, transcriptome analysis of dendritic cells migrating within collagen networks of increasing collagen concentration, and thus increasing complexity, identified the dual-specificity tyrosine phosphorylation-regulated kinase 3 (Dyrk3) to be upregulated in response to migration in more dense collagen matrices. Utilizing two well-described pharmacological Dyrk3 inhibitors, GSK-626616 and harmine (Wippich *et al.*, 2013; Rai *et al.*, 2018), demonstrated that both dendritic cells and Jurkat T cells, serving as an additional model for immune cell migration, depend on Dyrk3 function for their migration in complex microenvironments, which was further confirmed by transient expression of a dominant-negative kinase-dead point mutant of Dyrk3 (K218M) in Jurkat T cells.

While this study included a variety of reductionistic migration assays, ranging from collagen networks over microchannel assays to confining under-agarose assays, it would be interesting to investigate the effect of non-functional Dyrk3 in the physiological environment of an *in vivo* setting. This would require depletion of Dyrk3 on a genetic level, as transient inhibition of Dyrk3 with pharmacological inhibitors specifically e.g. in dendritic cells is not suitable for the evaluation of migration in vivo. In an attempt to generate stable Dyrk3 knockouts in precursor Hoxb8 cells, I employed the CRISPR/Cas9 technique via lentiviral transfection. Yet, this approach was not successful, probably owing to knockout-induced lethality. Importantly, Dyrk3 plays a crucial role during mitosis by regulating the dissolution of different membraneless organelles to prevent aberrant hybrid condensation (Rai et al., 2018). As a consequence, inhibition of Dyrk3 was previously shown to result in mitotic arrest (Rai et al., 2018). Since Hoxb8 cells are constantly undergoing mitosis under the influence of an estrogen-inducible Hoxb8 promotor (Redecke et al., 2013), a stable knockout of Dyrk3 is likely not favorable. Instead, transient alterations of Dyrk3 expression either on a genetic or on a transcriptome level should be pursued. For this purpose, I performed a transient knockdown of Dyrk3 expression via electroporation of Dyrk3-targeting siRNAs. In addition, as alternative approach, I generated a Hoxb8 cell line with doxycycline-inducible expression of a Dyrk3-targeting shRNA. Yet, the following applies to both of the approaches: confirmation of knockdown efficiency is typically performed by Western blot analysis. This requires careful testing of commercially available Dyrk3 antibodies, as many antibodies presented to be specific for Dyrk3 also often recognize the closely related Dyrk2 (Ramella et al., 2024). In fact, this has also proven challenging in my experiments and will require even further antibody testing to confirm that the approaches are effective. To circumvent this issue, RT-qPCR performed with Dyrk3-specific primers would allow to detect changes in Dyrk3 expression on the mRNA level. Furthermore, building on the C-Nap1 knockout utilized in this study, a similar system could be developed for Dyrk3. For this purpose, I generated Dyrk3-specific lentiviral sgRNA vectors. Furthermore, I have initiated the transfection of a Hoxb8 cell line, which expresses inducible Cas9 upon doxycycline addition, with a stably expressed sgRNA targeting Dyrk3. Doxycycline administration would induce Cas9 expression, which would then be directed to Dyrk3 by the sgRNA. Although cycling cells appear sensitive to Dyrk3 knockout, the optimal timing for Cas9 induction during dendritic cell differentiation could be determined. Subsequently, indel frequency around the cut site could be assessed using TIDE (Tracking of Indels by Decomposition) (Brinkman et al., 2014). Importantly, the inducible knockout system described here will consistently produce a mixed population of cells, containing both cells with differentially mutated Dyrk3 alleles and unaffected wild-type Dyrk3 cells. Therefore, achieving a high baseline gene editing efficiency is crucial to observe any effects in subsequent experiments. Once successfully established, these cells could be utilized for various *in vivo* migration experiments, such as footpad injections. In this setup, differently labeled wildtype and knockout cells are injected at a 1:1 ratio into the hind foot of a mouse. After 24-48 hours, the draining popliteal lymph nodes are excised, and the number of successfully homed dendritic cells from both genetic backgrounds can be evaluated to determine whether Dyrk3 is also necessary for immune cell migration *in vivo*. If this approach proves unsuccessful, *ex vivo* mouse ear explant assays performed by collaborators have already provided relevant insights (Weier *et al.*, 2022). In these assays, the ventral ear sheets were incubated in medium for 24 hours either under control conditions or in the presence of GSK-626616. Subsequently, dermal dendritic cells and lymphatic vessels were visualized using immunofluorescence staining. In accordance with the here-described *in vitro* data, Dyrk3 inhibition resulted in less migration towards the lymphatic vessels and reduced intravasation into the vessels (data not shown).

4.2 Forces acting on the centrosome resulting in fracturing

Centrosome fracturing in migrating dendritic cells upon rendering Dyrk3 non-functional or by genetic depletion of the linker protein C-Nap1 is highly dependent on the complexity of the surrounding microenvironment. This fracturing correlates with the formation of multiple explorative protrusions, that cells employ to navigate their path. Using reductionistic microchannel assays, this study revealed that the formation of two or more protrusions does not only result in a transient centriolar stretching during cellular pathfinding in untreated cells compared to cells migrating with a single protrusion, but also that it preferentially induces centrosome fracturing in the presence of mechanically unstable centrosomes. Thereby, protrusive cell fronts are identified as a source of mechanical forces acting on the centrosome. To further elucidate the underlying mechanism of force generation, co-inhibition experiments were performed either using Latrunculin A targeting actin polymerization or using para-nitroblebbistatin inhibiting myosin-II contractility. Surprisingly, this showed that centrosome fracturing is clearly reduced upon myosin-II inhibition and completely abolished upon actin inhibition in Dyrk3-inhibited cells. Similarly, myosin-II inhibition leads to a decrease in fracturing rates and actin inhibition to an almost complete reduction in C-Nap1-deficient cells. In addition, analysis of PCM shape deformations of migrating dendritic cells expressing PCNT-dTomato as a PCM marker revealed that not only the centriole pair is subject to mechanical forces, but also the surrounding pericentriolar material is deformed during cellular pathfinding. Importantly, these deformations, which were quantified by different shape descriptors, are likewise reduced upon inhibition of actin polymerization. Altogether, these data identify the actomyosin network as the underlying source of force exerted on the centrosome. Of note, the more pronounced effect of actin inhibition on centrosome fracturing compared to myosin-II inhibition could indicate that the force exerted by actin filaments themselves rather than the force generated by myosin-II-driven cellular contractility is responsible for centrosome fracturing. Although actomyosin forces could be identified as the underlying cause, it still remains elusive how exactly the actin cytoskeleton is acting on the centrosome in this context.

The two-sided relationship between actin and the centrosome has been subject to many studies. Dynamic actin networks were observed to be involved in the assembly and orientation of spindle poles in diverse species ranging from frog embryonic cells to mammalian cultured cells (Rosenblatt *et al.*, 2004; Cao *et al.*, 2010). During early ciliogenesis, actin is implicated in the centrosomal attachment to the cell cortex by the formation of stress-fiber- and focal-adhesion-like structures,

as well as in the preceding centrosomal movement towards the cell edge (Dawe et al., 2009; Antoniades et al., 2014). Of note, the actin cytoskeleton plays a more general role in centrosome positioning, for instance during immune synapse formation (Gomez et al., 2007; Tang & Marshall, 2012). In addition, the actin network was shown to reorganize and disassemble in the proximity of centrosomes when the latter reached the cell cortex during the formation of immune synapses (Stinchcombe et al., 2006). While few examples of direct interactions between actin and centrosome exist (Antoniades et al., 2014), the relation between actin filaments and microtubules is well-known. Physical crosslinking between both cytoskeletal networks usually occurs at growing plus-ends of microtubules in the cellular periphery, as most actin is typically localized at the plasma membrane (Blanchoin et al., 2014; Akhmanova & Steinmetz, 2015). Furthermore, the spatial distribution and network architecture of microtubules were shown to be influenced by the actin cytoskeleton (Dogterom & Koenderink, 2019). Yet, centrosomes isolated from Jurkat T cells were demonstrated to induce actin nucleation in vitro. In accordance, cloud-like centrosome-associated actin filaments were observed in Jurkat T cells and HEK293T cells. This process of centrosomal actin nucleation was dependent on PCM1-based Arp2/3 recruitment to the centrosome and promoted by the nucleation-promoting factor (NPF) WASH (WASp and SCAR homolog), as it was sensitive to Arp2/3 inhibition via CK666, but not formin inhibition via SMIFH2 (Farina et al., 2016). Similarly, the accumulation of actin at the centrosome during anaphase in mitotic cells is an Arp2/3- and WASH-dependent process. Interestingly, this actin accumulation is accompanied by a reduction of microtubule numbers, possibly because actin and microtubule filaments are competing for space in the small centrosomal area (Farina et al., 2019). Of note, this inverse correlation between an increase in actin and a concomitant decrease in the number of microtubule filaments was also observed in B-lymphocytes. Here, lymphocyte activation led to the disassembly of centrosome-associated actin and an increase in microtubule numbers. Subsequent in vitro reconstitution assays suggested that the actin filaments might constitute a physical barrier around the centrosome, thereby blocking microtubule elongation. In a cellular context, adhesion and cell spreading in response to cell activation could lead to a decrease in centrosomal actin, as adhesions compete for free actin monomers, ultimately resulting in an increase in microtubule nucleation. Consequently, this mechanism would couple the regulation of microtubule numbers to cell adhesion (Inoue et al., 2019).

In order to further elucidate the exact mechanism of force generation leading to centriolar splitting, it will be intriguing to see whether a specific type of actin is responsible for centrosome fracturing. Therefore, co-inhibition experiments employing CK666 to target Arp2/3-mediated branched actin nucleation or SMIFH2 to inhibit formin-mediated linear actin polymerization will allow to further narrow down potential underlying mechanisms. The genetic depletion of different NPFs, such as the WAVE (WASp-family verprolin-homologous protein) complex- which typically localizes to the tip of lamellipodia driving forward protrusive locomotion- through knockout of its subunit Hem1, could provide evidence if forward locomotion itself is able to generate the necessary force (Gaertner et al., 2022). Similarly, knockout of WASp (Wiskott-Aldrich syndrome protein), the other main NPF upstream of Arp2/3, which is implicated in the nucleation of vertically pushing actin patches in dendritic cells and T cells, and thereby enables locomotion in confining environments, will allow to investigate the role of this form of actin nucleation (Gaertner et al., 2022). In addition, through a knockout of WASH1, the role of WASH complex-driven actin nucleation at the centrosome can be further elucidated (Farina et al., 2016). Altogether, this will enable a more detailed dissection of the underlying mechanism. Importantly, an actin depolymerization-driven effect on microtubule nucleation as it was already described previously (Farina et al., 2019; Inoue et al., 2019), cannot be excluded so far. It is possible that actin depolymerization

by Latrunculin A results in increased microtubule nucleation at the centrosome due to reduced actin nucleation, thereby enhancing the microtubule-based centrosome linker and decreasing centrosome fracturing rates.

Overall, the role of microtubules in force generation or force transmission was not investigated in this study. Previous studies have demonstrated that depolymerization of microtubules induced by nocodazole treatment can result in centrosome fracturing under non-migratory conditions, due to the elimination of the microtubule-based linker (Meraldi & Nigg, 2001; Panic et al., 2015). In accordance with these reports, preliminary experiments investigating centrosome cohesion upon nocodazole treatment show a similar effect (data not shown), thereby rendering a generalized depolymerization of microtubules upon nocodazole treatment unsuitable for studying their role in force generation. However, the photoactivatable drug photostatin-1 might provide an opportunity to investigate the role of microtubules, as the photoactivation-driven mode of function provides temporal and spatial control over microtubule depolymerization, thereby also offering the opportunity to specifically exclude the inter-centriolar microtubule network (Borowiak et al., 2015). Of note, local activation of photostatin-1 in protruding cells fronts in order to investigate the impact of microtubules within protrusions on centrosome cohesion might likely result in the collapse and retraction of the respective protrusion owing to local release of Lfc and subsequent actomyosin activation (Kopf et al., 2020), thereby also disrupting the underlying cellular structure implicated in centrosome fracturing. Given that the binding and sequestration of regulatory molecules, such as Lfc, to microtubules is a common feature, the use of alternative localized depolymerization methods like opto-katanin—where light-induced recruitment of the microtubule-severing protein katanin results in localized microtubule depolymerization—will also not allow the uncoupling of these mechanisms (Meiring et al., 2022). Thus, investigating whether microtubules contribute to force generation or transmission to the centrosome remains a challenging issue that necessitates further research.

Regarding force transmission, it would be intriguing to speculate whether cellular adhesions also play a role. Amoeboid migrating cells, such as T cells or dendritic cells, can migrate independently of substrate adhesion, although they typically employ a low-adhesiveness migration mode (Kameritsch & Renkawitz, 2020). Previous studies have shown that adhesion-free migration relies on a retrograde actin flow that creates shear forces around the environmental topology. Thus, migration without integrins is possible in textured areas, but cells are immobile in smooth environments that lack suitable topology (Reversat et al., 2020). Therefore, the role of adhesions in centrosome fracturing could be investigated in integrin or talin knockout cells, thereby enforcing an adhesion-free migration mode that solely depends on environmental topology. Notably, previous reports indicate that cells incapable of forming adhesions have difficulties entering the microchannel devices used in this study (Reversat et al., 2020). Thus, utilizing these cells would necessitate either flushing them into the microchannel structures or injecting them underneath the agarose layer in an under-agarose bead assay. In addition to investigating the role of cellular adhesion on centrosome splitting, one could also examine whether a more pronounced topology, e.g. by the addition of serrated topographies to the surface of microchannels requiring a path decision, would lead to an increased retrograde actin flow, thereby accelerating intracellular forces and thus increasing centrosome fracturing rates compared to non-surface-textured microchannels.

To investigate the magnitude of forces required to disrupt a centrosome, the development of a genetically encoded centrosome force sensor would be an intriguing approach. These molecular tension sensors employ a mechanosensitive peptide that separates a pair of FRET (Förster resonance energy transfer) fluorophores. When force is applied, the mechanosensitive peptide under-

goes reversible extension, increasing the distance between the FRET fluorophores and consequently altering the FRET signal intensity. Importantly, these sensors are sensitive to forces in the piconewton-scale, which is relevant to the forces experienced within cells (Fischer *et al.*, 2021). Thus, incorporation of such a tension-sensitive sensor into centrosomal linker components would allow to measure the forces acting on the centriolar pair upon migration in different microenvironments, thereby eventually enabling to define a threshold of maximal force the linker can endure before breaking. Additionally, this approach would enable the characterization of the reduction in centrosome breakage caused by actin inhibition. Specifically, it would help determine whether this reduction is due to decreased force acting on the centrosome - confirming the direct involvement of actin-based forces - or whether there is no change in force, suggesting another mechanism, such as increased microtubule nucleation leading to microtubule-based linker stabilization. Furthermore, the generation of a tension sensor would facilitate the investigation of whether alterations of the biophysical PCM properties, as it was observed in this study upon Dyrk3 inhibition, also have an effect on force transmission on the centrosome.

4.3 How exactly is Dyrk3 influencing centrosome cohesion?

Mechanical forces exerted by competing explorative protrusions are able to transiently deform the centrosome during migration in complex microenvironments. This is manifested not only in the transient stretching of the centriolar pair but also in the deformation of the pericentriolar material (PCM) as cells make pathfinding decisions. The two centrioles within a centrosome are usually linked by two parallel mechanisms. One mechanism involves a fibrous proteinaceous linker primarily composed of Rootletin and CEP68 filaments, which are attached to a C-Nap1 ring positioned at the proximal ends of the centrioles, thereby directly connecting them (Fry et al., 1998; Mayor et al., 2000; Bahe et al., 2005; Graser et al., 2007; Vlijm et al., 2018). The second mechanism relies on microtubule interconnectivity. In this mechanism, the minus-end directed kinesin14 KIF3C connects microtubules originating from the mother centriolar subdistal appendages (SDAs) and those from the daughter centriolar pericentriolar material (PCM) microtubule network. By crosslinking microtubules and facilitating antiparallel microtubule sliding, KIF3C generates cohesive forces that bring the two centrioles closer together (Panic et al., 2015; Hata et al., 2019). In accordance with that, genetic depletion of the centriolar linker protein C-Nap1 in dendritic cells migrating in microchannels requiring cell navigation and path decision-making, frequently resulted in centrosome fracturing when experiencing mechanical forces. Interestingly, upon rendering Dyrk3 non-functional, the effects of these forces similarly extend beyond temporary centriolar stretching and result in centrosome fracturing. In order to elucidate the underlying mechanism, phospho-proteome analysis of dendritic cells migrating in collagen matrices upon Dyrk3 inhibition or under control conditions revealed that not only well-known targets of Dyrk3, such as SRRM1 and SRRM2, are differently phosphorylated when Dyrk3 is non-functional but also multiple centrosome-associated proteins like PCM1, CLASP1 and 2, or AKNA are affected (Wippich et al., 2013). Furthermore, fluorescence recovery after photobleaching (FRAP) experiments demonstrated that the diffusion properties of PCM-associated proteins like CEP120 or Dyrk3 itself are reduced upon Dyrk3 inhibition, while the signal recovery of PCM scaffold proteins like PCNT or AKNA remains largely unaffected, suggesting altered biophysical properties of the PCM mainly affecting the more diffusible, mobile components. Thus, there are multiple indications that Dyrk3 inhibition specifically affects the components and properties of the pericentriolar material (PCM).

What remains elusive so far, however, is the precise relationship between this phenomenon and the heightened incidence of centrosome fracturing.

The PCM is a proteinaceous matrix composed of different proteins and arising through liquidliquid phase separation. In vitro PCM reconstitution studies performed in C. elegans revealed that "young" (less than 2 minutes) condensates of the scaffold protein SPD-5 grew by isotropic expansion and displayed fast signal recovery after photobleaching, consistent with a liquid-like condensate. In contrast, "aged" (more than 10 minutes) condensates did not show any growth nor signal recovery, indicating that the PCM scaffold evolves and becomes less dynamic over time (Woodruff et al., 2017). The process by which a liquid-like state solidifies into a more viscous material is termed "aging" or "maturation" and has been documented as a pathological process in other biomolecular condensates (Patel et al., 2015). While the SPD-5 scaffold hardened, different client proteins remained dynamic, indicating that the PCM is a selective, yet porous condensate composed of scaffold proteins with low turnover and client proteins with higher turnover rates (Woodruff et al., 2017). Altogether, the authors proposed that the PCM exists in a gel-like state, which may support its function during mitosis by enabling it to incorporate new material and expand and withstand microtubule-dependent pulling forces during cell division (Woodruff et al., 2017). If now the effect of Dyrk3 inhibition appears to be confined to the PCM but leads to reduced centrosome stability, it would be intriguing to speculate that the biophysical properties of the PCM may not only play a role during cell division but also actively contribute to centrosome cohesion. Thus, the PCM could represent a third, parallel centrosomal linker mechanism, possibly facilitated by its gel-like state. If this is the case, the altered diffusion properties of PCM components upon Dyrk3 inhibition could indicate a more solid and less diffusible PCM state, resulting in a less gel-like but rather glass-like condensate state with reduced elasticity. Consequently, the application of force could lead to literal fracturing, as the PCM would lack the necessary flexibility to withstand mechanical stress. To further explore this hypothesis, the biophysical properties of the PCM must be investigated in greater detail. FRAP (fluorescence recovery after photobleaching) enables the assessment of the diffusion properties of a fluorescently labeled molecule, providing insights into its mobility within the condensate as well as with the surrounding cytosol. However, FRAP does not provide information about the material state of the condensate (Alshareedah et al., 2021). Importantly, FRAP measurements in multimolecular condensates might reveal different diffusion properties for different components of the same condensate, as it was also observed in this study. Therefore, in collaboration with Prof. Jochen Guck (Max Planck Institute for the Science of Light, Erlangen, Germany), I attempted to investigate the material properties of Dyrk3-inhibited cells using Optical Diffraction Tomography (ODT). This technique employs quantitative phase imaging to determine the optical density and the distribution of the refractive index within a cell, potentially revealing changes in material properties due to Dyrk3 inhibition (Schürmann et al., 2015; Kim et al., 2016). However, since extensive experimental adjustments were required to adapt the here-established migration assays to the technical requirements of ODT, this approach was not further pursued. Yet, methods such as single particle tracking represent another approach to investigate the viscosity of a condensate (Elbaum-Garfinkle et al., 2015; Feric et al., 2016). In principle, single-particle tracking involves monitoring the diffusion of an exogenous spherical particle within a biomolecular condensate, which is also applicable inside living cells (Shen et al., 2017). Importantly, another potential mechanism through which Dyrk3 might affect centrosome cohesion by modifying the biophysical characteristics of the PCM, which remains to be fully elucidated, is the reduction in the diffusion of linker components, such as Rootletin or CEP68, to their intended location. This could result in a weakening of the protein linker, thereby leading to an increased frequency of centrosome breakage. To further explore this hypothesis, localization and

amount of linker components could be evaluated by immunofluorescence staining. Thereby, one could draw conclusions regarding whether Dyrk3 inhibition results in a decreased number of linker proteins reaching the connection between the centrioles, and whether they localize to other regions instead. In addition, the concurrent inhibition of Dyrk3 and depletion of C-Nap1, thereby depleting the centriolar linker, would enable examination of whether their impact on centrosome fracturing is additive, suggesting the involvement of two independent mechanisms, or whether the effect is comparable, indicating their participation in the same mechanism. Preliminary experiments with Dyrk3-inhibited C-Nap1 knockout cells suggest the latter, as the individual effects do not appear to be additive. Of note, given that microtubule nucleation is not affected by Dyrk3 inhibition, the microtubule-based linker is presumably not implicated in the underlying mechanism. How exactly Dyrk3 can alter the biophysical properties of the PCM currently remains elusive. To investigate the underlying mechanism in more detail, the proteins identified in the analysis of the phosphoproteome upon Dyrk3 inhibition provide a good starting point. PCM1, for instance, is implicated in the recruitment of several centrosomal proteins, such as Pericentrin and Ninein. Therefore, PCM1 depletion was shown to result in impaired microtubule organization (Dammermann & Merdes, 2002). Furthermore, PCM1 is essential for Nek2 trafficking via centriolar satellites (Hames et al., 2005). Due to its centrosomal localization and its function as an essential microtubule organizing factor during cell delamination, AKNA might be another interesting candidate (Camargo Ortega et al., 2019). In addition, the stress-responsive protein Ndrg1 is not only associated with hereditary sensory and motor neuropathies and cancer, but was also shown to regulate microtubule dynamics and support spindle fiber formation during mitosis (Kalaydjieva et al., 2000; Kim et al., 2004). However, it must be emphasized that none of the phosphoproteome targets have been described in relation to centrosome cohesion or PCM properties. Therefore, further investigations will be necessary to elucidate the exact underlying mechanism.

The findings presented here intriguingly suggest that the biophysical properties of the PCM are important on a more general note. During mitosis, the centrioles are separated in a precise and controlled manner by Nek2 and PLK1 (Fry et al., 1998; Bahe et al., 2005). They are surrounded by an expanded PCM, which, while in a gel-like state, can still incorporate material and can also be divided to build the spindle body (Woodruff et al., 2017). Now the question arises whether cells actively alter the material state of the surrounding PCM, for instance through Dyrk3, to make the tightly connected centrioles more resistant to fracturing by mechanical forces, such as those occurring during cell migration. Given the effects of centrosome fracturing on cell migration, this may potentially highlight the importance of preserving and regulating the integrity of other membraneless organelles, such as stress granules, nucleoli, and splicing speckles, under mechanical stress. This consideration is particularly relevant as cells encounter mechanical stress during development, tissue homeostasis, and disease, thus bringing these organelles into greater focus.

4.4 FUNCTIONAL CONSEQUENCES OF CENTROSOME FRACTURING

Centrosome fracturing upon rendering Dyrk3 non-functional results in the emergence of two functional MTOCs within a single cell. The individual centrioles are able to nucleate and anchor microtubules, and are equipped with a functional PCM, as it was demonstrated by immunofluorescence staining of fractured centrosomes for α -tubulin, ninein, and γ -tubulin. Of note, there are minimal PCM fragments and no acentrosomal microtubule asters observed following fracturing. Despite the rapid and sudden nature of centrosome fracturing, the PCM persists in its association with the centrioles. Thus, upon centrosome fracturing, cells are suddenly equipped with two

equivalent MTOCs functioning as steering organelles. Importantly, cells typically display a hierarchical asymmetry between the centrioles of a centrosome, traditionally designated as mother and daughter centrioles. Due to the semiconservative mechanism of centrosome duplication, only the mother centriole possesses distal and subdistal appendages, which the newly formed daughter centriole will only acquire after the next duplication cycle (Kochanski & Borisy, 1990; Nigg & Stearns, 2011). The mother centriolar subdistal appendages are particularly associated with microtubule nucleation, as they recruit microtubule anchoring proteins such as ninein (Delgehyr et al., 2005). Consistent with this observation, the characterization of non-fractured centrosomes in dendritic cells using immunofluorescence staining and super-resolution microscopy confirmed that both centrioles function as a single functional unit at the center of a nucleating microtubule aster. Nevertheless, one centriole preferentially accumulates ninein, a characteristic feature of a mother centriole and the typical asymmetrical hierarchy (Piel et al., 2000; Nigg & Stearns, 2011). This raises the question of why both individual centrioles of a fractured centrosome exhibit the characteristics and appearance of mother centrioles. To further investigate this question, it would be logical to examine the localization and distribution of additional distal appendage (DA) and subdistal appendage (SDA) markers relative to the individual centrioles using immunofluorescence staining and super-resolution microscopy to see if both centrioles are fully decorated with appendages. This approach would provide a clearer understanding of whether, from a mechanistic and functional perspective, there are indeed two mother centrioles. The most suitable markers for this purpose would include sodium channel and clathrin linker 1 (SCLT1) or CEP89 for distal appendages, and centriolin or CEP170 for subdistal appendages (Ma et al., 2023). Additional existing evidence indicating that both individual centrioles harbor appendages is the symmetric distribution of AKNA following centrosome fracturing. AKNA plays an essential role in organizing microtubules as part of the subdistal appendages of the mother centriole during brain development and is critical for regulating cell delamination (Camargo Ortega et al., 2019). However, it remains unclear whether this suggests that the two individual centrioles are identified as mother centrioles and therefore actively equipped with appendages and needs to be further investigated. Notably, the composition and formation of distal and subdistal appendages are intricately linked to the centrosome duplication cycle and, consequently, to the cell cycle itself (Ma et al., 2023). Yet, dendritic cells are terminally differentiated cells that no longer undergo mitosis (Worbs et al., 2017; Weier et al., 2022). On one hand, this suggests that terminally differentiated cells must possess the capability to mature centrioles autonomously from the cell cycle and the cell cycle-dependent expression of various DA and SDA regulators (Ma et al., 2023). On the other hand, it could also imply that the presence of individual centrioles might initiate signaling pathways that induce maturation. If this phenomenon is not driven by an active cellular process, the distribution of PCM and microtubules could potentially occur randomly on the two centrioles upon splitting. However, this would not account for the presence of ninein and AKNA at both centrioles. Overall, further investigation is required to elucidate precisely how both centrioles can establish equivalent MTOCs and why the daughter centriole retains the capacity to function as an MTOC instead of being deactivated, maintaining the mother centriole as the sole MTOC.

As a consequence of centrosome fracturing upon Dyrk3 inhibition and the subsequent emergence of two MTOCs, cells with fractured centrosomes take particularly longer during cellular pathfinding in complex microenvironments. This is accompanied by longer competing protrusions (defined as the longest retracting protrusion), and more elongated cell shapes indicative of cellular entanglement. Surprisingly, the distance between individual centrioles and the time cells need to make a productive path decision even seem to correlate, suggesting a direct link between intracellular coordination of protrusions and localization of the two steering organelles. Thus, it would

be interesting to see whether cellular entanglement is even more pronounced if the two MTOCs are located in two different protrusions compared to a less dispersed localization. This might also provide insights into how cells ultimately make a path decision. Although centrosome fracturing results in prolonged passing time, the majority of cells manage to navigate through the path junction, indicating a decision-making process and coordination of protrusions. To better understand how they accomplish this, it would be intriguing to investigate whether ultimately a centriole randomly makes the decision or if additional mechanisms of cellular coordination are at play. Additionally, to directly demonstrate that the presence of the two MTOCs is the direct cause of entanglement, one could, for example, ablate one of the MTOCs during cell migration using a laser. In the case that two competing steering organelles are causative, one would expect cells with an ablated MTOC to navigate better than cells that still possess both MTOCs. Alternatively, using lightactivatable photostatin-1, the microtubule network around one of the two MTOCs could be specifically depolymerized, and the effect on the speed of path decision-making measured (Borowiak et al., 2015). However, it should again be noted here that targeted depolymerization of microtubules can lead to the release of proteins such as Lfc and induce retraction (Kopf et al., 2020). What already indicates that specifically centrosome fracturing is the cause of the migration defect is that cells whose centrosome was depleted using the PLK4 inhibitor centrinone, and thus cannot break, also show no effect on migration through complex environments when Dyrk3 is inhibited (Wong et al., 2015). Dendritic cells without a centrosome migrate as efficiently as cells with an unbroken centrosome, regardless of whether they are Dyrk3-inhibited or under control conditions. This shows that specifically a broken centrosome becomes a problem for cell migration. Importantly, these data do not necessarily mean that cells can migrate without an MTOC and microtubules. In fact, it is not unlikely that other organelles such as the Golgi apparatus instead take on the function as MTOC (Chabin-Brion et al., 2001). This could easily be investigated using immunofluorescence staining of α-tubulin in centrinone-treated cells. Together, these data indicate that centrosome fracturing and the resulting emergence of two MTOCs impair cellular navigation and lead to cellular entanglement. What remains elusive so far is the long-term consequences of this phenomenon.

As already demonstrated, centrosome fracturing leads to a migration defect in complex microenvironments that require efficient cell navigation and coordination. However, it remains unclear whether cells become stuck or even undergo apoptosis in the long term as a result. When considering this in a more physiological context such as immune responses, it could impact the generation of strong immune responses because, for example, fewer dendritic cells reach the draining lymph node to present antigens. The latter could be further investigated, as discussed earlier, through an *in vivo* experiment such as the footpad injection. Tracking cells with fractured centrosomes for a longer period of time during their migration could provide insights into longer-term consequences than those assessed during this study. This could also provide insights into whether cells are capable of reassembling and repairing fractured centrosomes. If this is the case, it could be imagined that the presumably necessary long-range interactions for this process are mediated by microtubules. In a similar mechanism to the microtubule-based linker itself, centrioles could be brought back together through crosslinking and antiparallel sliding mediated by kinesins (Hata *et al.*, 2019).

Analysis of Dyrk3-inhibited cells with non-fractured cells revealed that these cells exhibit a normal polarity, comparable to control cells, in terms of the nucleus-MTOC axis configuration and front-rear polarity with the polarity marker PH-Akt (Várnai & Balla, 1998). However, the effects of fracturing on polarity still require further investigation. One could hypothesize that the effect

of cellular entanglement and impaired coordination is due to an alteration in cell polarity resulting from the presence of two MTOCs.

Altogether, the here presented data show that the centrosome is subject to mechanical forces during cell migration, even leading to centrosome fracturing. These forces are exerted by the actomyosin cytoskeleton, although deciphering the underlying mechanism of force transmission requires further investigation. As a consequence of centrosome fracturing, two coexisting MTOCs emerge within a single cell, ultimately resulting in cellular entanglement and impaired pathfinding. Given that the centrosome as MTOC is crucial not only for cellular locomotion but also for trafficking, organelle positioning, and other functions, the question arises as to how centrosome fracturing also influences these roles (Conduit *et al.*, 2015). Considering that cells experience mechanical forces not only during migration through the body, but also during other cellular functions, such as cardiac fibroblasts or vascular endothelium, these findings suggest a broad relevance of maintaining centrosome coherence for physiology (Pesce *et al.*, 2023; Lim & Harraz, 2024).

REFERENCES

- Agircan, F.G., Schiebel, E. & Mardin, B.R. (2014) Separate to operate: control of centrosome positioning and separation. *Philosophical Transactions of the Royal Society of London. Series B, Biological Sciences*, 369(1650). Available from: https://doi.org/10.1098/rstb.2013.0461.
- Akhmanova, A. & Steinmetz, M.O. (2015) Control of microtubule organization and dynamics: two ends in the limelight. *Nature Reviews. Molecular Cell Biology*, 16(12), 711–726. Available from: https://doi.org/10.1038/nrm4084.
- Alshareedah, I., Kaur, T. & Banerjee, P.R. (2021) Methods for characterizing the material properties of biomolecular condensates. *Methods in Enzymology*, 646, 143–183. Available from: https://doi.org/10.1016/bs.mie.2020.06.009.
- Alvarez-Rodrigo, I., Steinacker, T.L., Saurya, S., Conduit, P.T., Baumbach, J. & Novak, Z.A. et al. (2019) Evidence that a positive feedback loop drives centrosome maturation in fly embryos. *ELife*, 8. Available from: https://doi.org/10.7554/eLife.50130.
- Anderson, P. & Kedersha, N. (2008) Stress granules: the Tao of RNA triage. *Trends in Biochemical Sciences*, 33(3), 141–150. Available from: https://doi.org/10.1016/j.tibs.2007.12.003.
- Anderson, P. & Kedersha, N. (2009) RNA granules: post-transcriptional and epigenetic modulators of gene expression. *Nature Reviews. Molecular Cell Biology*, 10(6), 430–436. Available from: https://doi.org/10.1038/nrm2694.
- Antoniades, I., Stylianou, P. & Skourides, P.A. (2014) Making the connection: ciliary adhesion complexes anchor basal bodies to the actin cytoskeleton. *Developmental Cell*, 28(1), 70–80. Available from: https://doi.org/10.1016/j.devcel.2013.12.003.
- Aranda, S., Laguna, A. & La Luna, S. de (2011) DYRK family of protein kinases: evolutionary relationships, biochemical properties, and functional roles. *FASEB Journal : Official Publication of the Federation of American Societies for Experimental Biology*, 25(2), 449–462. Available from: https://doi.org/10.1096/fj.10-165837.
- Astro, V., Chiaretti, S., Magistrati, E., Fivaz, M. & Curtis, I. de (2014) Liprin-α1, ERC1 and LL5 define polarized and dynamic structures that are implicated in cell migration. *Journal of Cell Science*, 127(Pt 17), 3862–3876. Available from: https://doi.org/10.1242/jcs.155663.
- Astro, V. & Curtis, I. de (2015) Plasma membrane-associated platforms: dynamic scaffolds that organize membrane-associated events. *Science Signaling*, 8(367), re1. Available from: https://doi.org/10.1126/scisignal.aaa3312.
- Azimzadeh, J., Hergert, P., Delouvée, A., Euteneuer, U., Formstecher, E. & Khodjakov, A. et al. (2009) hPOC5 is a centrin-binding protein required for assembly of full-length centrioles. *The Journal of Cell Biology*, 185(1), 101–114. Available from: https://doi.org/10.1083/jcb.200808082.
- Badano, J.L., Teslovich, T.M. & Katsanis, N. (2005) The centrosome in human genetic disease. *Nature Reviews. Genetics*, 6(3), 194–205. Available from: https://doi.org/10.1038/nrg1557.
- Badolato, R. (2013) Defects of leukocyte migration in primary immunodeficiencies. *European Journal of Immunology*, 43(6), 1436–1440. Available from: https://doi.org/10.1002/eji.201243155.
- Bahe, S., Stierhof, Y.-D., Wilkinson, C.J., Leiss, F. & Nigg, E.A. (2005) Rootletin forms centriole-associated filaments and functions in centrosome cohesion. *The Journal of Cell Biology*, 171(1), 27–33. Available from: https://doi.org/10.1083/jcb.200504107.
- Banani, S.F., Lee, H.O., Hyman, A.A. & Rosen, M.K. (2017) Biomolecular condensates: organizers of cellular biochemistry. *Nature Reviews. Molecular Cell Biology*, 18(5), 285–298. Available from: https://doi.org/10.1038/nrm.2017.7.

- Bear, J.E. & Haugh, J.M. (2014) Directed migration of mesenchymal cells: where signaling and the cytoskeleton meet. *Current Opinion in Cell Biology*, 30, 74–82. Available from: https://doi.org/10.1016/j.ceb.2014.06.005.
- Becker, W., Weber, Y., Wetzel, K., Eirmbter, K., Tejedor, F.J. & Joost, H.G. (1998) Sequence characteristics, subcellular localization, and substrate specificity of DYRK-related kinases, a novel family of dual specificity protein kinases. *The Journal of Biological Chemistry*, 273(40), 25893–25902. Available from: https://doi.org/10.1074/jbc.273.40.25893.
- Berg, S., Kutra, D., Kroeger, T., Straehle, C.N., Kausler, B.X. & Haubold, C. et al. (2019) ilastik: interactive machine learning for (bio)image analysis. *Nature Methods*, 16(12), 1226–1232. Available from: https://doi.org/10.1038/s41592-019-0582-9.
- Bergert, M., Erzberger, A., Desai, R.A., Aspalter, I.M., Oates, A.C. & Charras, G. et al. (2015) Force transmission during adhesion-independent migration. *Nature Cell Biology*, 17(4), 524–529. Available from: https://doi.org/10.1038/ncb3134.
- Bettencourt-Dias, M. & Glover, D.M. (2007) Centrosome biogenesis and function: centrosomics brings new understanding. *Nature Reviews. Molecular Cell Biology*, 8(6), 451–463. Available from: https://doi.org/10.1038/nrm2180.
- Bettencourt-Dias, M., Rodrigues-Martins, A., Carpenter, L., Riparbelli, M., Lehmann, L. & Gatt, M.K. et al. (2005) SAK/PLK4 is required for centriole duplication and flagella development. *Current Biology : CB*, 15(24), 2199–2207. Available from: https://doi.org/10.1016/j.cub.2005.11.042.
- Bhattacharyya, D. & Glick, B.S. (2007) Two mammalian Sec16 homologues have nonredundant functions in endoplasmic reticulum (ER) export and transitional ER organization. *Molecular Biology of the Cell*, 18(3), 839–849. Available from: https://doi.org/10.1091/mbc.E06-08-0707.
- Blanchoin, L., Boujemaa-Paterski, R., Sykes, C. & Plastino, J. (2014) Actin dynamics, architecture, and mechanics in cell motility. *Physiological Reviews*, 94(1), 235–263. Available from: https://doi.org/10.1152/physrev.00018.2013.
- Blangy, A., Lane, H.A., d'Hérin, P., Harper, M., Kress, M. & Nigg, E.A. (1995) Phosphorylation by p34cdc2 regulates spindle association of human Eg5, a kinesin-related motor essential for bipolar spindle formation in vivo. *Cell*, 83(7), 1159–1169. Available from: https://doi.org/10.1016/0092-8674(95)90142-6.
- Bodor, D.L., Pönisch, W., Endres, R.G. & Paluch, E.K. (2020) Of Cell Shapes and Motion: The Physical Basis of Animal Cell Migration. *Developmental Cell*, 52(5), 550–562. Available from: https://doi.org/10.1016/j.devcel.2020.02.013.
- Bornens, M. (2002) Centrosome composition and microtubule anchoring mechanisms. *Current Opinion in Cell Biology*, 14(1), 25–34. Available from: https://doi.org/10.1016/s0955-0674(01)00290-3.
- Borowiak, M., Nahaboo, W., Reynders, M., Nekolla, K., Jalinot, P. & Hasserodt, J. et al. (2015) Photoswitchable Inhibitors of Microtubule Dynamics Optically Control Mitosis and Cell Death. *Cell*, 162(2), 403–411. Available from: https://doi.org/10.1016/j.cell.2015.06.049.
- Brangwynne, C.P. (2013) Phase transitions and size scaling of membrane-less organelles. *The Journal of Cell Biology*, 203(6), 875–881. Available from: https://doi.org/10.1083/jcb.201308087.
- Brinkman, E.K., Chen, T., Amendola, M. & van Steensel, B. (2014) Easy quantitative assessment of genome editing by sequence trace decomposition. *Nucleic Acids Research*, 42(22), e168. Available from: https://doi.org/10.1093/nar/gku936.

- Buchan, J.R. & Parker, R. (2009) Eukaryotic stress granules: the ins and outs of translation. *Molecular Cell*, 36(6), 932–941. Available from: https://doi.org/10.1016/j.molcel.2009.11.020.
- Cabral, G., Laos, T., Dumont, J. & Dammermann, A. (2019) Differential Requirements for Centrioles in Mitotic Centrosome Growth and Maintenance. *Developmental Cell*, 50(3), 355-366.e6. Available from: https://doi.org/10.1016/j.devcel.2019.06.004.
- Cai, Y. & Sheetz, M.P. (2009) Force propagation across cells: mechanical coherence of dynamic cytoskeletons. *Current Opinion in Cell Biology*, 21(1), 47–50. Available from: https://doi.org/10.1016/j.ceb.2009.01.020.
- Camargo Ortega, G., Falk, S., Johansson, P.A., Peyre, E., Broix, L. & Sahu, S.K. et al. (2019) The centrosome protein AKNA regulates neurogenesis via microtubule organization. *Nature*, 567(7746), 113–117. Available from: https://doi.org/10.1038/s41586-019-0962-4.
- Cao, J., Crest, J., Fasulo, B. & Sullivan, W. (2010) Cortical actin dynamics facilitate early-stage centrosome separation. *Current Biology : CB*, 20(8), 770–776. Available from: https://doi.org/10.1016/j.cub.2010.02.060.
- Caswell, P.T. & Zech, T. (2018) Actin-Based Cell Protrusion in a 3D Matrix. *Trends in Cell Biology*, 28(10), 823–834. Available from: https://doi.org/10.1016/j.tcb.2018.06.003.
- Chabin-Brion, K., Marceiller, J., Perez, F., Settegrana, C., Drechou, A. & Durand, G. et al. (2001) The Golgi complex is a microtubule-organizing organelle. *Molecular Biology of the Cell*, 12(7), 2047–2060. Available from: https://doi.org/10.1091/mbc.12.7.2047.
- Cheng, H., Kao, Y.-L., Chen, T., Sharma, L., Yang, W.-T. & Chuang, Y.-C. et al. (2023) Actin filaments form a size-dependent diffusion barrier around centrosomes. *EMBO Reports*, 24(1), e54935. Available from: https://doi.org/10.15252/embr.202254935.
- Cho, N.H., Cheveralls, K.C., Brunner, A.-D., Kim, K., Michaelis, A.C. & Raghavan, P. et al. (2022) OpenCell: Endogenous tagging for the cartography of human cellular organization. *Science (New York, N.Y.)*, 375(6585), eabi6983. Available from: https://doi.org/10.1126/science.abi6983.
- Conduit, P.T., Wainman, A. & Raff, J.W. (2015) Centrosome function and assembly in animal cells. *Nature Reviews. Molecular Cell Biology*, 16(10), 611–624. Available from: https://doi.org/10.1038/nrm4062.
- Corthésy-Theulaz, I., Pauloin, A. & Pfeffer, S.R. (1992) Cytoplasmic dynein participates in the centrosomal localization of the Golgi complex. *The Journal of Cell Biology*, 118(6), 1333–1345. Available from: https://doi.org/10.1083/jcb.118.6.1333.
- Cunha-Ferreira, I., Rodrigues-Martins, A., Bento, I., Riparbelli, M., Zhang, W. & Laue, E. et al. (2009) The SCF/Slimb ubiquitin ligase limits centrosome amplification through degradation of SAK/PLK4. *Current Biology : CB*, 19(1), 43–49. Available from: https://doi.org/10.1016/j.cub.2008.11.037.
- Dammermann, A. & Merdes, A. (2002) Assembly of centrosomal proteins and microtubule organization depends on PCM-1. *The Journal of Cell Biology*, 159(2), 255–266. Available from: https://doi.org/10.1083/jcb.200204023.
- Dang, H. & Schiebel, E. (2022) Emerging roles of centrosome cohesion. *Open Biology*, 12(10), 220229. Available from: https://doi.org/10.1098/rsob.220229.
- Dawe, H.R., Adams, M., Wheway, G., Szymanska, K., Logan, C.V. & Noegel, A.A. et al. (2009) Nesprin-2 interacts with meckelin and mediates ciliogenesis via remodelling of the actin cytoskeleton. *Journal of Cell Science*, 122(Pt 15), 2716–2726. Available from: https://doi.org/10.1242/jcs.043794.

- Delgehyr, N., Sillibourne, J. & Bornens, M. (2005) Microtubule nucleation and anchoring at the centrosome are independent processes linked by ninein function. *Journal of Cell Science*, 118(Pt 8), 1565–1575. Available from: https://doi.org/10.1242/jcs.02302.
- Denais, C.M., Gilbert, R.M., Isermann, P., McGregor, A.L., Te Lindert, M. & Weigelin, B. et al. (2016) Nuclear envelope rupture and repair during cancer cell migration. *Science (New York, N.Y.)*, 352(6283), 353–358. Available from: https://doi.org/10.1126/science.aad7297.
- Di Vona, C., Bezdan, D., Islam, A.B.M.M.K., Salichs, E., López-Bigas, N. & Ossowski, S. et al. (2015) Chromatin-wide profiling of DYRK1A reveals a role as a gene-specific RNA polymerase II CTD kinase. *Molecular Cell*, 57(3), 506–520. Available from: https://doi.org/10.1016/j.molcel.2014.12.026.
- Dogterom, M. & Koenderink, G.H. (2019) Actin-microtubule crosstalk in cell biology. *Nature Reviews. Molecular Cell Biology*, 20(1), 38–54. Available from: https://doi.org/10.1038/s41580-018-0067-1.
- Dong, C., West, K.L., Tan, X.Y., Li, J., Ishibashi, T. & Yu, C.-H. et al. (2020) Screen identifies DYRK1B network as mediator of transcription repression on damaged chromatin. *Proceedings of the National Academy of Sciences of the United States of America*, 117(29), 17019–17030. Available from: https://doi.org/10.1073/pnas.2002193117.
- Doyle, A.D., Nazari, S.S. & Yamada, K.M. (2022) Cell-extracellular matrix dynamics. *Physical Biology*, 19(2). Available from: https://doi.org/10.1088/1478-3975/ac4390.
- Doyle, A.D., Petrie, R.J., Kutys, M.L. & Yamada, K.M. (2013) Dimensions in cell migration. *Current Opinion in Cell Biology*, 25(5), 642–649. Available from: https://doi.org/10.1016/j.ceb.2013.06.004.
- DuChez, B.J., Doyle, A.D., Dimitriadis, E.K. & Yamada, K.M. (2019) Durotaxis by Human Cancer Cells. *Biophysical Journal*, 116(4), 670–683. Available from: https://doi.org/10.1016/j.bpj.2019.01.009.
- Efimov, A., Kharitonov, A., Efimova, N., Loncarek, J., Miller, P.M. & Andreyeva, N. et al. (2007) Asymmetric CLASP-dependent nucleation of noncentrosomal microtubules at the trans-Golgi network. *Developmental Cell*, 12(6), 917–930. Available from: https://doi.org/10.1016/j.devcel.2007.04.002.
- Elbaum-Garfinkle, S., Kim, Y., Szczepaniak, K., Chen, C.C.-H., Eckmann, C.R. & Myong, S. et al. (2015) The disordered P granule protein LAF-1 drives phase separation into droplets with tunable viscosity and dynamics. *Proceedings of the National Academy of Sciences of the United States of America*, 112(23), 7189–7194. Available from: https://doi.org/10.1073/pnas.1504822112.
- Farina, F., Gaillard, J., Guérin, C., Couté, Y., Sillibourne, J. & Blanchoin, L. et al. (2016) The centrosome is an actin-organizing centre. *Nature Cell Biology*, 18(1), 65–75. Available from: https://doi.org/10.1038/ncb3285.
- Farina, F., Ramkumar, N., Brown, L., Samandar Eweis, D., Anstatt, J. & Waring, T. et al. (2019) Local actin nucleation tunes centrosomal microtubule nucleation during passage through mitosis. *The EMBO Journal*, 38(11). Available from: https://doi.org/10.15252/embj.201899843.
- Feric, M., Vaidya, N., Harmon, T.S., Mitrea, D.M., Zhu, L. & Richardson, T.M. et al. (2016) Coexisting Liquid Phases Underlie Nucleolar Subcompartments. *Cell*, 165(7), 1686–1697. Available from: https://doi.org/10.1016/j.cell.2016.04.047.
- Fischer, L.S., Rangarajan, S., Sadhanasatish, T. & Grashoff, C. (2021) Molecular Force Measurement with Tension Sensors. *Annual Review of Biophysics*, 50, 595–616. Available from: https://doi.org/10.1146/annurev-biophys-101920-064756.

- Friedl, P., Wolf, K. & Lammerding, J. (2011) Nuclear mechanics during cell migration. *Current Opinion in Cell Biology*, 23(1), 55–64. Available from: https://doi.org/10.1016/j.ceb.2010.10.015.
- Fritz-Laylin, L.K., Riel-Mehan, M., Chen, B.-C., Lord, S.J., Goddard, T.D. & Ferrin, T.E. et al. (2017) Actin-based protrusions of migrating neutrophils are intrinsically lamellar and facilitate direction changes. *ELife*, 6. Available from: https://doi.org/10.7554/eLife.26990.
- Fry, A.M., Mayor, T., Meraldi, P., Stierhof, Y.D., Tanaka, K. & Nigg, E.A. (1998) C-Nap1, a novel centrosomal coiled-coil protein and candidate substrate of the cell cycle-regulated protein kinase Nek2. *The Journal of Cell Biology*, 141(7), 1563–1574. Available from: https://doi.org/10.1083/jcb.141.7.1563.
- Gadadhar, S., Bodakuntla, S., Natarajan, K. & Janke, C. (2017) The tubulin code at a glance. *Journal of Cell Science*, 130(8), 1347–1353. Available from: https://doi.org/10.1242/jcs.199471.
- Gaertner, F., Reis-Rodrigues, P., Vries, I. de, Hons, M., Aguilera, J. & Riedl, M. et al. (2022) WASp triggers mechanosensitive actin patches to facilitate immune cell migration in dense tissues. *Developmental Cell*, 57(1), 47-62.e9. Available from: https://doi.org/10.1016/j.devcel.2021.11.024.
- Gallo, R., Rai, A.K., McIntyre, A.B.R., Meyer, K. & Pelkmans, L. (2023) DYRK3 enables secretory trafficking by maintaining the liquid-like state of ER exit sites. *Developmental Cell*, 58(19), 1880-1897.e11. Available from: https://doi.org/10.1016/j.devcel.2023.08.005.
- Godinho, S.A., Kwon, M. & Pellman, D. (2009) Centrosomes and cancer: how cancer cells divide with too many centrosomes. *Cancer Metastasis Reviews*, 28(1-2), 85–98. Available from: https://doi.org/10.1007/s10555-008-9163-6.
- Gomez, T.S., Kumar, K., Medeiros, R.B., Shimizu, Y., Leibson, P.J. & Billadeau, D.D. (2007) Formins regulate the actin-related protein 2/3 complex-independent polarization of the centrosome to the immunological synapse. *Immunity*, 26(2), 177–190. Available from: https://doi.org/10.1016/j.immuni.2007.01.008.
- Gönczy, P. (2012) Towards a molecular architecture of centriole assembly. *Nature Reviews. Molecular Cell Biology*, 13(7), 425–435. Available from: https://doi.org/10.1038/nrm3373.
- Graser, S., Stierhof, Y.-D. & Nigg, E.A. (2007) Cep68 and Cep215 (Cdk5rap2) are required for centrosome cohesion. *Journal of Cell Science*, 120(Pt 24), 4321–4331. Available from: https://doi.org/10.1242/jcs.020248.
- Greenan, G.A., Keszthelyi, B., Vale, R.D. & Agard, D.A. (2018) Insights into centriole geometry revealed by cryotomography of doublet and triplet centrioles. *ELife*, 7. Available from: https://doi.org/10.7554/eLife.36851.
- Guard, S.E., Poss, Z.C., Ebmeier, C.C., Pagratis, M., Simpson, H. & Taatjes, D.J. et al. (2019) The nuclear interactome of DYRK1A reveals a functional role in DNA damage repair. *Scientific Reports*, 9(1), 6539. Available from: https://doi.org/10.1038/s41598-019-42990-5.
- Guderian, G., Westendorf, J., Uldschmid, A. & Nigg, E.A. (2010) Plk4 trans-autophosphorylation regulates centriole number by controlling betaTrCP-mediated degradation. *Journal of Cell Science*, 123(Pt 13), 2163–2169. Available from: https://doi.org/10.1242/jcs.068502.
- Guichard, P., Hachet, V., Majubu, N., Neves, A., Demurtas, D. & Olieric, N. et al. (2013) Native architecture of the centriole proximal region reveals features underlying its 9-fold radial symmetry. *Current Biology : CB*, 23(17), 1620–1628. Available from: https://doi.org/10.1016/j.cub.2013.06.061.
- Habedanck, R., Stierhof, Y.-D., Wilkinson, C.J. & Nigg, E.A. (2005) The Polo kinase Plk4 functions in centriole duplication. *Nature Cell Biology*, 7(11), 1140–1146. Available from: https://doi.org/10.1038/ncb1320.

- Hageman, J. & Kampinga, H.H. (2009) Computational analysis of the human HSPH/HSPA/DNAJ family and cloning of a human HSPH/HSPA/DNAJ expression library. *Cell Stress & Chaperones*, 14(1), 1–21. Available from: https://doi.org/10.1007/s12192-008-0060-2.
- Hames, R.S., Crookes, R.E., Straatman, K.R., Merdes, A., Hayes, M.J. & Faragher, A.J. et al. (2005) Dynamic recruitment of Nek2 kinase to the centrosome involves microtubules, PCM-1, and localized proteasomal degradation. *Molecular Biology of the Cell*, 16(4), 1711–1724. Available from: https://doi.org/10.1091/mbc.e04-08-0688.
- Harada, Y., Tanaka, Y., Terasawa, M., Pieczyk, M., Habiro, K. & Katakai, T. et al. (2012) DOCK8 is a Cdc42 activator critical for interstitial dendritic cell migration during immune responses. *Blood*, 119(19), 4451–4461. Available from: https://doi.org/10.1182/blood-2012-01-407098.
- Hata, S., Pastor Peidro, A., Panic, M., Liu, P., Atorino, E. & Funaya, C. et al. (2019) The balance between KIFC3 and EG5 tetrameric kinesins controls the onset of mitotic spindle assembly. *Nature Cell Biology*, 21(9), 1138–1151. Available from: https://doi.org/10.1038/s41556-019-0382-6.
- He, R., Huang, N., Bao, Y., Zhou, H., Teng, J. & Chen, J. (2013) LRRC45 is a centrosome linker component required for centrosome cohesion. *Cell Reports*, 4(6), 1100–1107. Available from: https://doi.org/10.1016/j.celrep.2013.08.005.
- Heuzé, M.L., Sankara Narayana, G.H.N., D'Alessandro, J., Cellerin, V., Dang, T. & Williams, D.S. et al. (2019) Myosin II isoforms play distinct roles in adherens junction biogenesis. *ELife*, 8. Available from: https://doi.org/10.7554/eLife.46599.
- Hinchcliffe, E.H., Miller, F.J., Cham, M., Khodjakov, A. & Sluder, G. (2001) Requirement of a centrosomal activity for cell cycle progression through G1 into S phase. *Science (New York, N.Y.)*, 291(5508), 1547–1550. Available from: https://doi.org/10.1126/science.1056866.
- Hughes, H., Budnik, A., Schmidt, K., Palmer, K.J., Mantell, J. & Noakes, C. et al. (2009) Organisation of human ER-exit sites: requirements for the localisation of Sec16 to transitional ER. *Journal of Cell Science*, 122(Pt 16), 2924–2934. Available from: https://doi.org/10.1242/jcs.044032.
- Humphrey, S.J., Karayel, O., James, D.E. & Mann, M. (2018) High-throughput and high-sensitivity phosphoproteomics with the EasyPhos platform. *Nature Protocols*, 13(9), 1897–1916. Available from: https://doi.org/10.1038/s41596-018-0014-9.
- Hyman, A.A. & Simons, K. (2012) Cell biology. Beyond oil and water--phase transitions in cells. *Science (New York, N.Y.)*, 337(6098), 1047–1049. Available from: https://doi.org/10.1126/science.1223728.
- Infante, E., Castagnino, A., Ferrari, R., Monteiro, P., Agüera-González, S. & Paul-Gilloteaux, P. et al. (2018) LINC complex-Lis1 interplay controls MT1-MMP matrix digest-on-demand response for confined tumor cell migration. *Nature Communications*, 9(1), 2443. Available from: https://doi.org/10.1038/s41467-018-04865-7.
- Inoue, D., Obino, D., Pineau, J., Farina, F., Gaillard, J. & Guerin, C. et al. (2019) Actin filaments regulate microtubule growth at the centrosome. *The EMBO Journal*, 38(11). Available from: https://doi.org/10.15252/embj.201899630.
- Irianto, J., Xia, Y., Pfeifer, C.R., Athirasala, A., Ji, J. & Alvey, C. et al. (2017) DNA Damage Follows Repair Factor Depletion and Portends Genome Variation in Cancer Cells after Pore Migration. *Current Biology : CB*, 27(2), 210–223. Available from: https://doi.org/10.1016/j.cub.2016.11.049.
- Ishikawa, H., Kubo, A., Tsukita, S. & Tsukita, S. (2005) Odf2-deficient mother centrioles lack distal/subdistal appendages and the ability to generate primary cilia. *Nature Cell Biology*, 7(5), 517–524. Available from: https://doi.org/10.1038/ncb1251.

- Janke, C., Rogowski, K., Wloga, D., Regnard, C., Kajava, A.V. & Strub, J.-M. et al. (2005) Tubulin polyglutamylase enzymes are members of the TTL domain protein family. *Science (New York, N.Y.)*, 308(5729), 1758–1762. Available from: https://doi.org/10.1126/science.1113010.
- Kalaydjieva, L., Gresham, D., Gooding, R., Heather, L., Baas, F. & Jonge, R. de et al. (2000) N-myc downstream-regulated gene 1 is mutated in hereditary motor and sensory neuropathy-Lom. *American Journal of Human Genetics*, 67(1), 47–58. Available from: https://doi.org/10.1086/302978.
- Kameritsch, P. & Renkawitz, J. (2020) Principles of Leukocyte Migration Strategies. *Trends in Cell Biology*, 30(10), 818–832. Available from: https://doi.org/10.1016/j.tcb.2020.06.007.
- Kapitein, L.C., Peterman, E.J.G., Kwok, B.H., Kim, J.H., Kapoor, T.M. & Schmidt, C.F. (2005) The bipolar mitotic kinesin Eg5 moves on both microtubules that it crosslinks. *Nature*, 435(7038), 114–118. Available from: https://doi.org/10.1038/nature03503.
- Kato, M., Han, T.W., Xie, S., Shi, K., Du, X. & Wu, L.C. et al. (2012) Cell-free formation of RNA granules: low complexity sequence domains form dynamic fibers within hydrogels. *Cell*, 149(4), 753–767. Available from: https://doi.org/10.1016/j.cell.2012.04.017.
- Kedersha, N., Ivanov, P. & Anderson, P. (2013) Stress granules and cell signaling: more than just a passing phase? *Trends in Biochemical Sciences*, 38(10), 494–506. Available from: https://doi.org/10.1016/j.tibs.2013.07.004.
- Képiró, M., Várkuti, B.H., Végner, L., Vörös, G., Hegyi, G. & Varga, M. et al. (2014) para-Nitro-blebbistatin, the non-cytotoxic and photostable myosin II inhibitor. *Angewandte Chemie (International Ed. in English)*, 53(31), 8211–8215. Available from: https://doi.org/10.1002/anie.201403540.
- Khodjakov, A. & Rieder, C.L. (2001) Centrosomes enhance the fidelity of cytokinesis in vertebrates and are required for cell cycle progression. *The Journal of Cell Biology*, 153(1), 237–242. Available from: https://doi.org/10.1083/jcb.153.1.237.
- Kim, K., Cha, J.S., Cho, Y.-S., Kim, H., Chang, N. & Kim, H.-J. et al. (2018) Crystal Structure of Human Dual-Specificity Tyrosine-Regulated Kinase 3 Reveals New Structural Features and Insights into its Auto-phosphorylation. *Journal of Molecular Biology*, 430(10), 1521–1530. Available from: https://doi.org/10.1016/j.jmb.2018.04.001.
- Kim, K., Yoon, J. & Park, Y. (2016) Large-scale optical diffraction tomography for inspection of optical plastic lenses. *Optics Letters*, 41(5), 934–937. Available from: https://doi.org/10.1364/OL.41.000934.
- Kim, K.-T., Ongusaha, P.P., Hong, Y.-K., Kurdistani, S.K., Nakamura, M. & Lu, K.P. et al. (2004) Function of Drg1/Rit42 in p53-dependent mitotic spindle checkpoint. *The Journal of Biological Chemistry*, 279(37), 38597–38602. Available from: https://doi.org/10.1074/jbc.M400781200.
- Kitata, R.B., Choong, W.-K., Tsai, C.-F., Lin, P.-Y., Chen, B.-S. & Chang, Y.-C. et al. (2021) A data-in-dependent acquisition-based global phosphoproteomics system enables deep profiling. *Nature Communications*, 12(1), 2539. Available from: https://doi.org/10.1038/s41467-021-22759-z.
- Kochanski, R.S. & Borisy, G.G. (1990) Mode of centriole duplication and distribution. *The Journal of Cell Biology*, 110(5), 1599–1605. Available from: https://doi.org/10.1083/jcb.110.5.1599.
- Kopf, A., Renkawitz, J., Hauschild, R., Girkontaite, I., Tedford, K. & Merrin, J. et al. (2020) Microtubules control cellular shape and coherence in amoeboid migrating cells. *The Journal of Cell Biology*, 219(6). Available from: https://doi.org/10.1083/jcb.201907154.

- Kroll, J., Hauschild, R., Kuznetcov, A., Stefanowski, K., Hermann, M.D. & Merrin, J. et al. (2023) Adaptive pathfinding by nucleokinesis during amoeboid migration. *The EMBO Journal*, 42(24), e114557. Available from: https://doi.org/10.15252/embj.2023114557.
- Kroll, J. & Renkawitz, J. (2024) Principles of organelle positioning in motile and non-motile cells. *EMBO Reports*, 25(5), 2172–2187. Available from: https://doi.org/10.1038/s44319-024-00135-4.
- Kroll, J., Ruiz-Fernandez, M.J.A., Braun, M.B., Merrin, J. & Renkawitz, J. (2022) Quantifying the Probing and Selection of Microenvironmental Pores by Motile Immune Cells. *Current Protocols*, 2(4), e407. Available from: https://doi.org/10.1002/cpz1.407.
- Kuriyama, R. & Borisy, G.G. (1981) Centriole cycle in Chinese hamster ovary cells as determined by whole-mount electron microscopy. *The Journal of Cell Biology*, 91(3 Pt 1), 814–821. Available from: https://doi.org/10.1083/jcb.91.3.814.
- Lämmermann, T. & Germain, R.N. (2014) The multiple faces of leukocyte interstitial migration. *Seminars in Immunopathology*, 36(2), 227–251. Available from: https://doi.org/10.1007/s00281-014-0418-8.
- Lämmermann, T. & Kastenmüller, W. (2019) Concepts of GPCR-controlled navigation in the immune system. *Immunological Reviews*, 289(1), 205–231. Available from: https://doi.org/10.1111/imr.12752.
- Lämmermann, T., Renkawitz, J., Wu, X., Hirsch, K., Brakebusch, C. & Sixt, M. (2009) Cdc42-dependent leading edge coordination is essential for interstitial dendritic cell migration. *Blood*, 113(23), 5703–5710. Available from: https://doi.org/10.1182/blood-2008-11-191882.
- Lämmermann, T. & Sixt, M. (2009) Mechanical modes of 'amoeboid' cell migration. *Current Opinion in Cell Biology*, 21(5), 636–644. Available from: https://doi.org/10.1016/j.ceb.2009.05.003.
- Lane, H.A. & Nigg, E.A. (1996) Antibody microinjection reveals an essential role for human pololike kinase 1 (Plk1) in the functional maturation of mitotic centrosomes. *The Journal of Cell Biology*, 135(6 Pt 2), 1701–1713. Available from: https://doi.org/10.1083/jcb.135.6.1701.
- Lawo, S., Hasegan, M., Gupta, G.D. & Pelletier, L. (2012) Subdiffraction imaging of centrosomes reveals higher-order organizational features of pericentriolar material. *Nature Cell Biology*, 14(11), 1148–1158. Available from: https://doi.org/10.1038/ncb2591.
- Lawrence, E.J., Zanic, M. & Rice, L.M. (2020) CLASPs at a glance. *Journal of Cell Science*, 133(8). Available from: https://doi.org/10.1242/jcs.243097.
- Leithner, A., Eichner, A., Müller, J., Reversat, A., Brown, M. & Schwarz, J. et al. (2016) Diversified actin protrusions promote environmental exploration but are dispensable for locomotion of leukocytes. *Nature Cell Biology*, 18(11), 1253–1259. Available from: https://doi.org/10.1038/ncb3426.
- Li, S., Fernandez, J.-J., Marshall, W.F. & Agard, D.A. (2012) Three-dimensional structure of basal body triplet revealed by electron cryo-tomography. *The EMBO Journal*, 31(3), 552–562. Available from: https://doi.org/10.1038/emboj.2011.460.
- Li, S., Fernandez, J.-J., Marshall, W.F. & Agard, D.A. (2019) Electron cryo-tomography provides insight into procentriole architecture and assembly mechanism. *ELife*, 8. Available from: https://doi.org/10.7554/eLife.43434.
- Lim, X.R. & Harraz, O.F. (2024) Mechanosensing by Vascular Endothelium. *Annual Review of Physiology*, 86, 71–97. Available from: https://doi.org/10.1146/annurev-physiol-042022-030946.

- Lin, Y.-N., Wu, C.-T., Lin, Y.-C., Hsu, W.-B., Tang, C.-J.C. & Chang, C.-W. et al. (2013) CEP120 interacts with CPAP and positively regulates centriole elongation. *The Journal of Cell Biology*, 202(2), 211–219. Available from: https://doi.org/10.1083/jcb.201212060.
- Lomakin, A.J., Cattin, C.J., Cuvelier, D., Alraies, Z., Molina, M. & Nader, G.P.F. et al. (2020) The nucleus acts as a ruler tailoring cell responses to spatial constraints. *Science (New York, N.Y.)*, 370(6514). Available from: https://doi.org/10.1126/science.aba2894.
- Lu, H., Yu, D., Hansen, A.S., Ganguly, S., Liu, R. & Heckert, A. et al. (2018) Phase-separation mechanism for C-terminal hyperphosphorylation of RNA polymerase II. *Nature*, 558(7709), 318–323. Available from: https://doi.org/10.1038/s41586-018-0174-3.
- Ma, D., Wang, F., Teng, J., Huang, N. & Chen, J. (2023) Structure and function of distal and subdistal appendages of the mother centriole. *Journal of Cell Science*, 136(3). Available from: https://doi.org/10.1242/jcs.260560.
- Mahen, R. (2022) cNap1 bridges centriole contact sites to maintain centrosome cohesion. *PLoS Biology*, 20(10), e3001854. Available from: https://doi.org/10.1371/journal.pbio.3001854.
- Mayor, T., Stierhof, Y.D., Tanaka, K., Fry, A.M. & Nigg, E.A. (2000) The centrosomal protein C-Nap1 is required for cell cycle-regulated centrosome cohesion. *The Journal of Cell Biology*, 151(4), 837–846. Available from: https://doi.org/10.1083/jcb.151.4.837.
- Mediani, L., Antoniani, F., Galli, V., Vinet, J., Carrà, A.D. & Bigi, I. et al. (2021) Hsp90-mediated regulation of DYRK3 couples stress granule disassembly and growth via mTORC1 signaling. *EMBO Reports*, 22(5), e51740. Available from: https://doi.org/10.15252/embr.202051740.
- Meiring, J.C.M., Grigoriev, I., Nijenhuis, W., Kapitein, L.C. & Akhmanova, A. (2022) Opto-katanin, an optogenetic tool for localized, microtubule disassembly. *Current Biology : CB*, 32(21), 4660-4674.e6. Available from: https://doi.org/10.1016/j.cub.2022.09.010.
- Mennella, V., Keszthelyi, B., McDonald, K.L., Chhun, B., Kan, F. & Rogers, G.C. et al. (2012) Sub-diffraction-resolution fluorescence microscopy reveals a domain of the centrosome critical for pericentriolar material organization. *Nature Cell Biology*, 14(11), 1159–1168. Available from: https://doi.org/10.1038/ncb2597.
- Menon, V.R., Ananthapadmanabhan, V., Swanson, S., Saini, S., Sesay, F. & Yakovlev, V. et al. (2019) DYRK1A regulates the recruitment of 53BP1 to the sites of DNA damage in part through interaction with RNF169. *Cell Cycle (Georgetown, Tex.)*, 18(5), 531–551. Available from: https://doi.org/10.1080/15384101.2019.1577525.
- Meraldi, P. & Nigg, E.A. (2001) Centrosome cohesion is regulated by a balance of kinase and phosphatase activities. *Journal of Cell Science*, 114(Pt 20), 3749–3757. Available from: https://doi.org/10.1242/jcs.114.20.3749.
- Merbl, Y. & Kirschner, M.W. (2009) Large-scale detection of ubiquitination substrates using cell extracts and protein microarrays. *Proceedings of the National Academy of Sciences of the United States of America*, 106(8), 2543–2548. Available from: https://doi.org/10.1073/pnas.0812892106.
- Miller, P.M., Folkmann, A.W., Maia, A.R.R., Efimova, N., Efimov, A. & Kaverina, I. (2009) Golgi-derived CLASP-dependent microtubules control Golgi organization and polarized trafficking in motile cells. *Nature Cell Biology*, 11(9), 1069–1080. Available from: https://doi.org/10.1038/ncb1920.
- Mitchison, T. & Kirschner, M. (1988) Cytoskeletal dynamics and nerve growth. *Neuron*, 1(9), 761–772. Available from: https://doi.org/10.1016/0896-6273(88)90124-9.
- Mullee, L.I. & Morrison, C.G. (2016) Centrosomes in the DNA damage response--the hub outside the centre. *Chromosome Research: an International Journal on the Molecular, Supramolecular*

- *and Evolutionary Aspects of Chromosome Biology*, 24(1), 35–51. Available from: https://doi.org/10.1007/s10577-015-9503-7.
- Nakazawa, Y., Hiraki, M., Kamiya, R. & Hirono, M. (2007) SAS-6 is a cartwheel protein that establishes the 9-fold symmetry of the centriole. *Current Biology : CB*, 17(24), 2169–2174. Available from: https://doi.org/10.1016/j.cub.2007.11.046.
- Nazarov, S., Bezler, A., Hatzopoulos, G.N., Nemčíková Villímová, V., Demurtas, D. & Le Guennec, M. et al. (2020) Novel features of centriole polarity and cartwheel stacking revealed by cryo-to-mography. *The EMBO Journal*, 39(22), e106249. Available from: https://doi.org/10.15252/embj.2020106249.
- Nido, G.S., Méndez, R., Pascual-García, A., Abia, D. & Bastolla, U. (2012) Protein disorder in the centrosome correlates with complexity in cell types number. *Molecular BioSystems*, 8(1), 353–367. Available from: https://doi.org/10.1039/c1mb05199g.
- Nigg, E.A. & Stearns, T. (2011) The centrosome cycle: Centriole biogenesis, duplication and inherent asymmetries. *Nature Cell Biology*, 13(10), 1154–1160. Available from: https://doi.org/10.1038/ncb2345.
- Panic, M., Hata, S., Neuner, A. & Schiebel, E. (2015) The centrosomal linker and microtubules provide dual levels of spatial coordination of centrosomes. *PLoS Genetics*, 11(5), e1005243. Available from: https://doi.org/10.1371/journal.pgen.1005243.
- Park, J.-E., Zhang, L., Bang, J.K., Andresson, T., DiMaio, F. & Lee, K.S. (2019) Phase separation of Polo-like kinase 4 by autoactivation and clustering drives centriole biogenesis. *Nature Communications*, 10(1), 4959. Available from: https://doi.org/10.1038/s41467-019-12619-2.
- Patel, A., Lee, H.O., Jawerth, L., Maharana, S., Jahnel, M. & Hein, M.Y. et al. (2015) A Liquid-to-Solid Phase Transition of the ALS Protein FUS Accelerated by Disease Mutation. *Cell*, 162(5), 1066–1077. Available from: https://doi.org/10.1016/j.cell.2015.07.047.
- Pérez, M., García-Limones, C., Zapico, I., Marina, A., Schmitz, M.L. & Muñoz, E. et al. (2012) Mutual regulation between SIAH2 and DYRK2 controls hypoxic and genotoxic signaling pathways. *Journal of Molecular Cell Biology*, 4(5), 316–330. Available from: https://doi.org/10.1093/jmcb/mjs047.
- Pesce, M., Duda, G.N., Forte, G., Girao, H., Raya, A. & Roca-Cusachs, P. et al. (2023) Cardiac fibroblasts and mechanosensation in heart development, health and disease. *Nature Reviews. Cardiology*, 20(5), 309–324. Available from: https://doi.org/10.1038/s41569-022-00799-2.
- Petrie, R.J., Koo, H. & Yamada, K.M. (2014) Generation of compartmentalized pressure by a nuclear piston governs cell motility in a 3D matrix. *Science (New York, N.Y.)*, 345(6200), 1062–1065. Available from: https://doi.org/10.1126/science.1256965.
- Petrie, R.J. & Yamada, K.M. (2016) Multiple mechanisms of 3D migration: the origins of plasticity. *Current Opinion in Cell Biology*, 42, 7–12. Available from: https://doi.org/10.1016/j.ceb.2016.03.025.
- Petry, S. & Vale, R.D. (2015) Microtubule nucleation at the centrosome and beyond. *Nature cell biology*, 17(9), 1089–1093. Available from: https://doi.org/10.1038/ncb3220.
- Piel, M., Meyer, P., Khodjakov, A., Rieder, C.L. & Bornens, M. (2000) The respective contributions of the mother and daughter centrioles to centrosome activity and behavior in vertebrate cells. *The Journal of Cell Biology*, 149(2), 317–330. Available from: https://doi.org/10.1083/jcb.149.2.317.
- Puklowski, A., Homsi, Y., Keller, D., May, M., Chauhan, S. & Kossatz, U. et al. (2011) The SCF-FBXW5 E3-ubiquitin ligase is regulated by PLK4 and targets HsSAS-6 to control centrosome duplication. *Nature Cell Biology*, 13(8), 1004–1009. Available from: https://doi.org/10.1038/ncb2282.

- R Core Team (2021) R: A language and environment for statistical computing. *R Foundation for Statistical Computing, Vienna, Austria*. Available from: URL https://www.R-project.org/.
- Raab, M., Gentili, M., Belly, H. de, Thiam, H.R., Vargas, P. & Jimenez, A.J. et al. (2016) ESCRT III repairs nuclear envelope ruptures during cell migration to limit DNA damage and cell death. *Science (New York, N.Y.)*, 352(6283), 359–362. Available from: https://doi.org/10.1126/science.aad7611.
- Rai, A.K., Chen, J.-X., Selbach, M. & Pelkmans, L. (2018) Kinase-controlled phase transition of membraneless organelles in mitosis. *Nature*, 559(7713), 211–216. Available from: https://doi.org/10.1038/s41586-018-0279-8.
- Ramella, M., Ribolla, L.M., Surini, S., Sala, K., Tonoli, D. & Cioni, J.-M. et al. (2024) Dual specificity kinase DYRK3 regulates cell migration by influencing the stability of protrusions. *IScience*, 27(4), 109440. Available from: https://doi.org/10.1016/j.isci.2024.109440.
- Redecke, V., Wu, R., Zhou, J., Finkelstein, D., Chaturvedi, V. & High, A.A. et al. (2013) Hematopoietic progenitor cell lines with myeloid and lymphoid potential. *Nature Methods*, 10(8), 795–803. Available from: https://doi.org/10.1038/nmeth.2510.
- Remo, A., Li, X., Schiebel, E. & Pancione, M. (2020) The Centrosome Linker and Its Role in Cancer and Genetic Disorders. *Trends in Molecular Medicine*, 26(4), 380–393. Available from: https://doi.org/10.1016/j.molmed.2020.01.011.
- Remo, A., Manfrin, E., Parcesepe, P., Ferrarini, A., Han, H.S. & Mickys, U. et al. (2018) Centrosome Linker-induced Tetraploid Segregation Errors Link Rhabdoid Phenotypes and Lethal Colorectal Cancers. *Molecular Cancer Research : MCR*, 16(9), 1385–1395. Available from: https://doi.org/10.1158/1541-7786.MCR-18-0062.
- Renkawitz, J., Kopf, A., Stopp, J., Vries, I. de, Driscoll, M.K. & Merrin, J. et al. (2019) Nuclear positioning facilitates amoeboid migration along the path of least resistance. *Nature*, 568(7753), 546–550. Available from: https://doi.org/10.1038/s41586-019-1087-5.
- Renkawitz, J., Reversat, A., Leithner, A., Merrin, J. & Sixt, M. (2018) Micro-engineered "pillar forests" to study cell migration in complex but controlled 3D environments. *Methods in Cell Biology*, 147, 79–91. Available from: https://doi.org/10.1016/bs.mcb.2018.07.004.
- Renkawitz, J., Schumann, K., Weber, M., Lämmermann, T., Pflicke, H. & Piel, M. et al. (2009) Adaptive force transmission in amoeboid cell migration. *Nature Cell Biology*, 11(12), 1438–1443. Available from: https://doi.org/10.1038/ncb1992.
- Reversat, A., Gaertner, F., Merrin, J., Stopp, J., Tasciyan, S. & Aguilera, J. et al. (2020) Cellular locomotion using environmental topography. *Nature*, 582(7813), 582–585. Available from: https://doi.org/10.1038/s41586-020-2283-z.
- Robison, P., Caporizzo, M.A., Ahmadzadeh, H., Bogush, A.I., Chen, C.Y. & Margulies, K.B. et al. (2016) Detyrosinated microtubules buckle and bear load in contracting cardiomyocytes. *Science (New York, N.Y.)*, 352(6284), aaf0659. Available from: https://doi.org/10.1126/science.aaf0659.
- Rosenblatt, J., Cramer, L.P., Baum, B. & McGee, K.M. (2004) Myosin II-dependent cortical movement is required for centrosome separation and positioning during mitotic spindle assembly. *Cell*, 117(3), 361–372. Available from: https://doi.org/10.1016/s0092-8674(04)00341-1.
- Russo, E., Teijeira, A., Vaahtomeri, K., Willrodt, A.-H., Bloch, J.S. & Nitschké, M. et al. (2016) Intralymphatic CCL21 Promotes Tissue Egress of Dendritic Cells through Afferent Lymphatic Vessels. *Cell Reports*, 14(7), 1723–1734. Available from: https://doi.org/10.1016/j.celrep.2016.01.048.

- Sala, K., Raimondi, A., Tonoli, D., Tacchetti, C. & Curtis, I. de (2018) Identification of a membrane-less compartment regulating invadosome function and motility. *Scientific Reports*, 8(1), 1164. Available from: https://doi.org/10.1038/s41598-018-19447-2.
- Sawin, K.E., LeGuellec, K., Philippe, M. & Mitchison, T.J. (1992) Mitotic spindle organization by a plus-end-directed microtubule motor. *Nature*, 359(6395), 540–543. Available from: https://doi.org/10.1038/359540a0.
- Schaedel, L., John, K., Gaillard, J., Nachury, M.V., Blanchoin, L. & Théry, M. (2015) Microtubules self-repair in response to mechanical stress. *Nature Materials*, 14(11), 1156–1163. Available from: https://doi.org/10.1038/nmat4396.
- Schmidt, T.I., Kleylein-Sohn, J., Westendorf, J., Le Clech, M., Lavoie, S.B. & Stierhof, Y.-D. et al. (2009) Control of centriole length by CPAP and CP110. *Current Biology : CB*, 19(12), 1005–1011. Available from: https://doi.org/10.1016/j.cub.2009.05.016.
- Schneider, C.A., Rasband, W.S. & Eliceiri, K.W. (2012) NIH Image to ImageJ: 25 years of image analysis. *Nature Methods*, 9(7), 671–675. Available from: https://doi.org/10.1038/nmeth.2089.
- Schumann, K., Lämmermann, T., Bruckner, M., Legler, D.F., Polleux, J. & Spatz, J.P. et al. (2010) Immobilized chemokine fields and soluble chemokine gradients cooperatively shape migration patterns of dendritic cells. *Immunity*, 32(5), 703–713. Available from: https://doi.org/10.1016/j.immuni.2010.04.017.
- Schürmann, M., Scholze, J., Müller, P., Chan, C.J., Ekpenyong, A.E. & Chalut, K.J. et al. (2015) Refractive index measurements of single, spherical cells using digital holographic microscopy. *Methods in Cell Biology*, 125, 143–159. Available from: https://doi.org/10.1016/bs.mcb.2014.10.016.
- SenGupta, S., Parent, C.A. & Bear, J.E. (2021) The principles of directed cell migration. *Nature Reviews. Molecular Cell Biology*, 22(8), 529–547. Available from: https://doi.org/10.1038/s41580-021-00366-6.
- Shen, H., Tauzin, L.J., Baiyasi, R., Wang, W., Moringo, N. & Shuang, B. et al. (2017) Single Particle Tracking: From Theory to Biophysical Applications. *Chemical Reviews*, 117(11), 7331–7376. Available from: https://doi.org/10.1021/acs.chemrev.6b00815.
- Shin, Y. & Brangwynne, C.P. (2017) Liquid phase condensation in cell physiology and disease. *Science (New York, N.Y.)*, 357(6357). Available from: https://doi.org/10.1126/science.aaf4382.
- Singla, V., Romaguera-Ros, M., Garcia-Verdugo, J.M. & Reiter, J.F. (2010) Ofd1, a human disease gene, regulates the length and distal structure of centrioles. *Developmental Cell*, 18(3), 410–424. Available from: https://doi.org/10.1016/j.devcel.2009.12.022.
- Sivan, G., Kedersha, N. & Elroy-Stein, O. (2007) Ribosomal slowdown mediates translational arrest during cellular division. *Molecular and Cellular Biology*, 27(19), 6639–6646. Available from: https://doi.org/10.1128/MCB.00798-07.
- Sixt, M. & Lämmermann, T. (2011) In vitro analysis of chemotactic leukocyte migration in 3D environments. *Methods in Molecular Biology (Clifton, N.J.)*, 769, 149–165. Available from: https://doi.org/10.1007/978-1-61779-207-6_11.
- So, C., Menelaou, K., Uraji, J., Harasimov, K., Steyer, A.M. & Seres, K.B. et al. (2022) Mechanism of spindle pole organization and instability in human oocytes. *Science (New York, N.Y.)*, 375(6581), eabj3944. Available from: https://doi.org/10.1126/science.abj3944.
- Sonnen, K.F., Schermelleh, L., Leonhardt, H. & Nigg, E.A. (2012) 3D-structured illumination microscopy provides novel insight into architecture of human centrosomes. *Biology Open*, 1(10), 965–976. Available from: https://doi.org/10.1242/bio.20122337.

- Spector, D.L. & Smith, H.C. (1986) Redistribution of U-snRNPs during mitosis. *Experimental Cell Research*, 163(1), 87–94. Available from: https://doi.org/10.1016/0014-4827(86)90560-4.
- Stinchcombe, J.C., Majorovits, E., Bossi, G., Fuller, S. & Griffiths, G.M. (2006) Centrosome polarization delivers secretory granules to the immunological synapse. *Nature*, 443(7110), 462–465. Available from: https://doi.org/10.1038/nature05071.
- Taira, N., Mimoto, R., Kurata, M., Yamaguchi, T., Kitagawa, M. & Miki, Y. et al. (2012) DYRK2 priming phosphorylation of c-Jun and c-Myc modulates cell cycle progression in human cancer cells. *The Journal of Clinical Investigation*, 122(3), 859–872. Available from: https://doi.org/10.1172/JCI60818.
- Taira, N., Nihira, K., Yamaguchi, T., Miki, Y. & Yoshida, K. (2007) DYRK2 is targeted to the nucleus and controls p53 via Ser46 phosphorylation in the apoptotic response to DNA damage. *Molecular Cell*, 25(5), 725–738. Available from: https://doi.org/10.1016/j.molcel.2007.02.007.
- Takahara, T. & Maeda, T. (2012) Transient sequestration of TORC1 into stress granules during heat stress. *Molecular Cell*, 47(2), 242–252. Available from: https://doi.org/10.1016/j.molcel.2012.05.019.
- Tang, C.-J.C., Fu, R.-H., Wu, K.-S., Hsu, W.-B. & Tang, T.K. (2009) CPAP is a cell-cycle regulated protein that controls centriole length. *Nature Cell Biology*, 11(7), 825–831. Available from: https://doi.org/10.1038/ncb1889.
- Tang, N. & Marshall, W.F. (2012) Centrosome positioning in vertebrate development. *Journal of Cell Science*, 125(Pt 21), 4951–4961. Available from: https://doi.org/10.1242/jcs.038083.
- Tanos, B.E., Yang, H.-J., Soni, R., Wang, W.-J., Macaluso, F.P. & Asara, J.M. et al. (2013) Centriole distal appendages promote membrane docking, leading to cilia initiation. *Genes & Development*, 27(2), 163–168. Available from: https://doi.org/10.1101/gad.207043.112.
- Te Boekhorst, V., Preziosi, L. & Friedl, P. (2016) Plasticity of Cell Migration In Vivo and In Silico. *Annual Review of Cell and Developmental Biology*, 32, 491–526. Available from: https://doi.org/10.1146/annurev-cellbio-111315-125201.
- Theile, L., Li, X., Dang, H., Mersch, D., Anders, S. & Schiebel, E. (2023) Centrosome linker diversity and its function in centrosome clustering and mitotic spindle formation. *The EMBO Journal*, 42(17), e109738. Available from: https://doi.org/10.15252/embj.2021109738.
- Thiam, H.-R., Vargas, P., Carpi, N., Crespo, C.L., Raab, M. & Terriac, E. et al. (2016) Perinuclear Arp2/3-driven actin polymerization enables nuclear deformation to facilitate cell migration through complex environments. *Nature Communications*, 7, 10997. Available from: https://doi.org/10.1038/ncomms10997.
- Tinevez, J.-Y., Perry, N., Schindelin, J., Hoopes, G.M., Reynolds, G.D. & Laplantine, E. et al. (2017) TrackMate: An open and extensible platform for single-particle tracking. *Methods (San Diego, Calif.)*, 115, 80–90. Available from: https://doi.org/10.1016/j.ymeth.2016.09.016.
- Tiwary, A.K. & Zheng, Y. (2019) Protein phase separation in mitosis. *Current Opinion in Cell Biology*, 60, 92–98. Available from: https://doi.org/10.1016/j.ceb.2019.04.011.
- Tsou, M.-F.B. & Stearns, T. (2006) Mechanism limiting centrosome duplication to once per cell cycle. *Nature*, 442(7105), 947–951. Available from: https://doi.org/10.1038/nature04985.
- Tsou, M.-F.B., Wang, W.-J., George, K.A., Uryu, K., Stearns, T. & Jallepalli, P.V. (2009) Polo kinase and separase regulate the mitotic licensing of centriole duplication in human cells. *Developmental Cell*, 17(3), 344–354. Available from: https://doi.org/10.1016/j.devcel.2009.07.015.
- Uetake, Y., Loncarek, J., Nordberg, J.J., English, C.N., La Terra, S. & Khodjakov, A. et al. (2007) Cell cycle progression and de novo centriole assembly after centrosomal removal in untransformed human cells. *The Journal of Cell Biology*, 176(2), 173–182. Available from: https://doi.org/10.1083/jcb.200607073.

- van Goethem, E., Poincloux, R., Gauffre, F., Maridonneau-Parini, I. & Le Cabec, V. (2010) Matrix architecture dictates three-dimensional migration modes of human macrophages: differential involvement of proteases and podosome-like structures. *Journal of Immunology (Baltimore, Md.: 1950)*, 184(2), 1049–1061. Available from: https://doi.org/10.4049/jimmunol.0902223.
- Vander Haar, E., Lee, S.-I., Bandhakavi, S., Griffin, T.J. & Kim, D.-H. (2007) Insulin signalling to mTOR mediated by the Akt/PKB substrate PRAS40. *Nature Cell Biology*, 9(3), 316–323. Available from: https://doi.org/10.1038/ncb1547.
- Várnai, P. & Balla, T. (1998) Visualization of phosphoinositides that bind pleckstrin homology domains: calcium- and agonist-induced dynamic changes and relationship to myo-3Hinositol-labeled phosphoinositide pools. *The Journal of Cell Biology*, 143(2), 501–510. Available from: https://doi.org/10.1083/jcb.143.2.501.
- Venturini, V., Pezzano, F., Català Castro, F., Häkkinen, H.-M., Jiménez-Delgado, S. & Colomer-Rosell, M. et al. (2020) The nucleus measures shape changes for cellular proprioception to control dynamic cell behavior. *Science (New York, N.Y.)*, 370(6514). Available from: https://doi.org/10.1126/science.aba2644.
- Vitiello, E., Moreau, P., Nunes, V., Mettouchi, A., Maiato, H. & Ferreira, J.G. et al. (2019) Acto-myosin force organization modulates centriole separation and PLK4 recruitment to ensure centriole fidelity. *Nature Communications*, 10(1), 52. Available from: https://doi.org/10.1038/s41467-018-07965-6.
- Vlijm, R., Li, X., Panic, M., Rüthnick, D., Hata, S. & Herrmannsdörfer, F. et al. (2018) STED nanoscopy of the centrosome linker reveals a CEP68-organized, periodic rootletin network anchored to a C-Nap1 ring at centrioles. *Proceedings of the National Academy of Sciences of the United States of America*, 115(10), E2246-E2253. Available from: https://doi.org/10.1073/pnas.1716840115.
- Vorobjev, I.A. & Chentsov, Y. (1982) Centrioles in the cell cycle. I. Epithelial cells. *The Journal of Cell Biology*, 93(3), 938–949. Available from: https://doi.org/10.1083/jcb.93.3.938.
- Watson, P., Townley, A.K., Koka, P., Palmer, K.J. & Stephens, D.J. (2006) Sec16 defines endoplasmic reticulum exit sites and is required for secretory cargo export in mammalian cells. *Traffic (Copenhagen, Denmark)*, 7(12), 1678–1687. Available from: https://doi.org/10.1111/j.1600-0854.2006.00493.x.
- Weier, A.-K., Homrich, M., Ebbinghaus, S., Juda, P., Miková, E. & Hauschild, R. et al. (2022) Multiple centrosomes enhance migration and immune cell effector functions of mature dendritic cells. *The Journal of Cell Biology*, 221(12). Available from: https://doi.org/10.1083/jcb.202107134.
- Weigelin, B., Bakker, G.-J. & Friedl, P. (2012) Intravital third harmonic generation microscopy of collective melanoma cell invasion: Principles of interface guidance and microvesicle dynamics. *Intravital*, 1(1), 32–43. Available from: https://doi.org/10.4161/intv.21223.
- Weninger, W., Biro, M. & Jain, R. (2014) Leukocyte migration in the interstitial space of non-lymphoid organs. *Nature Reviews. Immunology*, 14(4), 232–246. Available from: https://doi.org/10.1038/nri3641.
- Wickham, H., Averick, M., Bryan, J., Chang, W., McGowan, L. & François, R. et al. (2019) Welcome to the Tidyverse. *Journal of Open Source Software*, 4(43), 1686. Available from: https://doi.org/10.21105/joss.01686.
- Wippich, F., Bodenmiller, B., Trajkovska, M.G., Wanka, S., Aebersold, R. & Pelkmans, L. (2013) Dual specificity kinase DYRK3 couples stress granule condensation/dissolution to mTORC1 signaling. *Cell*, 152(4), 791–805. Available from: https://doi.org/10.1016/j.cell.2013.01.033.

- Wolf, K., Alexander, S., Schacht, V., Coussens, L.M., Andrian, U.H. von & van Rheenen, J. et al. (2009) Collagen-based cell migration models in vitro and in vivo. *Seminars in Cell & Developmental Biology*, 20(8), 931–941. Available from: https://doi.org/10.1016/j.semcdb.2009.08.005.
- Wolf, K., Müller, R., Borgmann, S., Bröcker, E.-B. & Friedl, P. (2003) Amoeboid shape change and contact guidance: T-lymphocyte crawling through fibrillar collagen is independent of matrix remodeling by MMPs and other proteases. *Blood*, 102(9), 3262–3269. Available from: https://doi.org/10.1182/blood-2002-12-3791.
- Wolf, K., Te Lindert, M., Krause, M., Alexander, S., Te Riet, J. & Willis, A.L. et al. (2013) Physical limits of cell migration: control by ECM space and nuclear deformation and tuning by proteolysis and traction force. *The Journal of Cell Biology*, 201(7), 1069–1084. Available from: https://doi.org/10.1083/jcb.201210152.
- Wong, Y.L., Anzola, J.V., Davis, R.L., Yoon, M., Motamedi, A. & Kroll, A. et al. (2015) Cell biology. Reversible centriole depletion with an inhibitor of Polo-like kinase 4. *Science (New York, N.Y.)*, 348(6239), 1155–1160. Available from: https://doi.org/10.1126/science.aaa5111.
- Woodruff, J.B., Ferreira Gomes, B., Widlund, P.O., Mahamid, J., Honigmann, A. & Hyman, A.A. (2017) The Centrosome Is a Selective Condensate that Nucleates Microtubules by Concentrating Tubulin. *Cell*, 169(6), 1066-1077.e10. Available from: https://doi.org/10.1016/j.cell.2017.05.028.
- Woodruff, J.B., Wueseke, O., Viscardi, V., Mahamid, J., Ochoa, S.D. & Bunkenborg, J. et al. (2015) Centrosomes. Regulated assembly of a supramolecular centrosome scaffold in vitro. *Science* (*New York, N.Y.*), 348(6236), 808–812. Available from: https://doi.org/10.1126/science.aaa3923.
- Worbs, T., Hammerschmidt, S.I. & Förster, R. (2017) Dendritic cell migration in health and disease. *Nature Reviews. Immunology*, 17(1), 30–48. Available from: https://doi.org/10.1038/nri.2016.116.
- Yamada, K.M. & Sixt, M. (2019) Mechanisms of 3D cell migration. *Nature Reviews. Molecular Cell Biology*, 20(12), 738–752. Available from: https://doi.org/10.1038/s41580-019-0172-9.
- Yoo, S.K., Deng, Q., Cavnar, P.J., Wu, Y.I., Hahn, K.M. & Huttenlocher, A. (2010) Differential regulation of protrusion and polarity by PI3K during neutrophil motility in live zebrafish. *Developmental Cell*, 18(2), 226–236. Available from: https://doi.org/10.1016/j.devcel.2009.11.015.
- Zantl, R. & Horn, E. (2011) Chemotaxis of slow migrating mammalian cells analysed by video microscopy. *Methods in Molecular Biology (Clifton, N.J.)*, 769, 191–203. Available from: https://doi.org/10.1007/978-1-61779-207-6_13.
- Zhang, D., Li, K., Erickson-Miller, C.L., Weiss, M. & Wojchowski, D.M. (2005) DYRK gene structure and erythroid-restricted features of DYRK3 gene expression. *Genomics*, 85(1), 117–130. Available from: https://doi.org/10.1016/j.ygeno.2004.08.021.
- Zheng, Y., Wong, M.L., Alberts, B. & Mitchison, T. (1995) Nucleation of microtubule assembly by a gamma-tubulin-containing ring complex. *Nature*, 378(6557), 578–583. Available from: https://doi.org/10.1038/378578a0.
- Zwicker, D., Decker, M., Jaensch, S., Hyman, A.A. & Jülicher, F. (2014) Centrosomes are autocatalytic droplets of pericentriolar material organized by centrioles. *Proceedings of the National Academy of Sciences of the United States of America*, 111(26), E2636-45. Available from: https://doi.org/10.1073/pnas.1404855111.

CONTRIBUTIONS

Cell lines and plasmids used in this study were either self-generated or received as indicated in Tables 6 and 7.

Transcriptomics of migrating dendritic cells in collagen networks of varying complexity was performed by Prof. Jörg Renkawitz in collaboration with Dr. Thomas Penz and Prof. Christoph Bock (Fig. 5A). Initial transcriptome analysis was performed by Dr. Tobias Straub and Maximilian Götz (Fig. 5 B-D). Cell sorting was performed together with Pardis Khosravani from the Core Facility Flow Cytometry (Biomedical Center). Phosphoproteome analysis as well as the underlying collagen migration experiments were optimized and performed by Dr. Petra Kameritsch and Jingyuan Sheng (Fig. 8C). Peter Konopka and Prof. Eva Kiermaier generated the Hoxb8 CETN2-GFP indCas9 sgC-NAP1 cell line used for differentiation of C-Nap1-deficient dendritic cells employed for experiments shown in Fig. 11 and Fig. 12, B and C. Analysis of EB3 comet speed and number, as well as PCM shape analysis were performed by Dr. Robert Hauschild (Fig. 18, B and C, and Fig. 13 B). Mauricio Ruiz-Fernandez analyzed competing protrusion lengths and PH-Akt-based cell polarity (Fig. 22, B and C, and Fig. 24A).

ACKNOWLEDGEMENTS

First, I would like to express my deepest gratitude to my supervisor, Prof. Jörg Renkawitz, whose guidance, support, and encouragement during the last five years have been invaluable throughout my research and the writing of this dissertation. Your insights and expertise have profoundly shaped this work, and your endless scientific curiosity and motivation were always more than contagious!

Furthermore, I would like to thank the members of my Thesis Advisory Committee Dr. Ralph Böttcher and Prof. Dr. Axel Imhof for their helpful advice, insightful comments, and suggestions during our TAC meetings and beyond.

A special thanks goes to all the collaborators involved in this project. To Prof. Eva Kiermaier for providing us with the Centrin2-GFP Hoxb8 cell line that formed a cornerstone of the entire project, and all her expertise regarding dendritic cells and their centrosomes. To Petra Kameritsch and Jingyuan Cheng for establishing and conducting the phosphoproteome analysis of millions of DCs migrating in parallel. To Robert Hauschild for all his time and effort, and the fruitful discussions regarding image analysis and software. To Andreas Thomae from Core Facility Bioimaging for all his technical assistance and invaluable advice during the hours at the microscope. To Jack Merrin for providing us with all the different wafer designs for the microfluidic experiments. It was a pleasure working with you!

To my dear Renkawitz Lab: it has been a true joy! You made the long years of my PhD journey not only bearable but truly enjoyable. I will always cherish the memories of our time together. From our (sometimes endless) coffee breaks and your insightful suggestions during our (occasionally scientific) discussions to the mental-support chocolate and all the fun activities outside the lab. Thank you for everything!

I am incredibly grateful for all the friendships with my colleagues that have developed during our time in the lab. I truly appreciate all of you and the memories we've created together, and I'm more than excited about the adventures that lie ahead for us.

Lastly, I want to thank my non-lab friends and especially my family for their unwavering support, understanding, and encouragement throughout this challenging academic journey. Their belief in my abilities and unconditional support has been a constant source of motivation.



LUDWIG-MAXIMILIANS-UNIVERSITÄT MÜNCHEN

Dekanat Medizinische Fakultät Promotionsbüro



AFFIDAVIT

Schmitt, Madeleine		
Surname, first name		
Großhaderner Straße 9		
Street		
82152 Planegg-Martinsried, Germany		
Zip code, town, country		
I hereby declare, that the submitted thesis entitled		
"The Role of Dyrk3 in Centrosome Coherence during Cell Migration"		
is my own work. I have only used the sources indicated and have not made unauthorised use of services of a third party. Where the work of others has been quoted or reproduced, the source is always given.		
I further declare that the dissertation presented here has not been submitted in the same or similar form to any other institution for the purpose of obtaining an academic degree.		
München, 23.05.2025	Madeleine Tanja Schmitt	
Place, Date	Signature doctoral candidate	

Affidavit June 2024



LUDWIG-MAXIMILIANS-UNIVERSITÄT MÜNCHEN

Dekanat Medizinische Fakultät Promotionsbüro



CONFIRMATION OF CONGRUENCY BETWEEN PRINTED AND ELECTRONIC VERSION OF THE DOCTORAL THESIS

Schmitt, Madeleine	
Surname, first name	
Großhaderner Straße 9	
Street	
82152 Planegg-Martinsried, Germany	
Zip code, town, country	
I hereby declare, that the submitted thesis entitled	
"The Role of Dyrk3 in Centrosome Coherence during Cell	Migration"
is congruent with the printed version both in content and	format.
München, 23.05.2025	Madeleine Tanja Schmitt
Place, Date	Signature doctoral candidate

LIST OF PUBLICATIONS

Publications

Holtkamp SJ, Ince LM, Barnoud C, **Schmitt MT**, Sinturel F, Pilorz V, Pick R, Jemelin S, Mühlstädt M, Boehncke WH, Weber J, Laubender D, Philippou-Massier J, Chen CS, Holtermann L, Vestweber D, Sperandio M, Schraml BU, Halin C, Dibner C, Oster H, Renkawitz J, Scheiermann C (2021) Circadian clocks guide dendritic cells into skin lymphatics. *Nature Immunology* 22(11):1375-1381. doi: 10.1038/s41590-021-01040-x

Clausen BE, Amon L, Backer RA, Berod L, Bopp T, Brand A, Burgdorf S, Chen L, Da M, Distler U, Dress RJ, Dudziak D, Dutertre CA, Eich C, Gabele A, Geiger M, Ginhoux F, Giusiano L, Godoy GJ, Hamouda AEI, Hatscher L, Heger L, Heidkamp GF, Hernandez LC, Jacobi L, Kaszubowski T, Kong WT, Lehmann CHK, López-López T, Mahnke K, Nitsche D, Renkawitz J, Reza RA, Sáez PJ, Schlautmann L, **Schmitt MT**, Seichter A, Sielaff M, Sparwasser T, Stoitzner P, Tchitashvili G, Tenzer S, Tochoedo NR, Vurnek D, Zink F, Hieronymus T (2023). Guidelines for mouse and human DC functional assays. *European journal of immunology* 53(12), e2249925. https://doi.org/10.1002/eji.202249925

Submitted Manuscripts

Schmitt MT, Kroll J, Ruiz-Fernandez MJA, Hauschild R, Ghosh S, Kameritsch P, Merrin J, Schmid J, Stefanowski K, Thomae AW, Cheng J, Öztan GN, Konopka P, Camargo G, Penz T, Bock C, Straub T, Meissner F, Kiermaier E, Renkawitz J. Dyrk3 Prevents Mechanical Centrosome Fracturing during Cell Navigation. *Submitted Article*.

Braun MB, Reza RA, Kameritsch P, Ruiz-Fernandez MJA, **Schmitt MT**, Shnipova M, Krug A, Merrin J, Polleux J, Renkawitz J. Microenvironmental Regulation of Macropinocytosis Facilitates Extracellular Fluid Sampling. *Submitted Article*.